PRESSURE DROP IN HEADERS OF MICROCHANNEL HEAT EXCHANGERS

BY

AMIR CHAVOSHI

DISSERTATION

Submitted in partial fulfillment of the requirements
for the degree of Doctor of Philosophy in Mechanical Engineering
in the Graduate College of the
University of Illinois Urbana-Champaign, 2022

Urbana, Illinois

Doctoral Committee:

Professor Predrag S. Hrnjak, Chair
Professor Tony Jacobi
Assistant Professor Stefan Elbel
Professor Yuanhui Zhang

ABSTRACT

Microchannel heat exchangers (MCHXs) have been widely used in the heating, ventilating, air conditioning, and refrigeration (HVAC&R) industry for their compactness and high heat transfer coefficient. However, they often underperform because of the flow maldistribution among parallel microchannel tubes, which is caused by pressure drop, as well as uneven phase distribution in headers. This non-uniform distribution of refrigerant creates an unwanted superheated region, which has a lower heat transfer coefficient and a smaller temperature difference between the refrigerant and heat-source fluid, thus decreases the heat transfer rate. This dissertation presents an experimental and numerical study of pressure drop in inlet and outlet header for both single-phase and two-phase flow in MCHXs.

The first focus of this work is the experimental investigation of the pressure drop and the development of a new set of correlations for pressure loss coefficients for single-phase flow through round headers of parallel MCHXs. Compressed air is adopted as working fluid. The tested velocity through the header ranges from 1 m/s to 20 m/s while the velocity through the microchannel tube ranges from 6 m/s to 30 m/s, based on those commonly used in MCHXs. Correlations for predicting pressure drop of inlet header and outlet header are proposed, and 98% of experimental data fall into a deviation of ±15 Pa.

Then, the single-phase flow distribution in MCHXs is numerically investigated. The new generated correlations and two other methods are used in a 1-D finite volume approach to evaluate single-phase pressure drop in headers of MCHXs, to predict mass flow rate distribution in microchannel tubes, and the results are compared with a Hydraulic-CFD Linked model, in which the flow in headers are simulated in 3-D by ANSYS Fluent. The results show that the 1-D finite

volume models show a difference in the prediction of flow rate distribution. The model in which the flow passage in the header is assumed to be a series of dividing and combining T-manifolds shows a satisfactory agreement with the Hydraulic-CFD Linked model in the perspectives of mass flow rate distribution.

The last experimental part of this study presents an investigation of the pressure drop in two-phase flow, for which flow visualization and pressure drop measurements are conducted in a vertical upward flow in a round inlet header with R134a. Pressure profiles and flow regimes for different mass fluxes and vapor qualities are demonstrated. Results show that pressure drop in the header is affected significantly by flow morphology in the header. The influences of inlet mass flux and vapor quality on the pressure drop are also presented.

To my family, for their love and support

ACKNOWLEDGMENTS

First and foremost, I would like to thank my Ph.D. advisor, Professor Pega Hrnjak, for all his mentoring, guidance, and patience throughout my journey. He is a great and compassionate mentor, and I will always be indebted to him for all his support.

I would also like to thank my committee members, Professor Tony Jacobi, Professor Stefan Elbel, and Professor Yuanhui Zhang for their insightful comments. They were very helpful and understanding throughout my graduate studies.

I wish to give special thanks to my incredible colleague and friend, Hongliang Qian. This dissertation would have never been possible without his invaluable help. Many thanks to my former and current colleagues, for their companionship, and help during my years at the University of Illinois: Professor Blake Johnson, Professor Kyle Smith, Professor Nenad Miljkovic, Wenzhe Li, Jun Li, Abdel Rahman Farraj, Sugun Tej Inampudi, Tao Ren, Huize Li, Jiu Xu, Wenying Zhang, Lili Feng, Bruno Kimura de Carvalho, Yufang Yao, Bill Davies, Neal Lawrence, Yang Zou, Yuping Gao, Yupeng Wang, and many others. I would also like to thank Creative Thermal Solution and the sponsors of ACRC for their support of my work.

In addition, I want to express my deepest gratitude to my amazing parents, Hamid and Sedigheh, who have always been there for me, and my lovely siblings, Ali, Leila, and Goli. Being away from them was the hardest thing I had to go through all these years, and their unconditional love and support gave me the strength to move forward.

Last but certainly not least, I want to thank my wife, my best friend, and the love of my life, Zahra. We have shared this ride together and have been through all the ups and downs together. I feel lucky and blessed beyond words to have her by my side on this challenging path. I cannot thank her enough for all she has done for me.

TABLE OF CONTENTS

LIST OF FIGURES

LIST OF TABLES

NOMENCLATURE

D	Inner diameter	m
G	Mass flux	kg m^{-2} s^{-1}
P	Pressure	Pa
S	Perimeter	m
g	Acceleration of gravity	m s^{-2}
l	Length	m
v	Velocity	m s^{-1}
α	Void fraction	
ζ	Diverging/converging loss coefficient	
λ	Frictional loss coefficient	
μ	Dynamic viscosity	Pa s
ρ	Density	kg m^{-3}

Subscripts

acc	Acceleration
c	Confluence flow in the header
conv	Converging
div	Diverging
eff	Effective friction loss
f	Friction
h	Hydraulic
header	Quantity in the header
i	i^{th} section of the header
in	Quantity at the inlet
l	Liquid phase
out	Quantity at the outlet
t	Tube
tot	Total
v	Vapor phase

CHAPTER 1

INTRODUCTION

1.1 INTRODUCTION

Microchannel heat exchangers (MCHXs) have come to the frontier of the heating, ventilation, air conditioning, and refrigeration (HVAC&R) industry for their advantages in high overall heat transfer coefficient, compactness, and possible charge reduction. MCHX condensers started to become popular as a replacement for the traditional round-tube-plate-fin RTPF condensers in the 1990s. Microchannel heat exchangers have been successful in automotive air conditioning systems and recently started to appear in residential and commercial air conditioning and refrigeration systems.

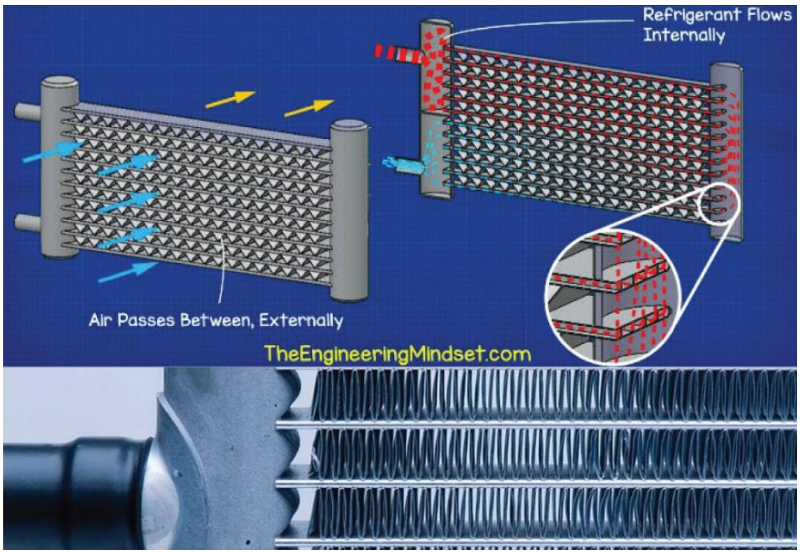

Figure 1-1: Microchannel heat exchanger (from TheEngineeringMindset.com and hydro.com)

As demonstrated in Figure 1-1, a MCHX essentially consists of multiple parallel microchannel tubes, where the heat transfer between the refrigerant and the outside fluid happens, and headers, whereat the refrigerant is collected from or distributes between microchannel tubes. Microchannel tubes consist of multiple ports in a variety of shapes, as shown in Figure 1-2, and are typically made of aluminum.

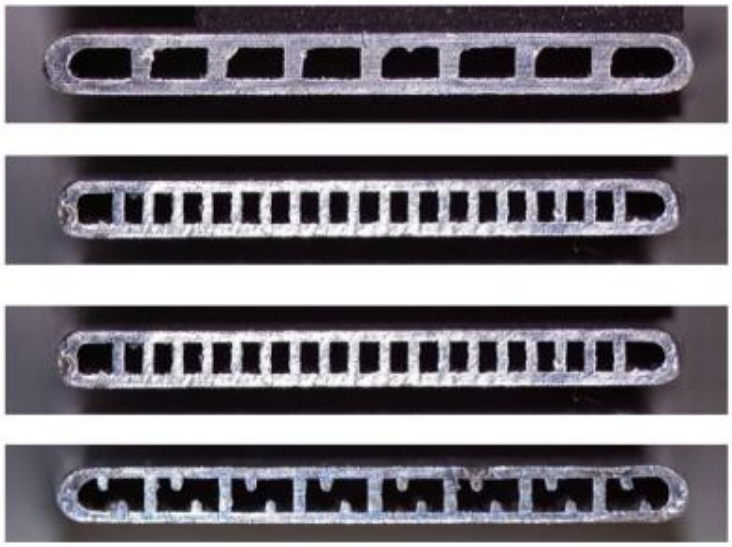

Figure 1-2: Types of microchannel ports

Microchannel heat exchangers suffer from the problem of refrigerant distribution in parallel microchannel tubes and such a maldistribution generally leads to deterioration of heat exchanger performance. Figure 1-3 shows an example of refrigerant maldistribution in an evaporator, resulting in unwanted superheated regions which have a lower heat transfer coefficient and a smaller temperature difference between the refrigerant and the heat-source fluid, leading to lower heat exchanger performance.

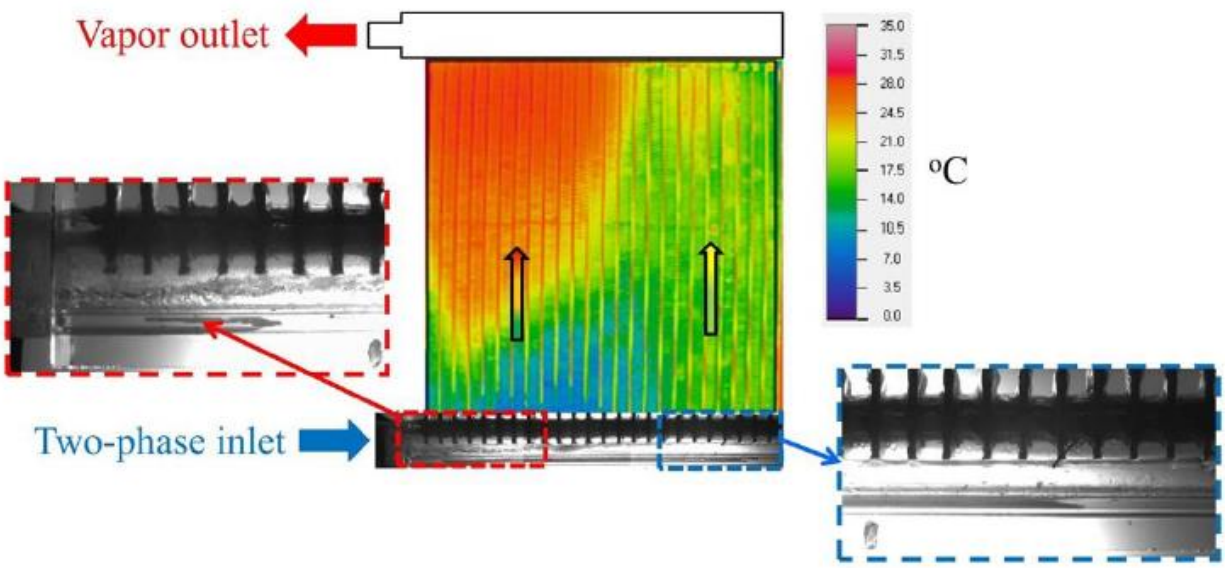

Figure 1-3: Refrigerant maldistribution in the microchannel evaporator, (Tuo and Hrnjak, 2013)

Thus, it is important to better understand the mechanisms behind the flow maldistribution. Difficulties in achieving good distribution, assuming uniform load from the airside, come mainly from two factors: First, unequal quality distribution at the inlet to each microchannel tube which is happening in two-phase flow, as a result of the thermophysical difference between liquid and vapor; second, pressure drop in the headers, particularly in the vapor phase, which is the main cause in the single-phase flow case. Single-phase flow is common in inlet headers (gas coolers, condensers, etc.), and outlet headers (directed expansion and flash gas bypass evaporators, etc.). Pressure drop in the headers results in uneven pressure drop along microchannel tubes, and consequently uneven mass flow rates in microchannel tubes, as shown in Figure 1-4.

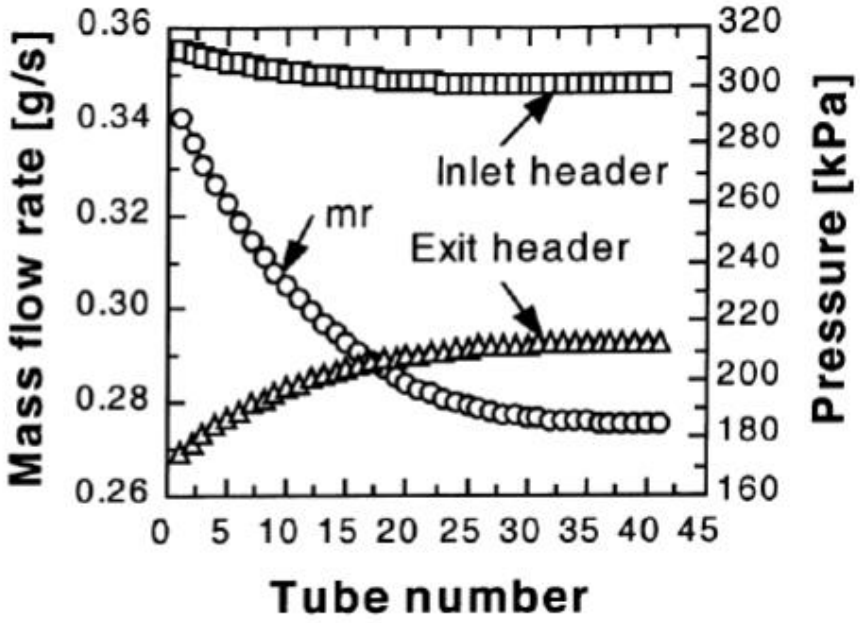

Figure 1-4: Pressure profile and flow distribution of single-phase N_2 in the MCHX (Yin *et al.*, 2000)

The flow distribution in the microchannel heat exchanger tubes has been extensively studied, as presented in the next chapter. However, due to the complex geometries of headers and refrigerant flow patterns within them, there are very limited works reported regarding the local pressure variation along the headers, for both single-phase and two-phase flow. Thus, the first focus of this research is the investigation of pressure drop in single-phase flow through round inlet and outlet headers of MCHXs and the development of new correlations for pressure loss coefficients. Then, single-phase flow distribution in MCHXs is numerically investigated and compared by four different simulation approaches. The third part of this research aims the investigation of two-phase flow in headers of MCHXs. Pressure drop, as well as mass flow rates in the header and each microchannel tube, are measured simultaneously. Visualization of two-phase flow along the header is also utilized for a better understanding of the behavior of two-phase flow in headers.

1.2 STRUCTURE OF THE DISSERTATION

Besides this introductory chapter, this thesis includes 5 chapters. Chapter 2 presents a literature review of previous studies regarding the pressure drop in headers in single-phase and two-phase flow, as well as the distribution in the microchannel tubes. The review covers both the results from past experimental studies and the different modeling approaches that attempt to predict distribution. The need for additional research is discussed and the objectives of the present study are stated. Chapter 3 presents the experimental results of the pressure drop for single-phase flow through round inlet and outlet headers, and only focuses on the pressure loss coefficient for the diverging/converging pressure drop. In this chapter, a new set of correlations for the prediction of pressure loss coefficient in headers is proposed. Chapter 4 proposes three 1-D finite volume mass flow rate distribution models in single-phase flow and compares their prediction to a CFD-based approach, which is very reliable in single-phase flow. Chapter 5 demonstrates experimental results of the pressure drop in the inlet header of MCHXs with careful observation of the header flow patterns. Chapter 6 provides conclusions from the present study and recommends areas for future research.

CHAPTER 2

LITERATURE REVIEW

Refrigerant distribution in microchannel heat exchangers plays an important role in the performance of HVAC&R systems. The performance of MCHX and thus the system capacity and efficiency is reduced as a result of refrigerant maldistribution (Bowers *et al.*, 2006; Forinash, 2015; Vist and Pettersen, 2004; Zou and Hrnjak, 2010, Nielsen *et. al.*, 2012). Kulkarni *et al.* (2004) showed that the performance of a microchannel evaporator was reduced by 20% due to the effect of maldistribution induced by the pressure drop in the horizontal header. Byun and Kim (2011) presented results showing the capacity of a two-pass microchannel heat exchanger was degraded by up to 13.4% by maldistribution of R410A, compared to the uniform distribution case. As shown in Figure 2-1, For the inlet header, a pool is formed at the bottom, so the bottom tubes have more liquid than the top tubes. For the second pass header, two-phase jets enter the header and form a liquid film. Because of the high axial momentum, only a small number of liquid branches out through the bottom tube. The most liquid exits through the middle tubes. When mass flux is increased, the distribution is changed: most liquid exits from the top tubes. Zou *et al.* (2014) showed a capacity reduction of up to 30% and 5% for R410A and R134a maldistribution in a two-pass outdoor MCHX under HP mode, respectively. Thus, there has been a significant interest in the research on the distribution of refrigerant among parallel tubes of MCHXs during recent decades.

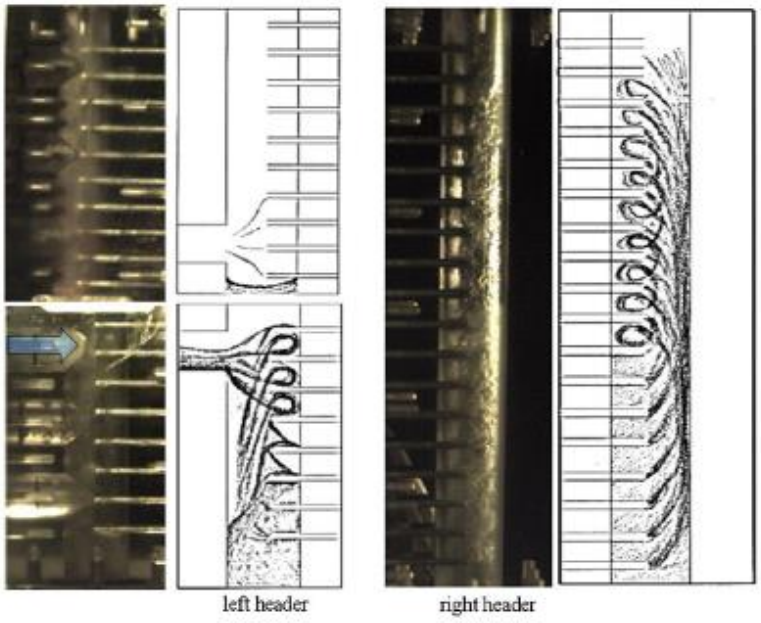

Figure 2-1: Flow pattern with top inlet and bottom outlet (Byun and Kim, 2011)

There are two major causes of refrigerant maldistribution in parallel tubes of a MCHX: 1) pressure drop in the headers, in particular, the vapor phase; 2) the quality distribution of refrigerant in headers. For two-phase inlet conditions, the distribution is usually poor and particularly affected by the flow regime in the inlet header (Fei and Hrnjak, 2004; Kim and Sin, 2006; Hwang *et al.*, 2007; Zou and Hrnjak, 2013; Mahvi and Garimella, 2017). For instance, as shown in Figure 2-2, when the inlet quality was above 0.35, the flow regime in the header became jet in horizontal headers with upward tubes, and this resulted in much less liquid into the middle tubes than the tubes at two ends (Ahmad *et al.*, 2009). Although inlet conditions have been broadly studied, there are discrepancies between the results. For example, many authors conclude that increasing the inlet mass flux improves the overall distribution (Lee and Lee, 2004; Hwang *et al.*, 2007; Kim *et al.*, 2011; Wijayanta *et al.*, 2017), but others find that it does not have a significant effect (Vist and Pettersen, 2004). This disagreement can be explained by the ranges of inlet mass fluxes tested in each study.

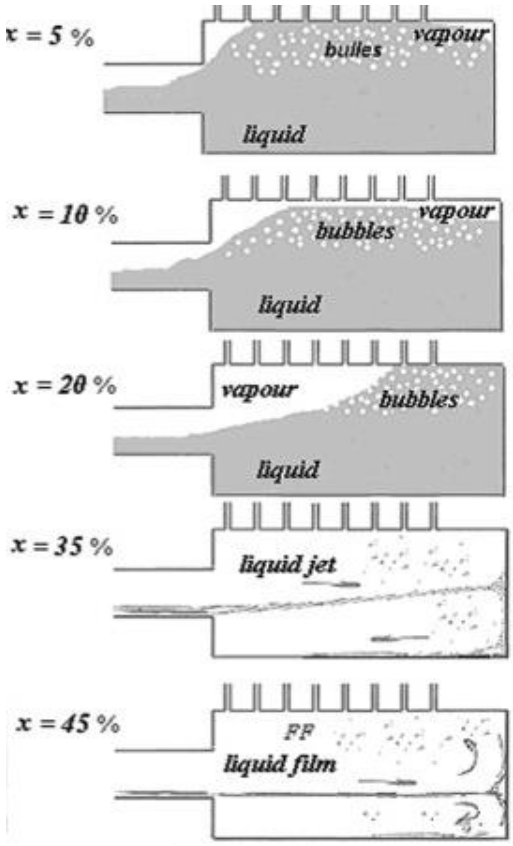

Figure 2-2: Flow pattern in horizontal header with upward tubes (Ahmed *et al.*, 2009)

In addition to a flow regime, studies show maldistribution is affected by tube protrusion in the header, geometry, orientation of header, inlet mass flux, quality, fluid properties, etc. (Hrnjak, 2004; Webb and Chung, 2005). Dario *et al.* (2015) conducted the most comprehensive study on the effect of heat exchanger orientation on two-phase flow distribution. They measured the liquid distribution of an air-water mixture into 9 parallel outlet channels when subjected to inlet mass fluxes between 72 and 216 kg m^{-2} s^{-1} and qualities between 0 and 0.75. The experiments were repeated on a vertical-downward header with horizontal channels and a horizontal header with horizontal, vertical-upward, and vertical-downward channels. They found that the header and channel orientations affect the flow patterns in the header, which results in different distribution

characteristics. It should be noted that the flow experiences a large expansion when it enters the test section in their header design ($A_{header}/A_{inlet\ tube} = 100$), which also affects the flow pattern. Dario *et al.* (2015) found that horizontal headers generally outperform vertical headers, which was also concluded in an earlier study by Cho *et al.* (2003).

2.1 PRESSURE DROP IN HEADERS

Connecting the inlet of MCHX to the exit of the outlet header, multiple flow paths are formed, and each flow path must have an equal pressure drop. This dictates pressure inequality along the headers, and consequently, nonuniform mass flow rate among microchannel tubes. Therefore, even in single-phase flow in MCHX, maldistribution exists (Datta and Majumdar, 1980; Kim *et al.*, 2004). It should be noted that single-phase flow is typical in inlet headers (gas coolers, condensers, evaporators with FGB, etc.), and outlet headers (evaporators).

Most previous studies focused on single-phase water flow distribution in laminar flow (Ghani *et al.*, 2012; Kim *et al.*, 1995; Wang and Yu, 1989). Yin *et al.* (2000) measured single-phase pressure drops inside the headers of a microchannel CO_2 gas cooler and determined empirical loss coefficients based on conventional hydraulic equations by Idelchik (1994). Later, Yin *et al.* (2002) measured pressure drop in headers and generated a model based on the assumption that the pressure loss coefficients are uniform. They also showed that due to the pressure drop of inlet and outlet headers, the first tube (closest to inlet and exit of C-type MCHX) has the highest mass flow rate, and the mass flow rate decreases by about 20% for the tubes located farthest from the inlet and outlet. Tuo and Hrnjak (2013) presented that such single-phase

maldistribution due to pressure drop in the outlet header of MCHX with horizontal headers significantly affected the heat exchanger and system performance.

Even though there has been some, limited progress over the past several decades on the development of effective header designs to alleviate maldistribution in heat exchangers in single-phase flows (Anbumeenakshi and Thansekhar, 2016; Bassiouny and Martin, 1984; Dharaiya *et al.*, 2009; Said *et al.*, 2015), there is still a need to better understand and predict pressure drop in headers of microchannel heat exchangers. This lack of knowledge in understanding pressure drop in headers is much more profound when it comes to two-phase flows, due to the significant complexity of flow characteristics inside the header (Webb and Chung, 2005).

Pioneer researchers opted for air-water mixture for the working fluid in studying two-phase flow (Rong *et al.*, 1995; Marchitto *et al.*, 2008). Tompkins *et al.* (2002) studied the two-phase pressure drop of the air-water mixture in the horizontal header. They concluded that pressure loss in the header was small, and the pressure slightly recovered at the end of the header, due to the stagnation. Kim *et al.* (2013) reported a similar trend in the horizontal header. However, two-phase refrigerant was more commonly used in recent studies, as the distribution characteristics of refrigerants are very different from the air-water mixture (Fei and Hrnjak, 2004; Wijayanta *et al.*, 2017). That is because the properties, mostly density ratio of liquid-vapor refrigerant is much higher than the water-air mixture.

In general, to the author's knowledge, single-phase and two-phase pressure drop in the header was seldom examined locally, and a systematic procedure to calculate two-phase pressure drop in the header is not available.

2.2 MODELING OF DISTRIBUTION

Various modeling methods have been proposed in the literature to predict two-phase flow distribution in headers of microchannel heat exchangers. These methods span from simple empirical correlations to complex computational fluid mechanics models.

Some experimental work on two-phase flow distribution in headers has been utilized to generate empirical correlations for common header geometries. These correlations generally predict the take-off ratio, which is the fraction of the inlet flow rate in the header (immediately upstream of the T-junction containing the channel of interest) that enters a branch channel. One of the first correlations for the liquid take-off ratio in a manifold (header) was developed by Watanabe *et al.* (1995). They related the liquid take-off ratio with the vapor-phase Reynolds number. Although the correlation predicts their data well, it does not include variables that could influence distribution in headers, including the inertia of the liquid phase, gravity, surface tension, and the effects of geometry. As a result, the model has poor predictive capabilities for geometries and operating conditions other than those for which it was developed (Panghat and Mehendale, 2016; Vist, 2004).

Kim *et al.* (2012) developed a similar empirical model based solely on the vapor Reynolds number for the liquid and vapor take-off ratio in a tubular header with protruding channels. Models were developed using a regression analysis for headers with a parallel, normal, and vertical inlet feeder tube. The results for the normal inlet condition are shown in Equations 2-1 and 2-2. The model predictions fit their data relatively well, with average R^2 values of ~78% (although errors are large in some cases, especially at low vapor Reynolds numbers).

$$\frac{\dot{m}_{Liq\ tube,i}}{\dot{m}_{Liq\ header,i}} = 2.01\mathrm{Re}_v[i]^{-0.55} \tag{2-1}$$

$$\frac{\dot{m}_{\mathrm{Vap}\ tube,i}}{\dot{m}_{\mathrm{Vap}\ header,i}} = 3.38\mathrm{Re}_v[i]^{-0.92} \tag{2-2}$$

Again, the Kim *et al.* (2012) model oversimplifies the flow in the header by just considering the inertial and viscous forces of the vapor phase. This could result in large errors when the model is applied to conditions other than those used in the regression analysis. Additionally, the model can predict non-physical results. For example, at low vapor Reynolds numbers, the model predicts take-off ratios greater than one, implying that more liquid enters the channel than is available in the header. Also, the flow distribution in a multichannel heat exchanger is constrained by pressure drop. A simple heat exchanger is governed by the equity of pressure drop in each flow path. The pressure change across each flow path must be equal so that the inlet and exit pressure are the same for each path. The path pressure drop is dependent on the liquid and vapor flow rates into each channel. The Kim *et al.* (2012) correlation proposes a method to calculate both the liquid and vapor flow rates through each path but does not consider the path pressure drops in the calculation. This can lead to predictions that are not physically possible because the pressure drop constraint is not satisfied.

Recently, Wijayanta *et al.* (2017) proposed another model for the liquid and vapor take-off ratios in vertical-downward channels connected to a common horizontal header. They found that the take-off ratios could be modeled using the local liquid Reynolds and Froude numbers and the two-phase Reynolds and Weber numbers in the header, as shown here.

$$\frac{\dot{m}_{Liq\ tube,i}}{\dot{m}_{Liq\ header,i}} = \frac{6}{N_{tube}} 0.426(\mathrm{Re}_{l,\ header}[i]^{-0.5} Fr_{l,\ header})^{-0.3} \tag{2-3}$$

$$\frac{\dot{m}_{Vap\ tube,i}}{\dot{m}_{Vap\ header,i}} = (\frac{6}{N_{tube}})^2\ 0.392e^{-0.002}(\mathrm{Re}_{tp,\ header}[i]^{0.5} We_{tp,\ header}[i]) \tag{2-4}$$

These parameters account for the effects of inertia, viscosity, gravity, and surface tension, which are all important in these types of two-phase flows. Predicting the liquid and vapor flow rates in a channel with no consideration for the path pressure drop may lead to non-physical results. Empirical models can be an effective way to predict flow distribution in heat exchangers if they account for the relevant physical phenomena. However, they are often oversimplified and do not capture the underlying physics, which can lead to poor predictive capabilities outside of the data range used in the data analysis.

1-D mechanistic models have been used to predict single-phase and two-phase flow distribution in heat exchangers (Ablanque *et al.*, 2010; Vist, 2004; Yin *et al.*, 2002). However, the results are highly dependent on the correlations used. Bajura (1971) derived the governing equation of the manifolds by applying the 1-D mass and momentum conservation equations to correlate flow rate and pressure profiles in dividing and combining manifolds. Further, Bajura and Jones (1976) connected the governing equations of two manifolds by the discharge equation, which described the relationship between the pressure differential between the manifolds and the lateral flow rate and obtained an analytical model for the manifold system. The control volumes for the combing and dividing manifolds are shown in Figure 2-3. The 1-D assumption oversimplified the complex flow conditions in the manifolds, so the authors proposed two coefficients to correct. One coefficient corrected the non-uniform velocity profile in the manifolds,

and the other one accounted for the axial momentum transfer to the lateral flow. These two correction coefficients were assumed to be constant and selected based on the experiments.

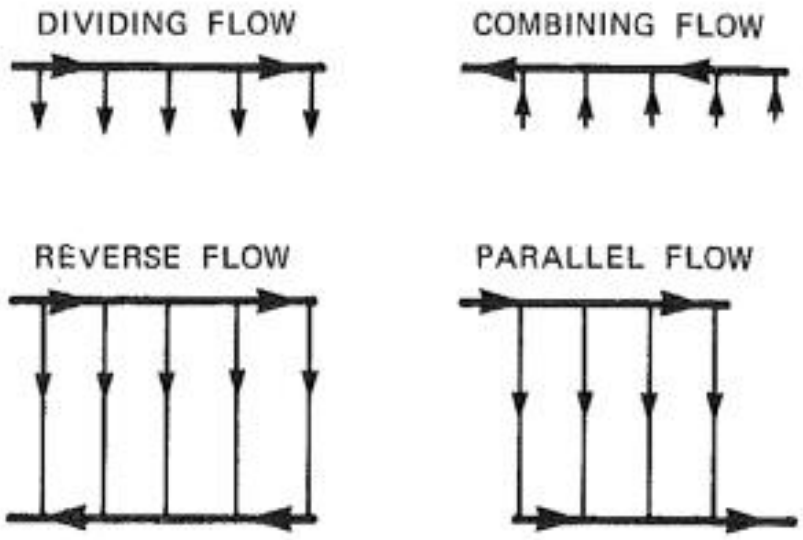

Figure 2-3: Control volume for dividing and combining manifold (Bajura and Jones, 1976)

Datta and Majumdar (1980) employed a 1-D finite-difference procedure, as shown in Figure 2-4, to predict single-phase flow distribution in parallel and reverse flow manifolds as defined by Bajura and Jones (1976), and the numerical results agreed with Bajura and Jones' data satisfactorily. Based on the single-phase study, Datta and Majumdar (1983) developed a 1-D numerical model of the homogeneous air-water mixture in various types of manifolds. For better accuracy of segmental models, proper pressure drop and phase-separation correlations must be selected based on the geometry of the heat exchanger and the flow conditions. In 1-D mechanistic models, the headers and the channels of the heat exchanger are discretized. In addition, existing correlations are employed to predict flow distribution. In these models, the pressure drop in the channels is calculated using correlations from the literature (Friedel, 1979; Garimella *et al.*, 2005;

Kim and Mudawar, 2012). There are many models in the literature to predict the phase-splitting and pressure drop characteristics of two-phase flows entering a T-junction (Hwang *et al.*, 1988; Tae and Cho, 2006), which can be used to predict the inlet quality into each channel. Pressure drop and phase-splitting models in T-junctions are usually based on experimental measurements when a fully developed two-phase flow enters the junction. Although these models can be used, they may not perform well in headers because the flow does not have space to fully develop between consecutive protruded microchannel tubes (Lee, 2009; Vist, 2004).

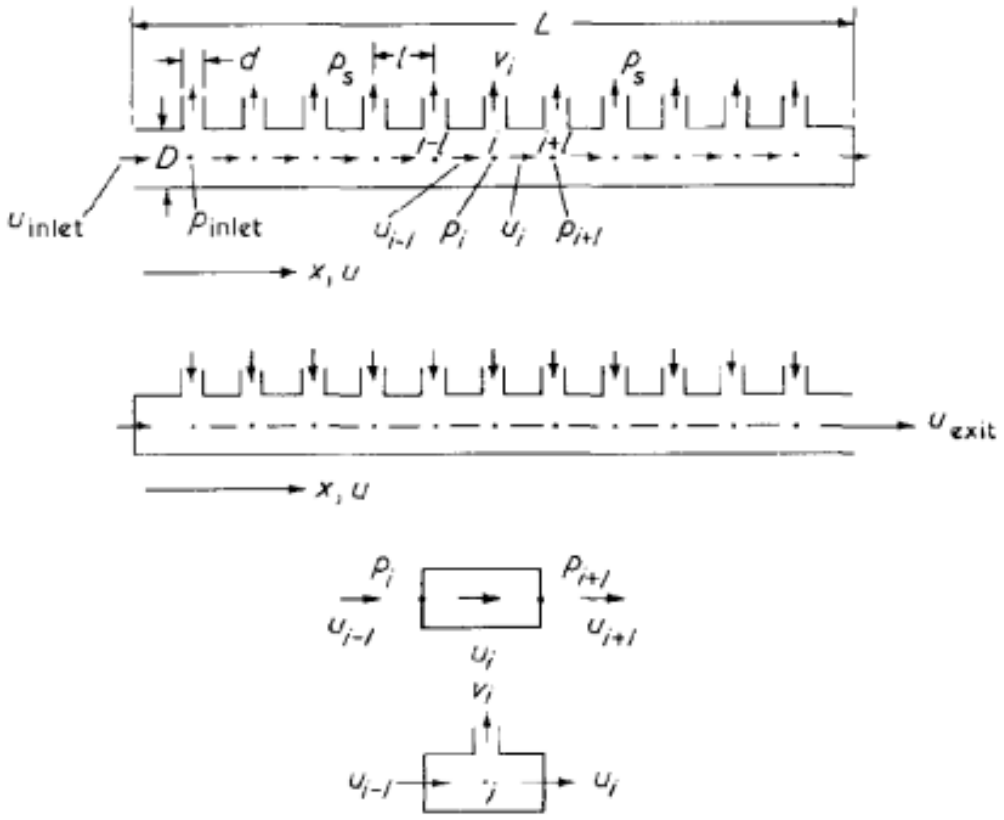

Figure 2-4: Control volume for dividing and combining manifold (Datta and Majumdar, 1980)

Computational Fluid Dynamic (CFD) models are also sometimes used to characterize flow distribution in heat exchangers. Most past works have focused on the distribution of single-phase flow into headers (Bhutta *et al.*, 2012; Luan *et al.*, 2017; Kumaran *et al.*, 2013; Tong *et al.*, 2009; Zhang and Li, 2003). Huang *et al.* (2014) simulated R134a vapor in the inlet header of the automotive microchannel condenser and integrated the CFD model with an ε-NTU based segmented condenser model, as shown in Figure 2-5. Good agreement on heating capacity with their experimental data was achieved.

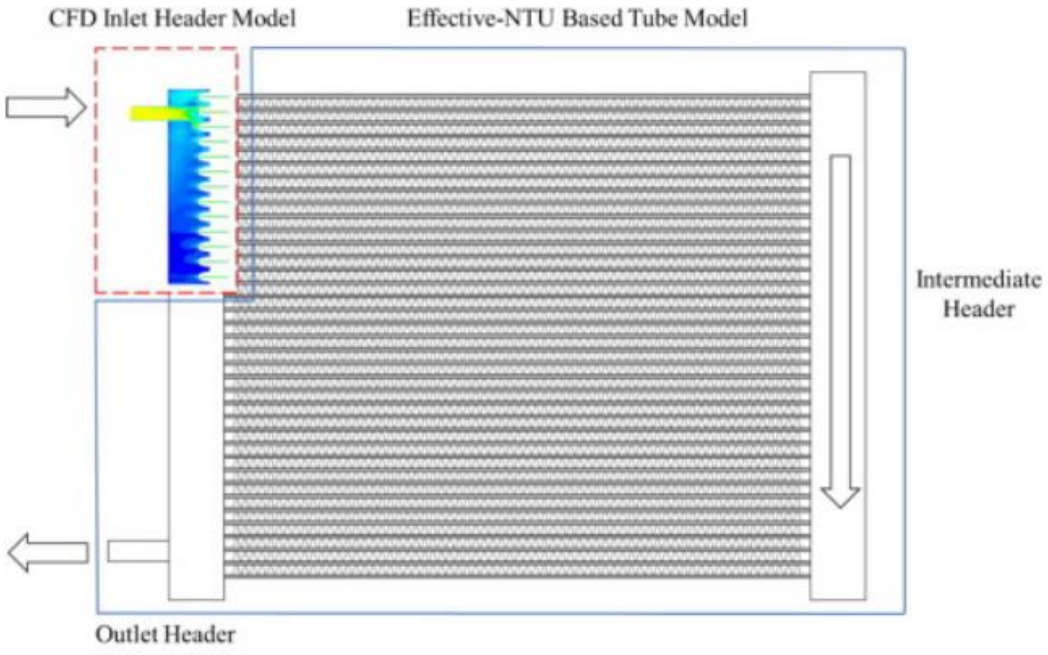

Figure 2-5: Condenser computational model (Huang *et al.*, 2014)

However, studies on two-phase flows are very limited. Fei and Hrnjak (2004) used a 3-D Eulerian-Eulerian approach to model two-phase flow distribution in a heat exchanger using FLUENT (a commercial CFD software). They compared the results with experimental data and

found that the model could qualitatively predict the measured trends, but some channels had large quantitative errors. They concluded that this approach was not accurately capturing the characteristics of the inlet expansion and flow recirculation at the far end of the header. They also presented the pressure and velocity fields inside the header for one inlet case, focusing on the formation and dissipation of the liquid jet, as shown in Figure 2-6.

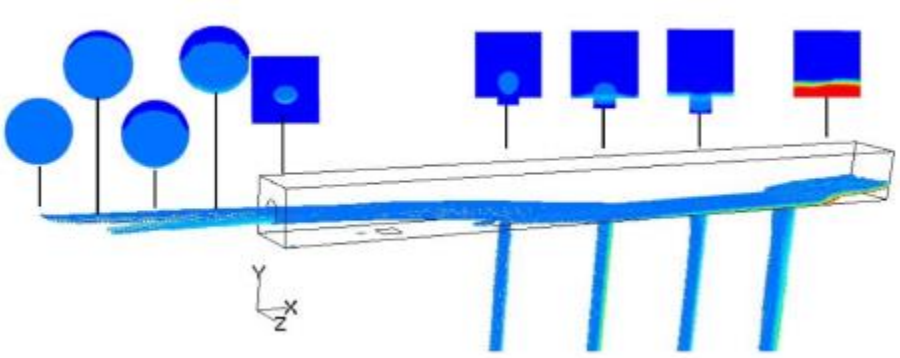

Figure 2-6: Flow pattern in inlet header (Fei and Hrnjak, 2004)

Zou and Hrnjak (2014) studied the flow distribution of R134a and R410A in the intermediate vertical header of a two-pass evaporator experimentally and numerically. A 3-D numerical model was developed in FLUENT using the Eulerian-Eulerian multiphase model with the standard k-ε turbulence model for both phases. Although the model does correctly predict the flow rate in some channels, the errors between the measured inlet qualities and the CFD predictions are large in many cases and generally do not follow the same trends. Zou and Hrnjak (2016) also presented the local liquid volume fractions and velocity profiles computed by the numerical model, which show some interesting flow phenomena, but further work is needed to develop a CFD simulation that accurately predicts the experimental results. Stevanovic and Hrnjak (2017) later on

improved the model by considering oil flow and compared the model results to oil retention data from experiments using R134a and R1234yf with PAG oil, as shown in Figure 2-7.

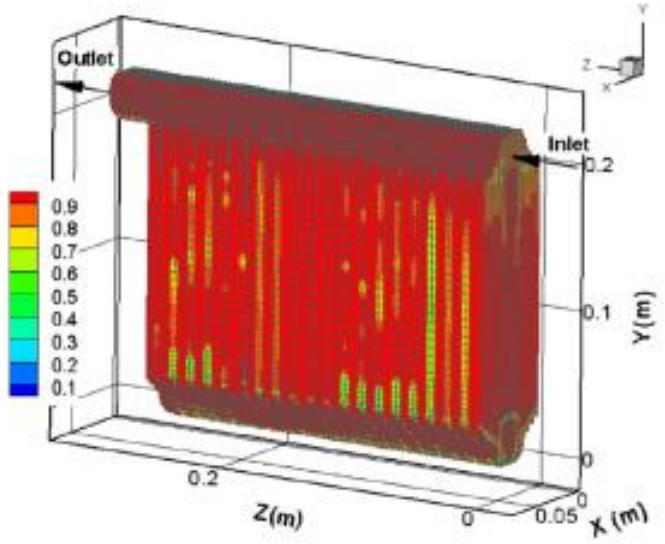

Figure 2-7: Void fraction prediction in the evaporator (Stevanovic and Hrnjak, 2017)

Computational Fluid Dynamics (CFD) studies could help improve the understanding of two-phase flow distribution by providing detailed information about the local pressures and velocities in headers; however, past work in this area is limited. Additionally, the models that have been developed either have not been specifically validated in distributors or do not accurately match experimental data. Future work is needed to advance this area of research so that it can be leveraged to help explain the factors affecting two-phase flow distribution.

CHAPTER 3

SINGLE-PHASE FLOW PRESSURE DROP IN THE HEADER

3.1 INTRODUCTION

This chapter presents the investigation of the pressure drop in headers of microchannel heat exchangers and the development of correlation for pressure loss coefficient for single-phase flow through round cylindrical headers of parallel MCHXs. The purpose to develop a correlation to evaluate pressure drops in a header is to predict the mass flow rate distribution among microchannel tubes. There are several mass flow rate distribution models available in the literature, such as Ren *et al.* (2013), and Tuo and Hrnjak (2013). In these models, the mass flow rate distribution is iteratively calculated by the pressure drop of the microchannel tube and that of the header. To the best of the author's knowledge, there is no prior work to predict the local loss coefficient accurately. Yin *et al.* (2002) measured pressure drop in headers and generated a correlation based on the assumption that the pressure loss coefficients are uniform. Although Yin's correlation provided a satisfactory prediction of the total pressure drop in headers compared to his experimental data, it is not certain that the correlation is fit for predicting the pressure drop of i^{th} section (Dp_i) in headers, i.e that the prediction will be satisfactory for headers of shorter or longer headers. Therefore, the predictability of Yin's correlation to the experimental data of the present study is uncertain and it will be investigated first. Figure 3-1 shows the deviation of pressure drop

of the inlet header and outlet header predicted by Yin's correlation to the data from the present study. It is shown that Yin's correlation does not predict well the pressure drop of i^{th} section (Dp_i) for both inlet and outlet headers. For the inlet header, the correlation over predicts all local pressure drops so the average is also over predicted. For the outlet header the deviation at the first two tubes is even higher than in the inlet header, but thanks to downstream pressure drops, the average value for total pressure drop gives reasonable predictions. As the number of tubes (header length) increases (as was in Yin's experiment) prediction for average pressure drop will be even more correct. Therefore, the non-uniformity of pressure loss coefficient in headers and the impacts of velocities through microchannel tubes and headers affect prediction for headers of various (especially shorter) sizes and will be reflected in the new correlation.

3.2 TEST FACILITY

The test system consists of a gas tank, a temperature pre-conditioner, and a header connected to 10 microchannel tubes. The temperature pre-conditioner is used to equalize the gas temperature with the room temperature. As shown in Figure 3-2, for the inlet header test, flow passes through m_0, and then enters the header. Part of the gas leaves the header through the first 4 microchannel tubes (MC tubes #1 to #4), with each mass flow rate measured, and the rest exits to the atmosphere through the header outlet. For the outlet header test, the gas goes through the first five microchannel tubes (MC tubes #1 to #5) with individual measurements. The mass flow rate transducer m_0 is used to measure the mass flow rate through MC tube #5.

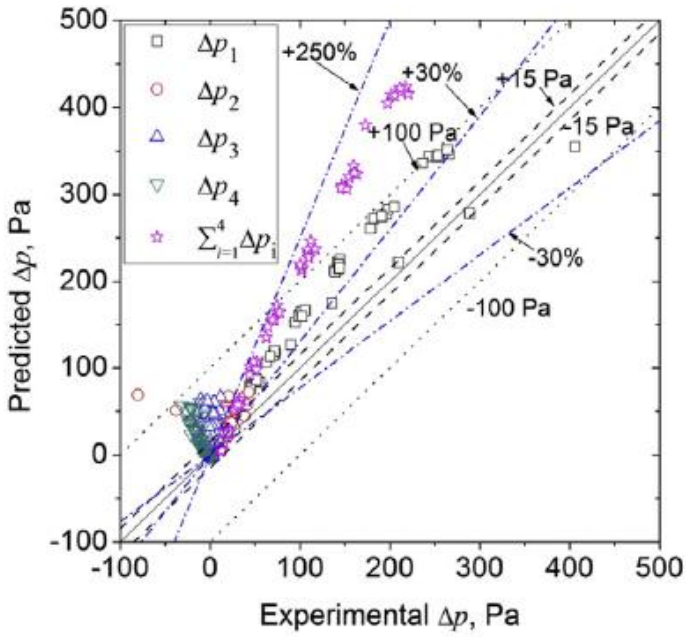

(a) Inlet header

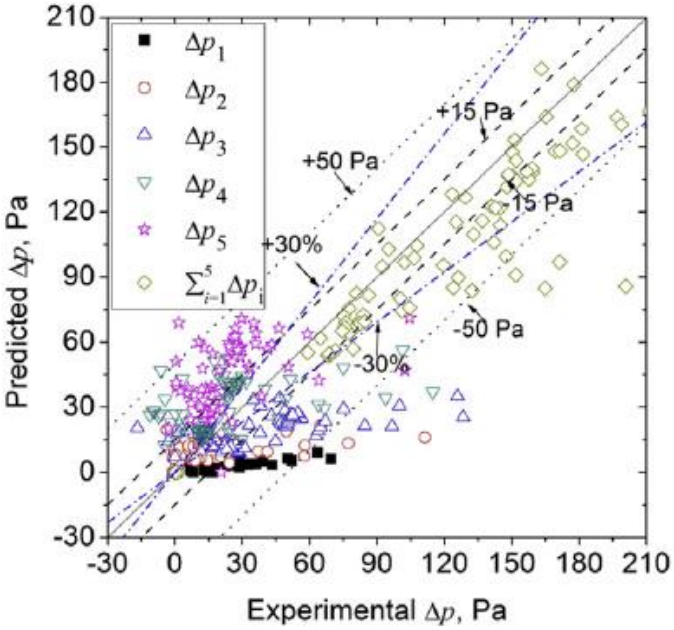

(b) Outlet header

Figure 3-1: Comparison of the experimental data of the present study with the predicted values obtained by Yin *et al.* (2002) correlation

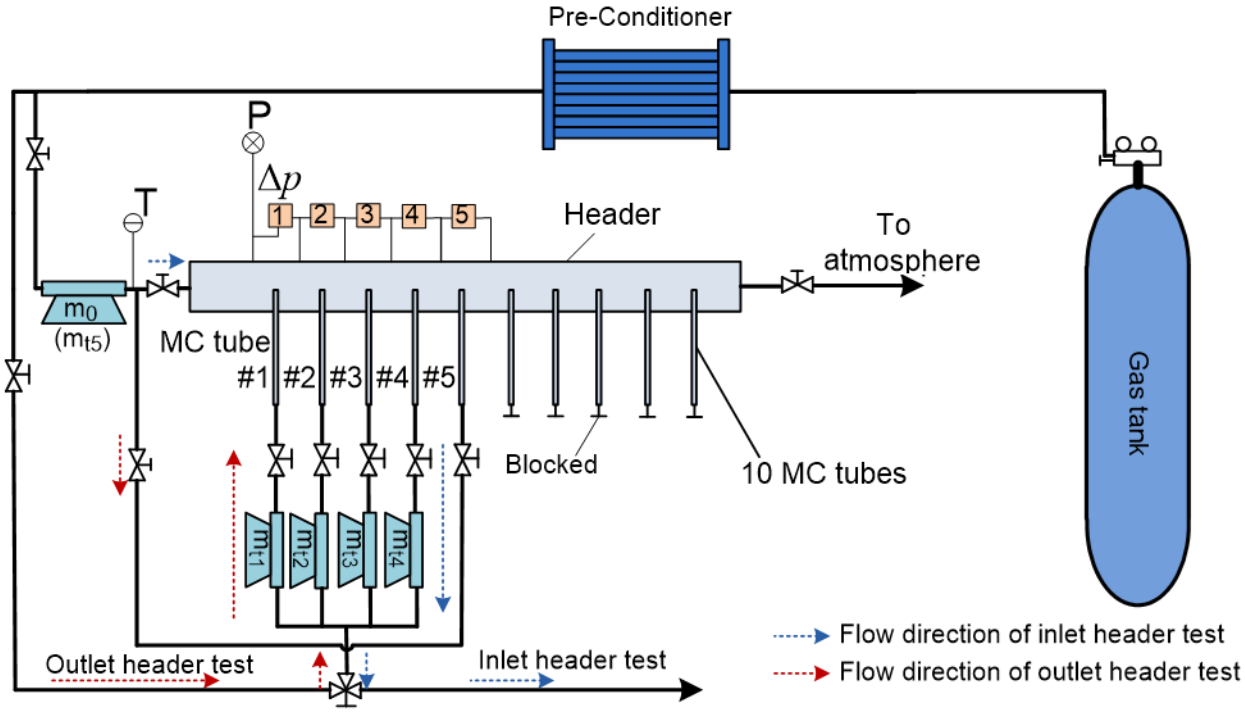

Figure 3-2: Test apparatus

The header consists of a transparent PVC tube and ten microchannel tubes. As shown in Figure 3-3, the tube spacing is 12.0 mm and the protrusion is 50%. The inner diameter of the PVC tube is 18.4 mm and the length is 200 mm. The microchannel tube has 23 ports with 1.5 mm in thickness and 17.9 mm in width. The length and width of each port are 0.84 mm and 0.64 mm, respectively.

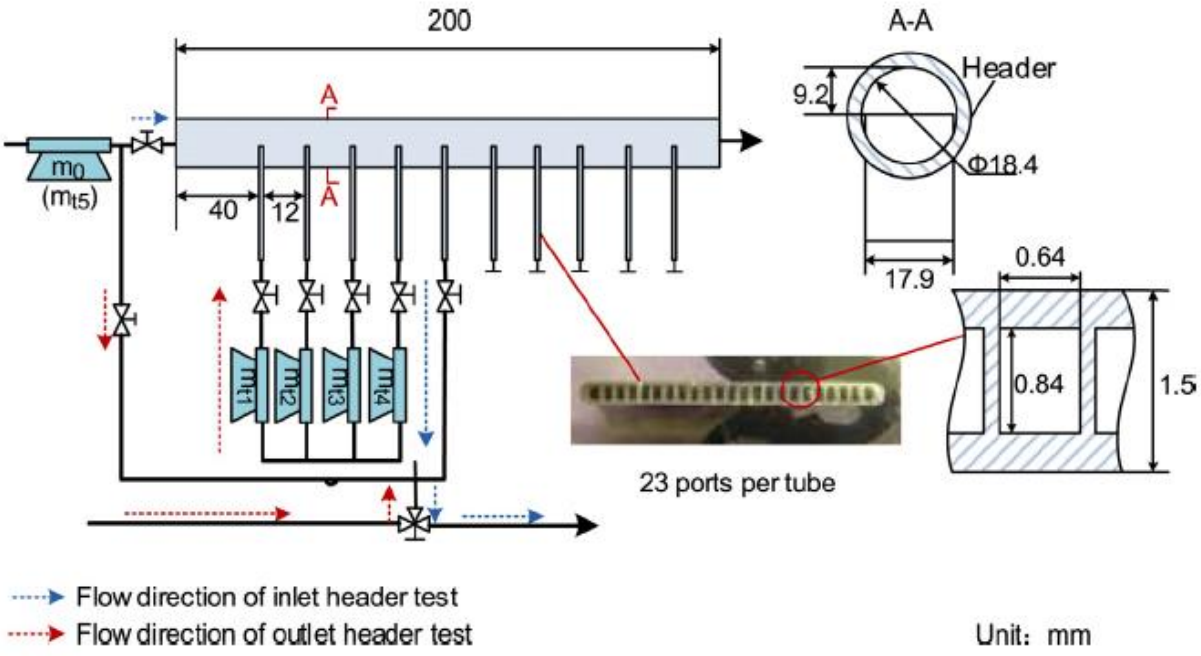

Figure 3-3: Configuration of the test section

The velocity through headers ranges from 1 m/s to 20 m/s while the velocity through microchannel tubes is in the range from 6 m/s to 30 m/s, which covers the most realistic working conditions in the residential and automotive air conditioning systems, according to the literature shown in Table 3-1.

In order to predict the mass flow rate distribution, the perfect location to place the pressure taps in the header is the surface of microchannel tube ends. However, directly placing the pressure taps at that surface may generate a great error because the working fluid may blow into the pressure taps resulting in much higher pressure than it would be. Therefore, as a compromise, the pressure taps are placed (10°) below the surface of the microchannel tube ends to avoid the flow directly blowing into the pressure taps, as shown in Figure 3-4. This figure shows the structure and location of pressure taps. A pressure tap comprises two sections. The first section is close to the inner

surface of the header with a diameter of 1.6 mm and a length of around 1.5 mm. The second section is close to the outer surface of the header with a diameter of 3.2 mm and a length of around 2 mm. The distance of l_i is 12 mm. The lengths of the connection tubes from the pressure taps to the transducer itself are larger than 500 mm, depending on the location of the transducer.

Table 3-1: Single-phase vapor velocities through header and microchannel tube in literature

Authors/Year	**AC type**	**HX type**	**Ref.**	**Vapor velocity through header [m s^{-1}]**	**Vapor velocity through MC tube [m s^{-1}]**
Park and Hrnjak, 2008	Residential	Condenser	R410A	3.5	2.2-8.8
Qi et al., 2010	Automotive	Evaporator	R134a	7.4-12.0	11.0-18.0
Peterson et al., 1998	Automotive	Gas Cooler	CO_2	3.9	6.0
Cho and Cho, 2007	Residential	Evaporator	R22	10.5-13.4	23-30
Kim and Bullard, 2001	Automotive	Evaporator	CO_2	1.6-5.0	5.5-14.7
Tuo et al., 2012	Automotive	Evaporator	R134a	8.7	6.1
Yin et al., 2001	N.A.	Gas Cooler	CO_2	5.2-14.4	4.3-12.4
Garcia-Cascales et al., 2010	Residential	Condenser	R410A	1.0-5.5	3.8-20.7
Zhao et al., 2012	Automotive	Evaporator	R1234yf	8.2-17.7	9.8-21.2

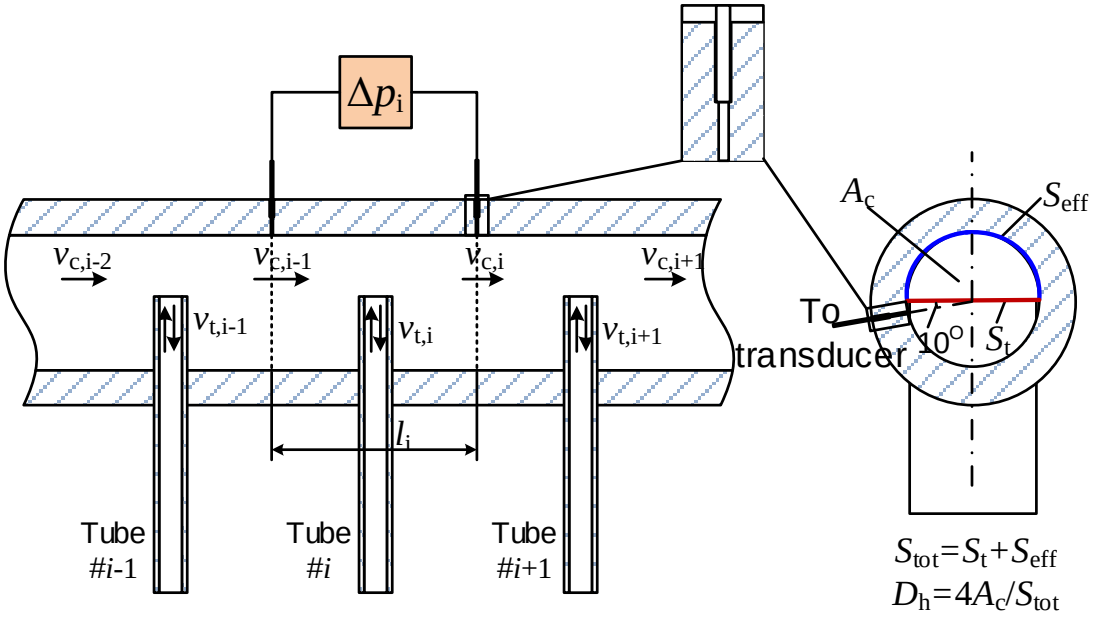

Figure 3-4: Schematic drawing of the header at i[th] section

3.3 DATA REDUCTION

The pressure drop at the i[th] section shown in Figure 3-4 consists of the diverging/converging loss pressure drop $\Delta p_{\zeta,\,i}$, acceleration pressure drop $\Delta p_{acc,\,i,}$ and frictional pressure drop $\Delta p_{f,\,i}$, as shown in Equation (3-1). In Equation (3-1), the acceleration pressure drop and friction pressure drop are computed by Equation (3-2) and Equation (3-3), respectively. Thus, the diverging/converging loss coefficient in the i[th] section is defined by the velocity at the i[th] section by Equation (3-4), as shown in Figure 3-4.

$$\Delta p_{\zeta,\,i} = \Delta p_i - \Delta p_{acc,\,i} - \Delta p_{f,\,i} \tag{3-1}$$

$$\Delta p_{acc,\,i} = \rho v_{c,i}^2 / 2 - \rho v_{c,i-1}^2 / 2 \tag{3-2}$$

$$\Delta p_{\mathrm{f,\,i}} = \lambda_{\mathrm{i\text{-}1}} \frac{l_i}{2D_{\mathrm{h}}} \frac{S_{\mathrm{eff}}}{S_{\mathrm{tot}}} \rho v_{\mathrm{c,i\text{-}1}}^2 / 2 + \lambda_{\mathrm{i}} \frac{l_i}{2D_{\mathrm{h}}} \frac{S_{\mathrm{eff}}}{S_{\mathrm{tot}}} \rho v_{\mathrm{c,i}}^2 / 2 \tag{3-3}$$

$$\zeta_{\mathrm{i}} \equiv \begin{cases} \dfrac{\Delta p_{\zeta,\,\mathrm{i}}}{\rho v_{\mathrm{c,i}}^2 / 2} & \text{Converging case} \\ \dfrac{\Delta p_{\zeta,\,\mathrm{i}}}{\rho v_{\mathrm{c,i\text{-}1}}^2 / 2} & \text{Diverging case} \end{cases} \tag{3-4}$$

$$v_{c,i} = \frac{m_i}{\rho A_c} \tag{3-5}$$

$$\lambda_i = \frac{0.3164}{\mathrm{Re}_i^{0.25}} \tag{3-6}$$

where ρ is the density; $v_{\mathrm{c,i\text{-}1}}$ and $v_{\mathrm{c,i}}$ are the average velocities of the flow through the header at sections i-1 and i, respectively, as Equation (3-5); $\lambda_{\mathrm{i\text{-}1}}$ and λ_{i} are the friction loss coefficients at sections i-1 and i, respectively, as Equation (3-6); l_i is the header length of i^{th} section; D_{h} is the hydraulic diameter of the header; S_{eff} and S_{tot} are the effective friction perimeter and total perimeter of the header, respectively. A_c is the free flow area in the header.

The instrumentation used in the test and their accuracies are listed in Table 3-2. The accuracies of the instrumentations specified in Table 3-2 are the nominal accuracy given by the manufacturer. The theoretical uncertainties of deduced parameters are estimated based on the analysis of error propagation reported by Moffat (1998). Based on the uncertainties of test transducers shown in Table 3-2, the uncertainties of calculated parameters are determined, and the maximum uncertainty of the deduced parameter diverging/converging loss pressure drop $\Delta p_{\zeta,i}$ is ±3.7 Pa. The mass balance check for the mass flow rate meters has been conducted. The maximum

difference between m_0 and the sum of m_1 to m_4 is within 0.05 g s^{-1}, and this error is also included in the uncertainty calculation. The compromise on placing the pressure taps may generate some extra errors. Thanks to the protrusions of the microchannel tube, this error is negligible because the secondary flow in the space between the protrusions is much weaker than the main flow (flow in the free flow area in A_c as shown in Figure 3-4) and the pressure taps are placed only around 0.5 mm below the surface of microchannel tube ends. The average error for the pressure loss coefficient is within 10%. The maximum uncertainty of deduced parameter pressure loss coefficient occurs when the loss pressure drop $\Delta p_{\zeta,i}$ is very low, and the value is very high (over 100%). Fortunately, when $\Delta p_{\zeta,i}$ approaches 0, the absolute value of diverging/converging pressure drop $\Delta p_{\zeta,i}$ is meaningless, having no impact on the mass flow rate distribution prediction and no impact on the prediction of total pressure drop. In order to show the uncertainty of tested values and deduced values, the error bars are added to the figures.

Table 3-2: The uncertainty of test instruments in single-phase experiment

Instrument	Measurement	Range	Unit	Uncertainty
Setra 206	Pressure (P)	0-136	kPa	± 0.13% FS
T-type Copper Constantan	Temperature (T)	0-220	^oC	± 0.5 ^oC
Micromotion DS12	m_0 and m_{t1}	0-37.5	g/s	± 0.15% flow rate
Micromotion DS6	m_{t2}, m_{t3} and m_{t4}	0-19	g/s	± 0.15% flow rate
Rosemount 1151	Δp_1~Δp_5	0-1270	Pa	±0.25% FS

3.4 RESULTS AND DISCUSSION

3.4.1 INLET HEADER

Figure 3-5 shows the pressure drop of the inlet header at different locations. The CFD results shown in Figure 3-5 (a) are obtained by solving coupled steady-state incompressible Navier-Stokes equations using SIMPLE scheme and a standard k-ε model for turbulence, and the boundary condition is the same as that of the experiment. The results show that Δp_1 is much larger than Δp_2 to Δp_4 (see Figure 3-5b). The reason is that a big contraction only occurs when flow cross over the protrusion of microchannel tube #1 as illustrated by a CFD simulation shown in Figure 3-5 (a). As the flow passes over microchannel tube #1, the flow area decreases by 50%, and thus pressure decreases sharply due to the flow acceleration and some extra unrecoverable pressure losses accompanied by the combined effect of contraction and diverging flow to microchannel tube #1. When the flow passes microchannel tube #1, the fluid will mostly flow through the free flow area A_c as shown in Figure 3-4, because the ratio of tube spacing and hydraulic diameter is too small (close to 1) to allow flow expansion, and thus there is insignificant contraction effect when flow passes over other microchannel tubes. Figure 3-5 also shows that the pressure drop of the i^{th} section decreases along the header. The possible reason is explained as follows. Due to the contraction when the flow passes over microchannel tube #1, the velocity in the free flow area A_c becomes non-uniform. The velocity close to the header inner surface S_{eff} as shown in Figure 3-4 is larger than that close to the surface S_t (see Figure 3-5(a)). As a result, it will generate more unrecoverable pressure loss when flow diverges to the microchannel tube. Further downstream the velocity of the fluid through the header will gradually become more uniform and diverging pressure loss will become smaller. In addition, as the fluid goes further, the mass is removed from

the main flow in the header resulting in a lower average velocity in the header. Therefore, the pressure drop gradually decreases as the flow goes further.

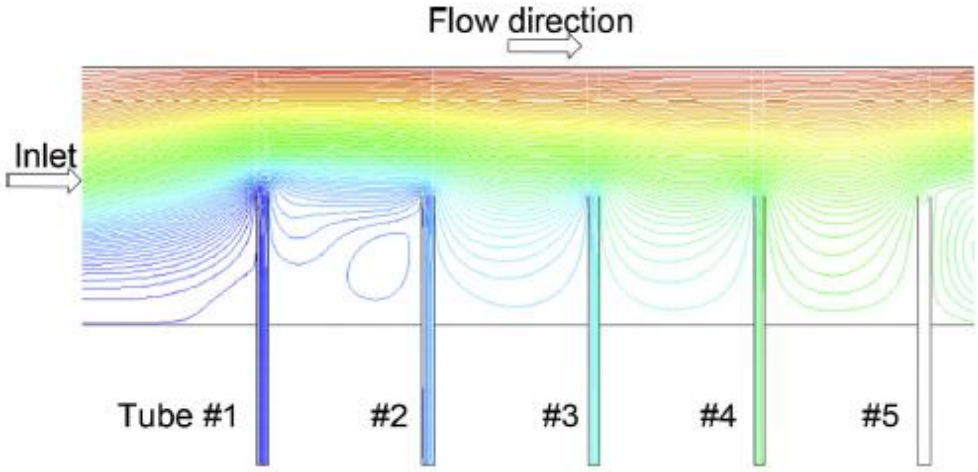

(a) Typical streamline in inlet header

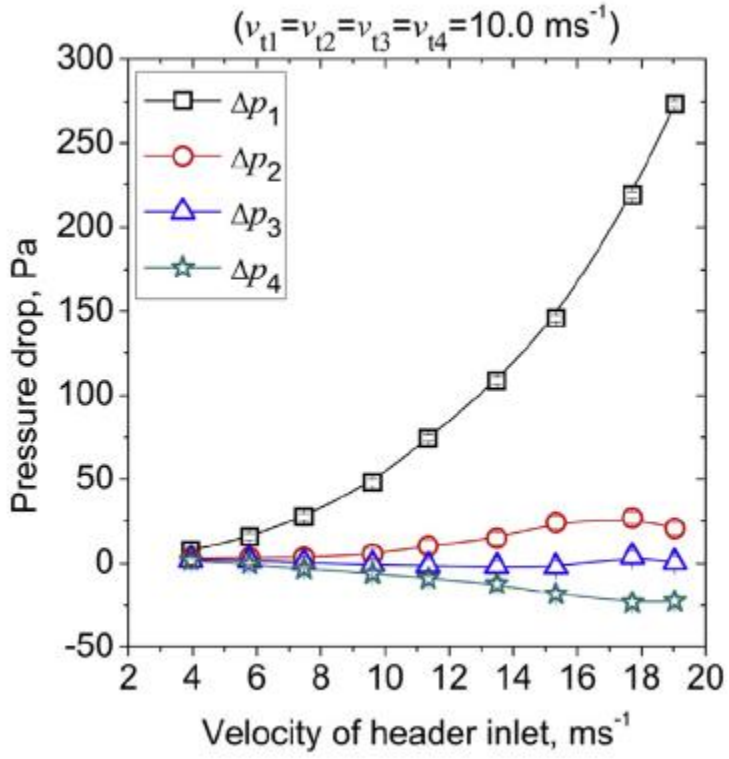

(b) Pressure drop along the inlet header

Figure 3-5: Effect of location in inlet header on pressure drop

Figure 3-6 shows the effect of velocity through the ith microchannel tube on Δp_i. Figure 3-6(a) shows that under a certain flow velocity through the header (v_{c0}), the velocity through the microchannel tube (v_{t1}) decreases the pressure drop (Δp_1) when flows pass over microchannel tube #1. This is because the contraction makes a very strong secondary flow between the microchannel tubes #1 and #2, and as the velocity through microchannel tube #1 increases, the suction force from the microchannel tube becomes stronger and pulls some of the fluid into the volume between the microchannel tubes #1 and #2 and below the line St shown in Figure 3-4. So, the flow through the microchannel tube affects the formation of secondary flow in the space behind. Figures 3-6(b) to 3-5(d) show that Δpi decreases as the velocity through the ith microchannel tube increases. t is due to the increase of deceleration pressure drop. Moreover, the effect becomes smaller as the velocity through the microchannel tube increases, which means the diverging pressure loss increases as the mass flow rate through the microchannel tube increases. The reason is that at higher velocity through the microchannel tube the expansion loss is larger.

Figure 3-7 shows the effect of the velocity through upstream microchannel tubes on Δpi. It shows that the velocity through microchannel tube #1 (v_{t1}) has a significant impact on Δp_2, but has no impact on Δp_3, as shown in Figures 3-7(a) and 3-7(b). Further, when v_{t1} is 5.8 m s^{-1}, Δp_2 will decrease as the velocity through the header increases, but when v_{t1} is larger than 7.7 m s^{-1}, Δp_2 will increase as the velocity through the header increases. This is because v_{t1} has a great impact on the flow situation between microchannel tubes #1 and #2 but has no impact on the following flow development. When v_{t1} is low, the contraction effect is dominant, and an eddy zone is formed between microchannel tubes #1 and #2, resulting in a local low-pressure region in that area and a negative Δp_2, as shown in Figure 3-5. When v_{t1} increases, the eddy zone between microchannel tubes #1 and #2 will be affected because the pressure behind the microchannel tube #1 will increase

and reduce the pressure drop. The results of the experiment also indicate that the velocities through microchannel tubes #2 and #3 have no impact on Δp_3 and Δp_4, respectively, as shown in Figures 3-7(c) and 3-7(d). This is because the velocity profile is more developed and so the effect of diverging flow through the tube on the eddy zone behind the tube has almost no impact on the main flow through the header.

Figure 3-8 shows the effect of the velocity through downstream microchannel tubes $v_{t,\, i+1}$ on Δp_i. It shows that the velocity through downstream microchannel tubes has no impact on the pressure drop. This is because the flow separation and eddy zone are formed after the flow diverging, and thus the change of velocity through the downstream microchannel tubes has no impact on the upstream flow inside the header.

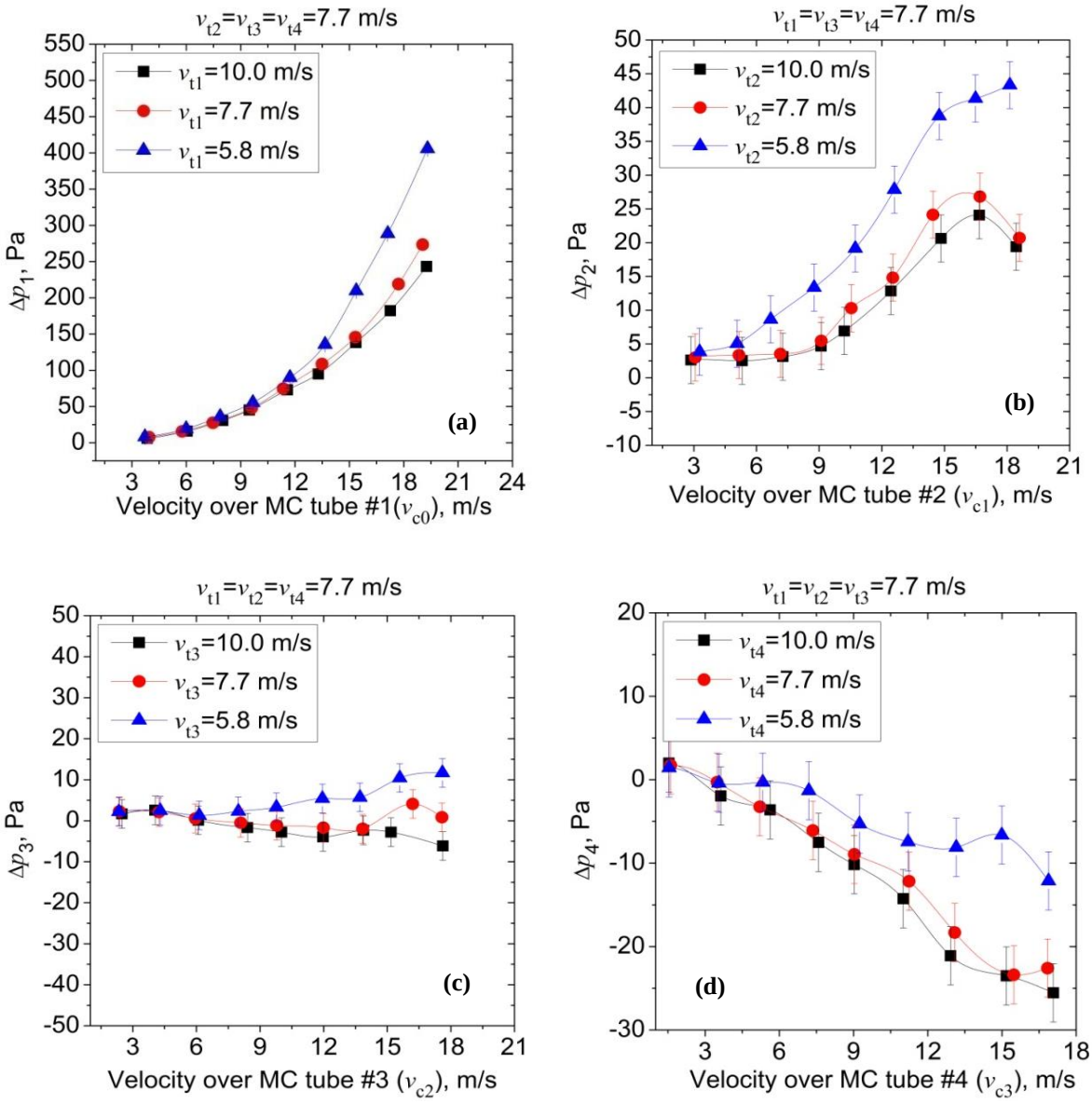

Figure 3-6: Effect of velocity in the i[th] microchannel tube on Δp_i

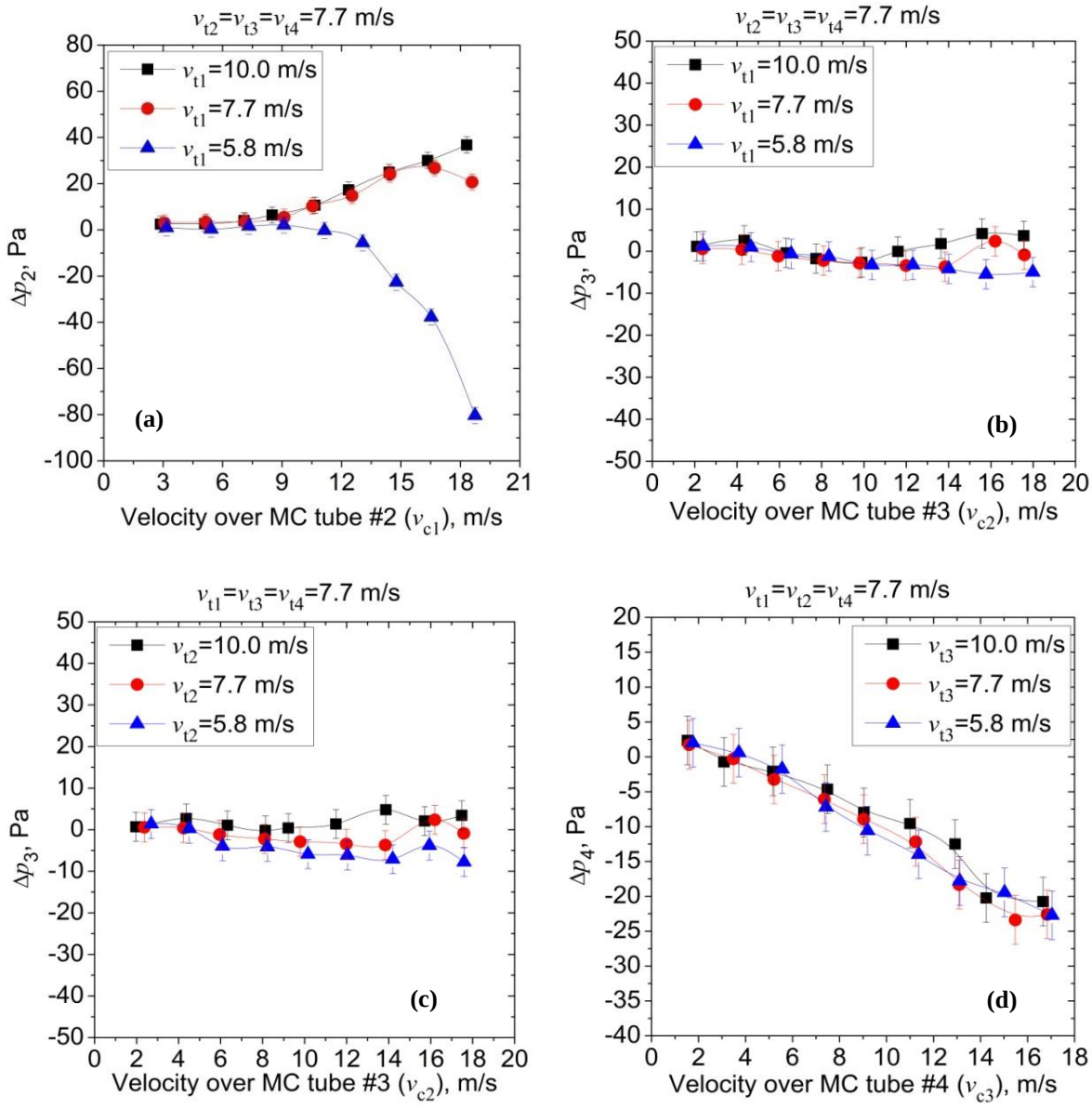

Figure 3-7: Effect of velocity through upstream microchannel tubes on Δp_i

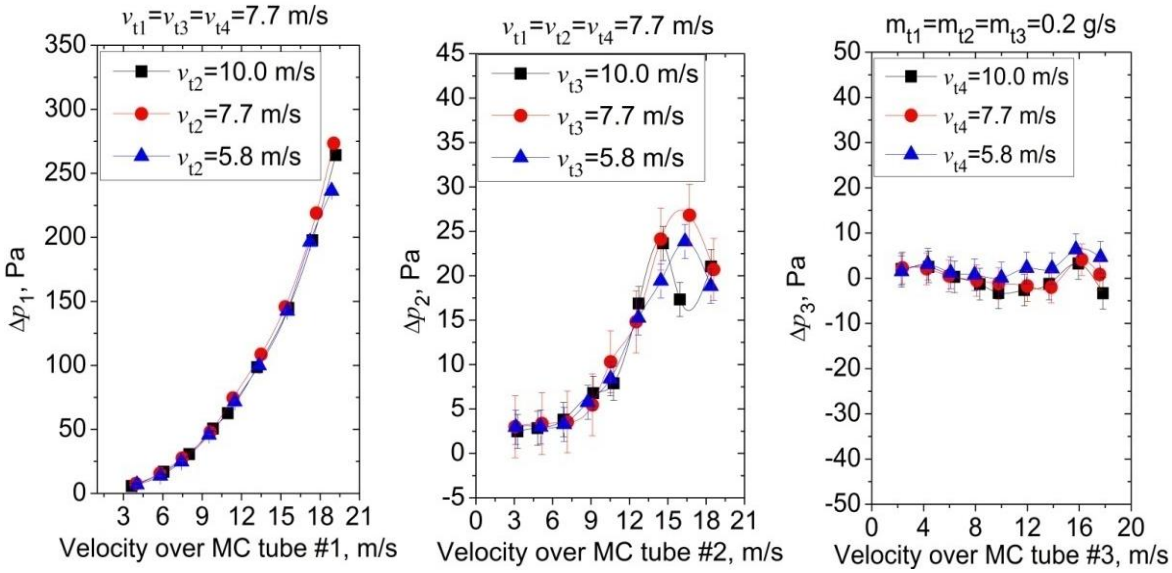

Figure 3-8: Effect of velocity through downstream microchannel tubes on Δp_i

Based on the experimental results, it can be said that:

(i) The pressure drop of the i^{th} section (Δp_i) is a function of the velocity through the i^{th} microchannel tube ($v_{t,i}$) and the velocity through the header before flow diverging at the i^{th} section ($v_{c,i-1}$);

(ii) The velocity through the $(i-1)^{th}$ microchannel tube ($v_{t,i-1}$) has no impact on the pressure drop of i^{th} section (Δp_i), except $v_{t,1}$ which has a great impact on Δp_2 due to the contraction;

(iii) The velocity through the $(i+1)^{th}$ microchannel tube ($v_{t,i+1}$) has no impact on the pressure drop of i^{th} section (Δp_i);

(iv) The location has some impact on the pressure drop in headers.

As a result, a correlation that is used to predict the pressure drop of an inlet header needs to include the parameters of the velocity through the i^{th} microchannel tube ($v_{t,i}$), the velocity through the

header at i^{th} section ($v_{c,i-1}$) and location. Moreover, the impact of $v_{t,1}$ on ζ_2, also needs to be addressed.

Figure 3-9 shows the relations between the pressure loss coefficient of the i^{th} section (ζ_i) as defined in Equation 3-4 and the parameters of the i^{th} microchannel tube ($v_{t,i}$), the velocity through the header before flow diverging at the i^{th} section ($v_{c,i-1}$) and locations, and the relations between ζ_2 and $v_{t,1}$. It shows that:

(i) if i is equal or larger than 3, ζ_i is a linear function of $v_{t,i}/v_{c,i-1}$.

(ii) at a specified value of $v_{t,i}/v_{c,i-1}$, ζ_i decreases as the value of $v_{t,i}$ increases;

(iii) when $v_{t,2}/v_{c,1}$ is smaller than 1, ζ_2 will sharply decrease as $v_{t,1}$ decreases due to the effect of contraction.

(iv) $v_{t,1}/v_{c,0}$ is smaller than 1, ζ_1 will sharply increases as $v_{t,1}/v_{c,0}$.

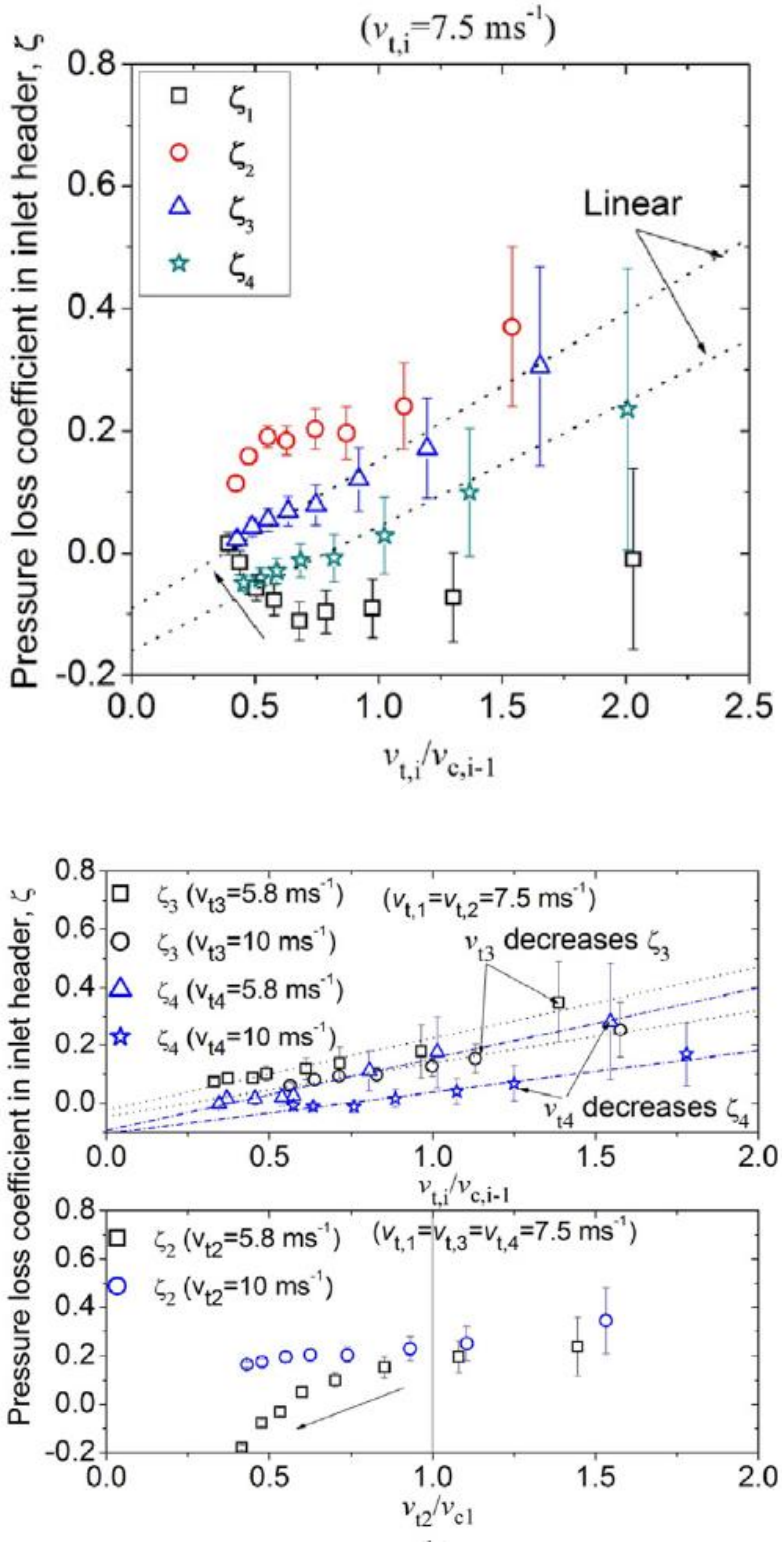

Figure 3-9: Pressure loss coefficients in inlet header as a function of $v_{t,i}/v_{c,i-1}$, $v_{t,i}$ and $v_{t,i-1}$

As a result, the correlation for ζ_i should describe the pressure loss coefficient of contraction and diverging flow separately for ζ_1 and ζ_2, while others ζ_i (i≥3) can be treated equally as a linear function of $v_{t,i}/v_{c,i-1}$ while adding the effect of $v_{t,i}$ and location. Based on that, the correlation for pressure loss coefficient in inlet header ζ_i is expressed as Equation 3-7. Using nonlinear fitting method, the values of a_1~a_{13} in Equation 3-7 are found to be: -14.582, 4.017, 0.111, -0.218, -24.230, 7.261, 0.242, -0.031, 0.269, 0.297, -0.044, 17.340, -1.715 and 0.165, respectively.

$$\zeta_i \equiv \frac{\Delta p}{\rho v_{c,i\text{-}1}^2/2} = \begin{cases} 0.75\exp\left(a_1 \dfrac{v_{t,i}}{v_{c,i\text{-}1}}\right) + a_2 \dfrac{v_{t,i}^2}{v_{c,i\text{-}1}^2} + a_3 \dfrac{v_{t,i}}{v_{c,i\text{-}1}} & \text{if } i = 1 \\ -0.4\exp\left(a_4 \dfrac{v_{t,i\text{-}1}}{v_{c,i\text{-}2}} + a_5\right) + a_6 \dfrac{v_{t,i}}{v_{c,i\text{-}1}} + a_7 v_{t,i} + a_8 & \text{if } i = 2 \\ a_9 \dfrac{v_{t,i}}{v_{c,i\text{-}1}} + a_{10} v_{t,i} + a_{11}\exp\left(a_{12}\cdot i\right) + a_{13} & \text{if } i \geq 3 \end{cases} \quad (3\text{-}7)$$

The correlation is validated by the experimental data, as shown in Figure 3-10. The predicted pressure drops of the i^{th} section of the inlet header (Δp_i) using the correlation agree with 98% of the experimental data (292 points) obtained in the present study within a deviation of ±15 Pa. In addition, the predicted total pressure drop ($\Sigma\Delta p_i$) agrees with 95% of experiment data within a deviation of ±15 Pa, which means the developed correlation has good accuracy to predict the total pressure drop of the header.

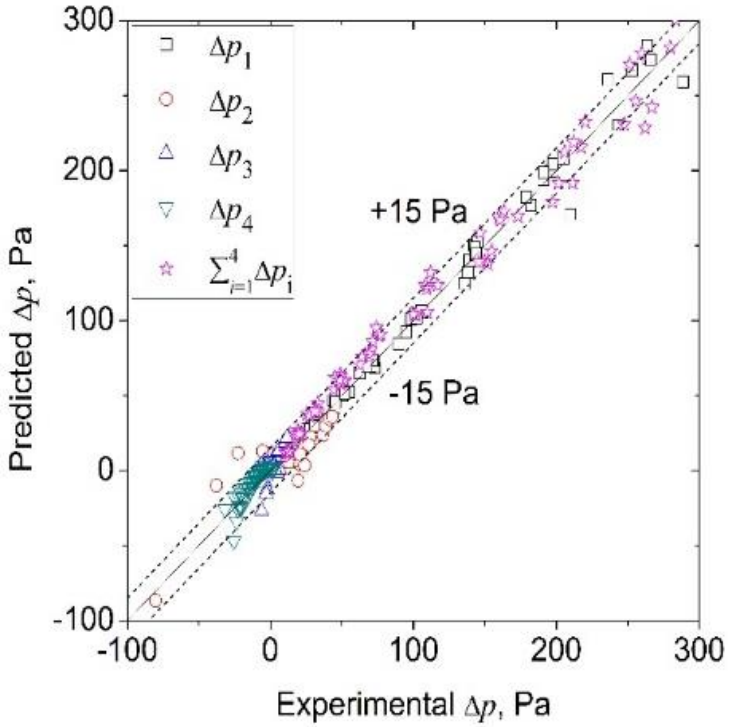

Figure 3-10: Accuracy of the generated correlation for inlet header

3.4.2 OUTLET HEADER

Figure 3-11 shows the pressure drop in the outlet header at different locations, indicating that Dp_3 is higher than the rest. In addition, with the increase of the velocities through all microchannel tubes, the pressure drop rises, but the trend of pressure drop distribution keeps the same. This is because the flow regimes and converging loss in the header change with the locations due to the one-by-one flow converging from the microchannel tubes, as shown in Figure 3-11 (a). The CFD results shown in Figure 3-11 (a) is obtained by solving coupled steady-state incompressible Navier-Stokes equations using SIMPLE scheme and a standard k-ε model for turbulence, and the boundary condition is the same as that of the experiment. At the beginning,

there is no flow in the microchannel tube, the fluid from microchannel tube #1 flows close to the inner surface of the header (S_{eff}) due to 90° flow turning and the main pressure loss is due to the secondary flow before the microchannel tube #1, the change of flow direction and subsequent expansion. As more fluid gets to the header, the contraction loss at the point of flow turning will increase due to the fluid occupying all open flow area (A_c) in the header. As a result, Dp_3 is much higher than Dp_2. However, as the flow goes further, the ratio of velocity through the microchannel tube and that through the header (v_{ti}/v_{ci}) will decrease due to the increase of velocity through the header, resulting in the decrease of contraction loss. That is why the Dp_4 and Dp_5 are smaller than Dp_3. Further, v_{ti}/v_{ci} will keep the same when the velocity through all microchannel tubes increases simultaneously, so the trend of pressure drop distribution along locations keeps the same. The trend will be more apparent with the introduction of the pressure loss coefficient. Figure 3-11 also indicates Dp_2 is lower than Dp_1 while Dp_5 is a little higher than Dp_4. The reason why Dp_2 is lower than Dp_1 is due to an extra eddy zone formed between the header end and the first microchannel tube resulting in a higher pressure loss. Dp_5 is a little higher than Dp_4 because the velocity in the header over the microchannel tube #5 is 25% larger than that over microchannel tube #4. The pressure drop is proportional to the square of velocity in the header. This means the Dp_5 is more than 50% higher than Dp_4 if the pressure loss coefficient keeps the same. Due to the obvious decrease in pressure loss coefficient, Dp_5 is just a little bit higher than Dp_4, less than 10%.

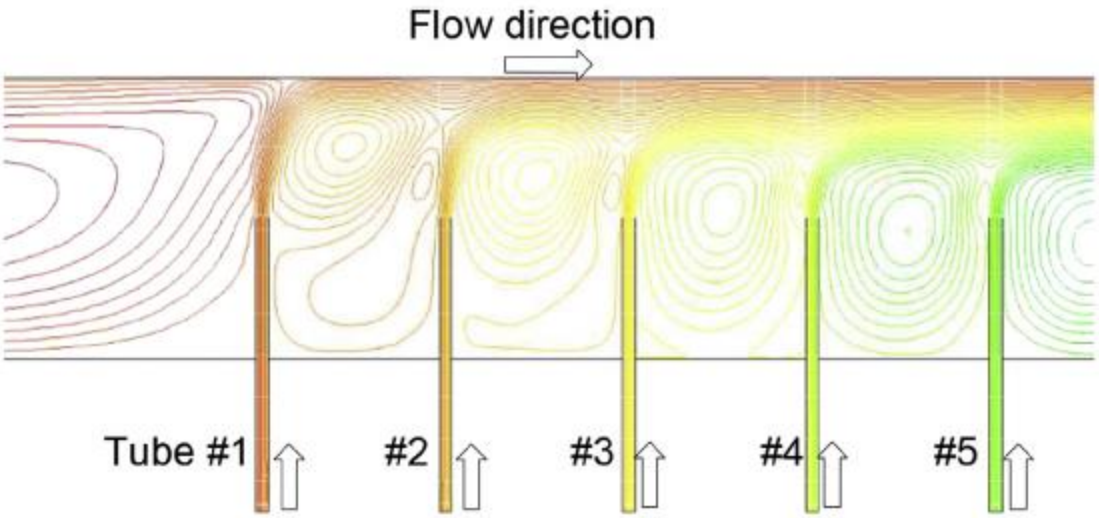

(a) Typical streamline in outlet header

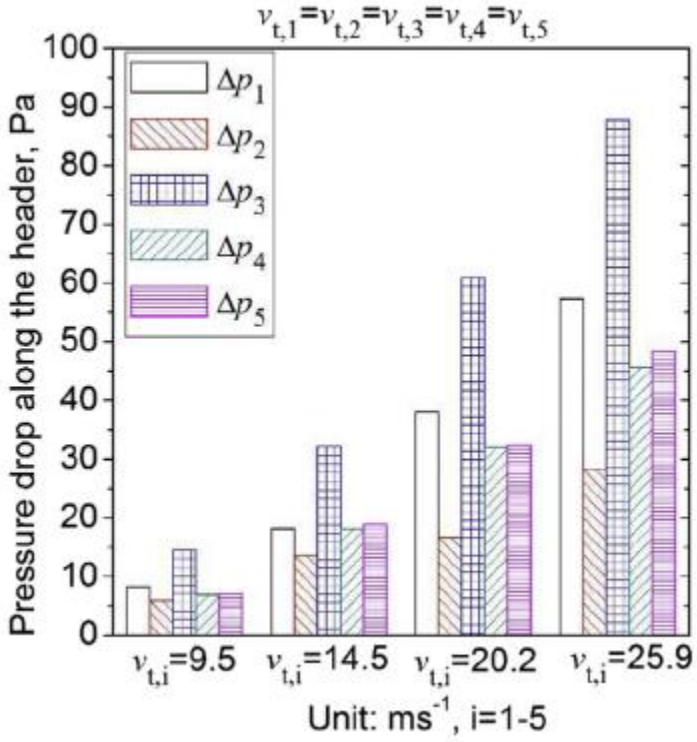

(b) Pressure drop along the outlet header

Figure 3-11: Effect of location in outlet header on pressure drop

Figure 3-12 shows the effect of velocity through the i^{th} microchannel tube on Δp_i of the outlet header. It shows that Δp_i increases as a quadratic function of velocity through the i^{th} microchannel tube. The reason might be that as the velocity through the microchannel tube (v_{ti}) increases, the secondary flow after converging, the shock of turbulent flow mixtures, the contraction at the point of the flow converging and its subsequent expansion becomes stronger, resulting in a higher unrecoverable pressure loss. Moreover, as the velocity through the microchannel tube increases, the acceleration pressure drop due to flow converging will increase too.

Figure 3-12 shows that Dp_i is also affected by the velocity through the neighboring microchannel tubes. Unlike Dp_1, Dp_i increases as the velocity through the neighboring microchannel tubes decreases. Take Dp_2 for an example, when v_{t1} and v_{t3} to v_{t5} increase from 13 m s^{-1} to 19 m s^{-1}, the Dp_2 decreases under the same v_{t2}. This is because the flow converging from neighboring microchannel tube is not fully developed in headers due to the small ratio of tube space and hydraulic diameter of the header (close to 1).

Figure 3-13 shows the effect of velocity through upstream microchannel tubes on Δp_i of the outlet header. It shows that Δp_i of outlet header decreases as the velocities through $(i-1)^{th}$ and $(i-2)^{th}$ microchannel tubes increase. The reason is that as the velocity in the upstream microchannel tube increases, v_{ci} increases, and consequently acceleration pressure drop decreases. In addition, this results in decreasing of $v_{t,i}/v_{c,i}$, resulting in the decrease of the converging loss coefficient of the current section (ζ_i). The expansion after the flow converging in the upstream section affects the flow converging in the current section because the ratio of tube space and hydraulic diameter of the header is too small to allow the flow to fully expand, resulting in the pressure increase during the flow expansion. The larger velocity through upstream microchannel tubes, the stronger effect

of flow expansion. For that reason, in some cases, Dp_i is even negative, as shown in Figure 3-13 (c).

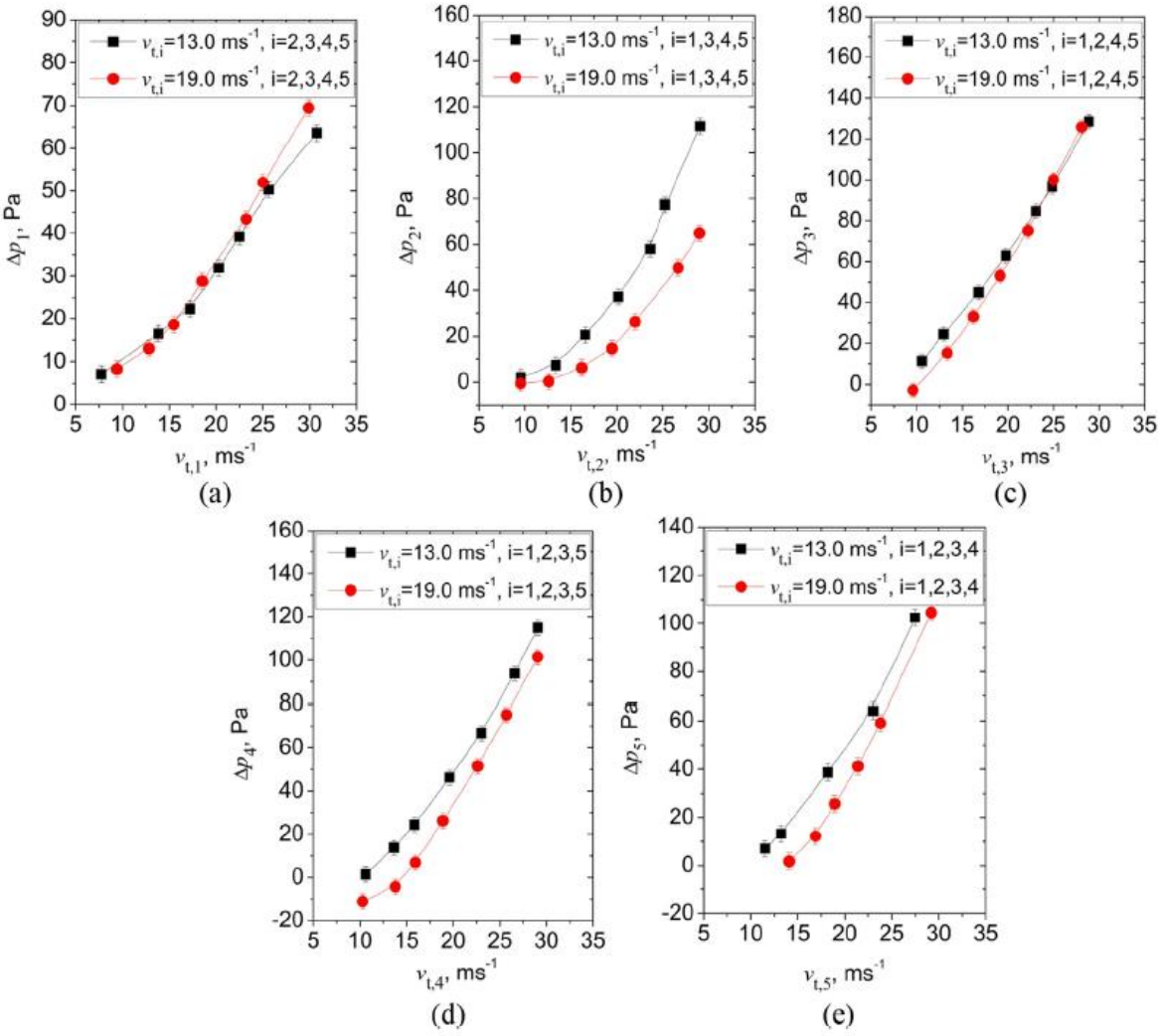

Figure 3-12: Effect of velocity through the i^{th} microchannel tube on Δp_i in the outlet header

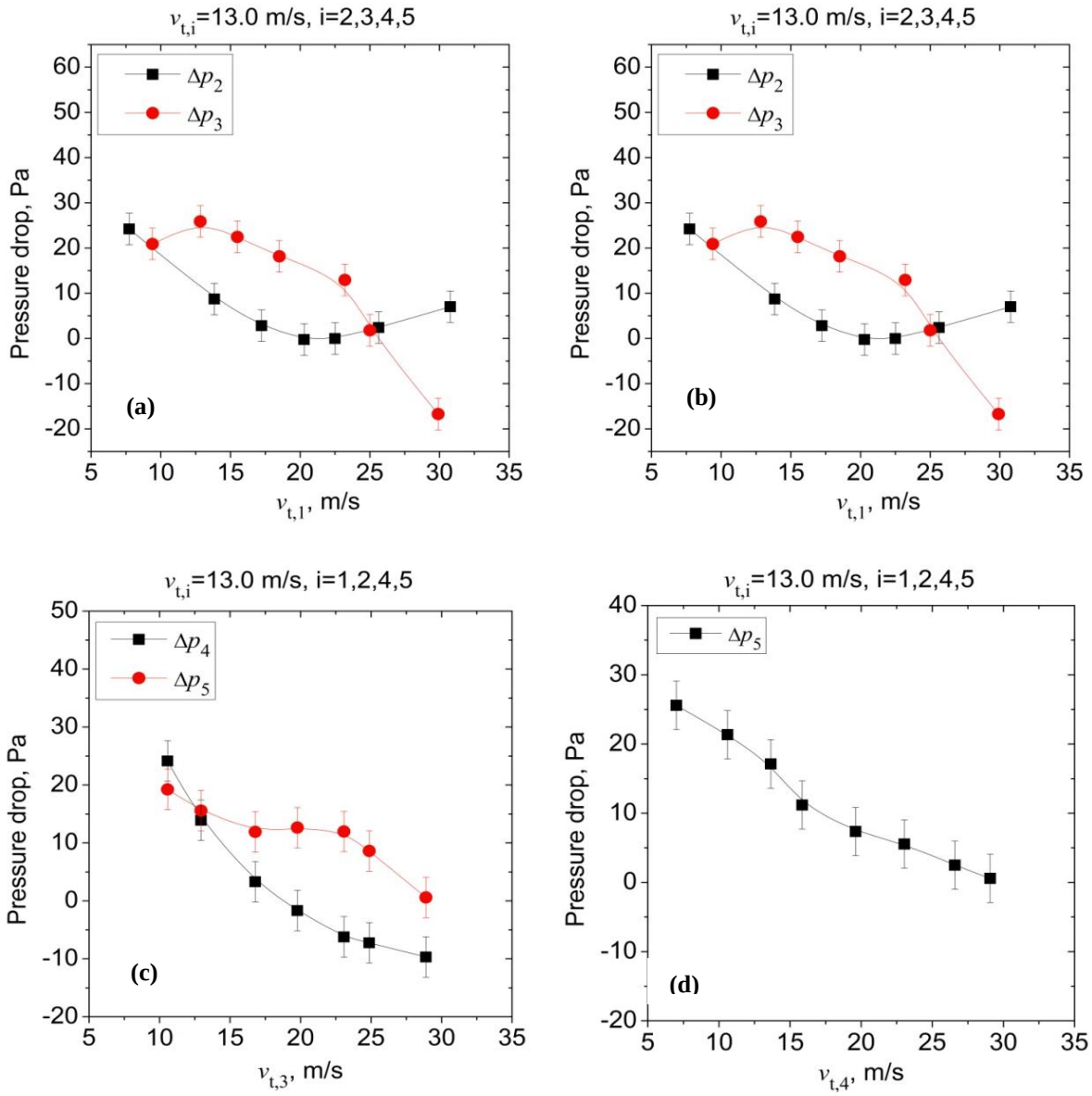

Figure 3-13: Effect of velocity through the upstream microchannel tubes on Δp_i in the outlet header

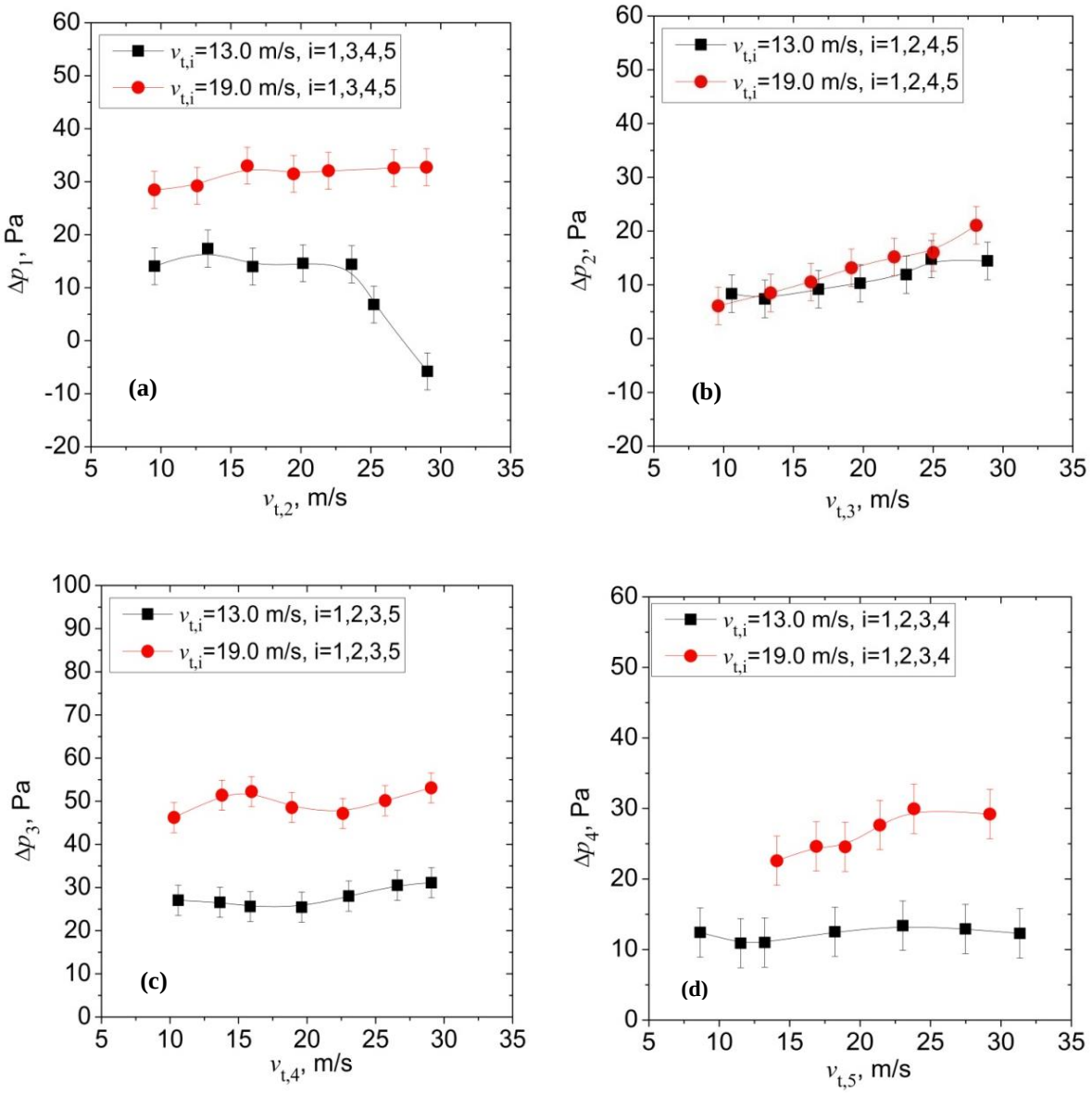

Figure 3-14: Effect of velocity through the downstream microchannel tube on Δp_i in the outlet header

Figure 3-14 shows the effect of velocity through the downstream microchannel tube on Δp_i in the outlet header. It shows that like the inlet header case, the velocity through the $(i+1)^{th}$ microchannel tube has no impact on Δp_i of the outlet header except the velocity through microchannel tube #2. This is because the eddy zone, flow contraction, and its subsequent expansion occur after the flow convergence, and thus the changes of velocity through the $(i+1)^{th}$ microchannel tube have no impact on the flow regimes of i^{th} section inside the header. As shown in Figure 3-14(a), the only different case is at high velocity through tube #2 ($v_{t,2}$) and low velocity through tube #1, or through the header ($v_{c,1}$). The velocity through the $(i+1)^{th}$ microchannel tube is so large that the flow through it almost blocks the flow through the header.

Based on the experimental results, it can be said that:

(i) The pressure drop of the i^{th} section (Δp_i) is a function of the velocity through the i^{th} microchannel tube ($v_{t,i}$) and the velocity through the header after flow converging at the i^{th} section ($v_{c,i}$);

(ii) The velocities through the $(i-1)^{th}$ and $(i-2)^{th}$ microchannel tubes ($v_{t,i-1}$ and $v_{t,i-2}$) have a great impact on the pressure drop of i^{th} section (Δp_i);

(iii) The velocity through the $(i+1)^{th}$ microchannel tube ($v_{t,i+1}$) has no impact on the pressure drop of i^{th} section (Δp_i);

(iv) The location also has some impact on the pressure drop in the headers.

As a result, a correlation that is used to predict the pressure drop of an outlet header needs to include the parameters of the velocity through the i^{th} microchannel tube ($v_{t,i}$), the velocity through the $(i-1)^{th}$ microchannel tube ($v_{t,i-1}$), the velocity through the $(i-2)^{th}$ microchannel tube ($v_{t,i-2}$) and the velocity through header at i^{th} section ($v_{c,i-1}$).

Figure 3-15 shows the relations between the pressure loss coefficient of i^{th} section (ζ_i) as defined in Equation 3-4 and the parameters of the velocity through the i^{th} microchannel tube ($v_{t,i}$), the velocity through the $(i\text{-}1)^{th}$ microchannel tube ($v_{t,i-1}$), the velocity through the $(i\text{-}2)^{th}$ microchannel tube ($v_{t,i-2}$) and the velocity through the header after flow converging at i^{th} section (v_c). It shows that:

(i) ζ_i is a quadratic function of $v_{t,i}/v_{c,i}$,

(ii) when i is equal to or larger than 3, ζ_i follows the same trend with $v_{t,i}/v_{c,i}$;

(iii) ζ_i decreases as the values of $v_{t,i-1}/v_{c,i}$ and $v_{t,i-2}/v_{c,i}$ increase.

As a result, the correlation for ζ_i has to be based on the fact that ζ_i is a quadratic function of $v_{t,i}/v_{c,i}$, and also $v_{t,i-1}/v_{c,i}$, and $v_{t,i-2}/v_{c,i}$ and location have some effect. Based on that, the formulation of ζ_i is expressed as Equation 3-8, and by using nonlinear fitting method, the values of a_1~a_9 in Equation 4.6 are from our data determined to be: 0.048, -0.888, -1.273, 3.352, 0.059, -0.221, -0.276, -0.112, 0.252 respectively.

$$\zeta_i \equiv \frac{\Delta p}{\rho v_{c,i}^2/2} = \begin{cases} 0.125\dfrac{v_{t,i}^2}{v_{c,i}^2} & \text{if } i=1 \\ \dfrac{v_{t,i}v_{t,i-1}}{v_{c,i}^2}\cdot\left(a_1\dfrac{v_{t,i}^2}{v_{c,i}^2}+a_2\dfrac{v_{t,i}}{v_{c,i}}+a_3\ln\dfrac{v_{t,i-1}}{v_{t,i}}+a_4\right) & \text{if } i=2 \\ \dfrac{v_{t,i-1}v_{t,i-2}}{v_{c,i}^2}\cdot\left(a_5\dfrac{v_{t,i}^2}{v_{c,i}^2}+a_6\dfrac{v_{t,i}}{v_{c,i}}+a_7\ln\dfrac{v_{t,i-1}}{v_{t,i}}+a_8\ln\dfrac{v_{t,i-2}}{v_{t,i}}+a_9\right) & \text{if } i\geq 3 \end{cases} \quad (3\text{-}8)$$

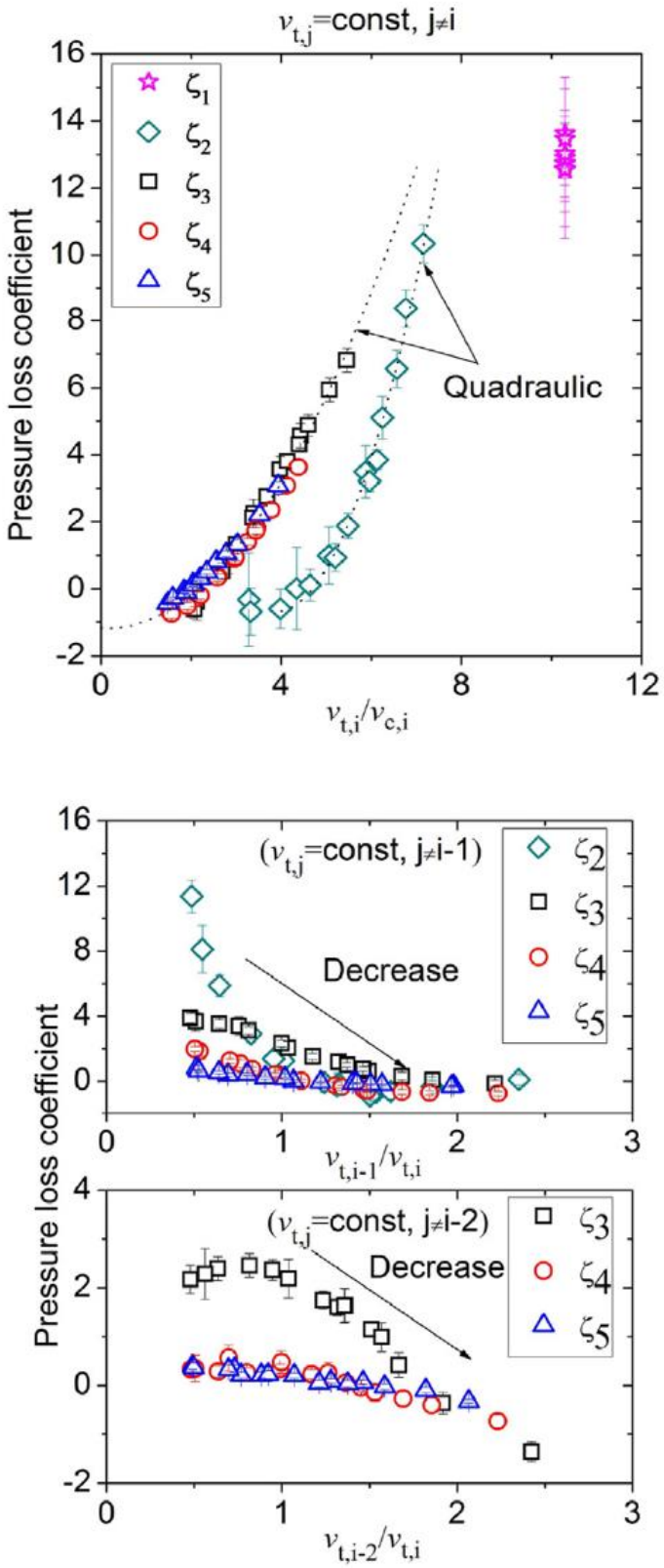

Figure 3-15: Pressure loss coefficient in outlet header as a function of $v_{t,i}/v_{c,i}$, $v_{t,i-1}/v_{t,i}$ and $v_{t,i-2}/v_{t,i}$

The correlation is validated by the experimental data. The correlation well predicts the pressure drop along the outlet headers and the predicted pressure drops of outlet header using the correlation agree with 98% of the experimental data (393 data points) obtained in the present study within a deviation of ±15 Pa as shown in Figure 3-16 In addition, the predicted total pressure drop ($\Sigma\Delta p_i$) agrees with 90% of experiment data within a deviation of ±15 Pa.

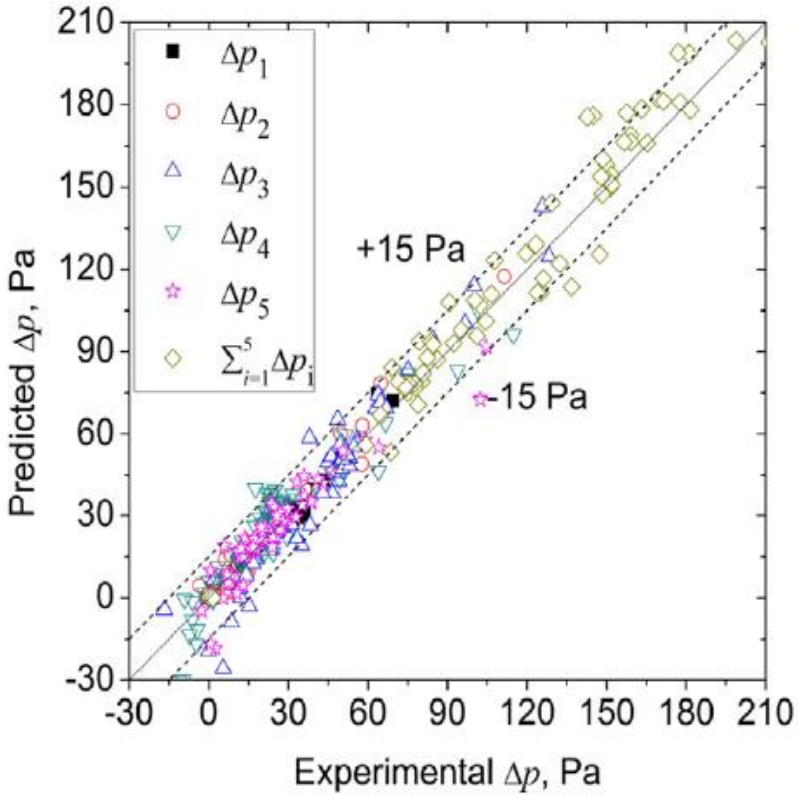

Figure 3-16: Accuracy of the generated correlation for outlet header

3.5 SUMMARY AND CONCLUSION

This chapter presents the investigation of pressure drop in the headers of microchannel heat exchangers in single-phase flow. The non-uniformity of pressure loss coefficient in the headers is observed and the impact of velocities through microchannel tubes is studied. Correlations based on experimental measurements are developed which are within ±15Pa accuracy for both inlet and outlet headers. The correlations developed in the present study were obtained from statistical analysis of the present data and thus they are valid only for the range of geometry and operating conditions of the experiments.

CHAPTER 4

SINGLE-PHASE FLOW DISTRIBUTION IN MCHXS

4.1 INTRODUCTION

This chapter presents numerical investigation of single-phase flow distribution in microchannel heat exchangers. For single-phase flow, there are many numerical simulations, for which the majority of the CFD was done in commercial software Fluent (Zhang and Li, 2003; Wen and Li, 2004; Muhana and Novog, 2008). Huang *et al.* (2014) simulated R134a vapor in the inlet header of an automotive microchannel condenser and integrated the CFD model with a 1-D ε-NTU based condenser model. Good agreement on heating capacity with their experimental data was achieved.

Despite the effectiveness and accuracy of 3-D CFD simulations, due to the complexity and the effort needed for that, 1-D finite volume models are desired, if possible. As a result, four distribution models are developed based on the principle of equal total pressure drop for all flow paths. Three models find the pressure profile in the headers, and the mass flow rate distribution in the microchannel heat exchanger, by 1-D mass and momentum conservation equations. Their mass flow rate predictions are then compared to the distribution generated by the hydraulic-CFD model, in which the pressure drop in the headers is calculated by 3-D CFD modeling of the headers.

The geometry of the two condensers was measured and summarized in Table 4-1.

Table 4-1: Microchannel heat exchanger geometry used in models

Parameter	Value
Number of passes	1
Number of MC tubes	36
Number of ports per MC tube	10
Width w/ headers [mm]	355
Width w/o headers [mm]	330
Microchannel tube depth [mm]	17.8
Microchannel tube thickness [mm]	1.8
Microchannel tube pitch [mm]	9.9
Microchannel tube port [mm]	1.3×1.53
Fin thickness [mm]	0.1
Fin pitch [mm]	1.64
Fin length [mm]	8.1
Louver pitch [mm]	0.9
Louver length [mm]	7.3
Louver angle [-]	26
Header shape	Round
Header equivalent diameter [mm]	19.3

4.2 HYDRAULIC-CFD LINKED MODEL

The single-phase pressure drop of MCHX could be broken down into two parts: pressure drop in microchannel tubes and that in headers. The single-phase pressure drops in the microchannel tubes are well studied (Graham and Dunn, 1995; Heun and Dunn, 1995; Yin *et al.*, 2001, etc.; Hrnjak and Tu, 2007), and the results showed that the correlation of Churchill (1977) has a good prediction for the laminar and turbulent flow regimes in the microchannel tubes.

Therefore, a model is developed in which to predict refrigerant distribution among parallel microchannel tubes of a single-pass microchannel heat exchanger, a 1-D model is used for forecasting thermal and hydraulic performance of flow within the microchannel tubes, while CFD simulation, using ANSYS Fluent, is employed to solve flow characteristics in the headers, as shown in Figure 4-1.

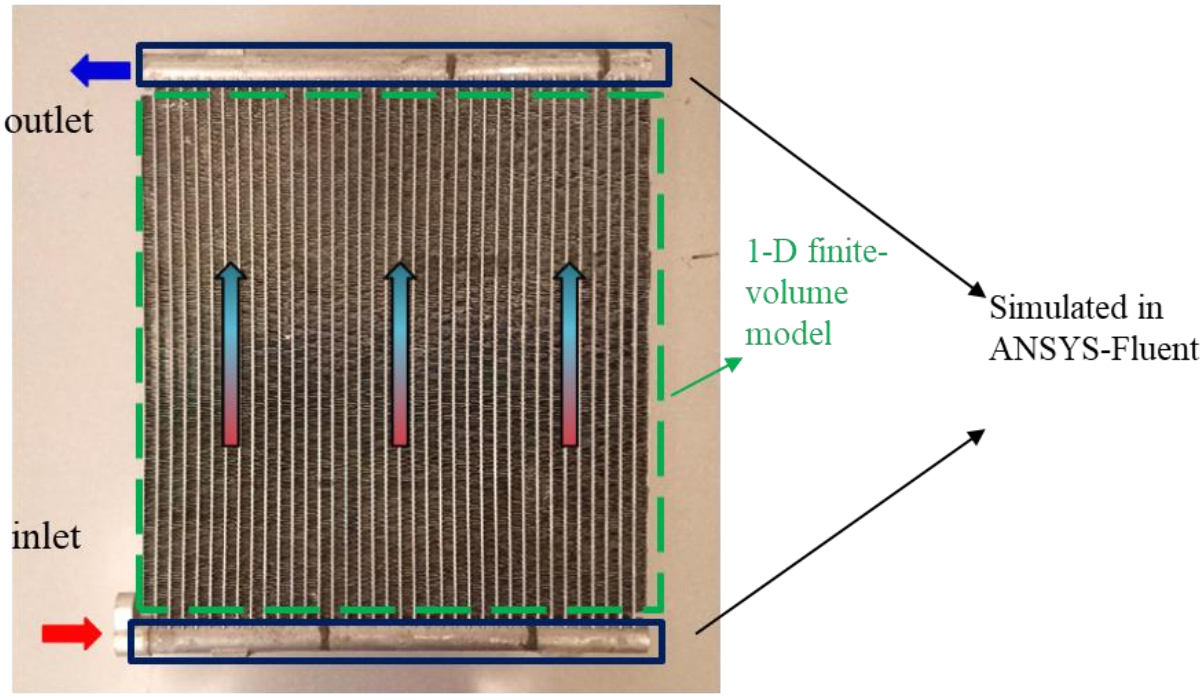

Figure 4-1: Single-pass MCHX

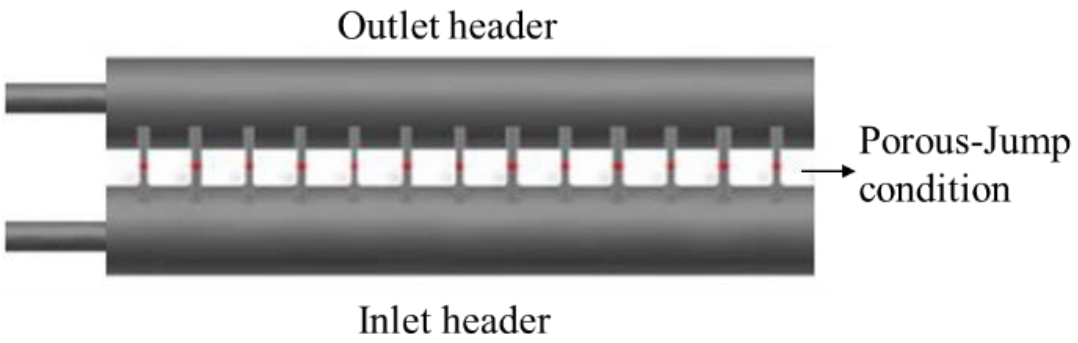

Figure 4-2: CFD simulation domain

In the Hydraulic-CFD Linked model, to make a solution domain to simulate using CFD, the microchannel tubes are removed, and the headers are directly attached together. In the place of the connection between the headers, however, to compromise the removal of microchannel tubes, a porous jump boundary is used in the CFD simulation as the representative of the pressure drop within microchannel tubes, as shown in Figure 4-2. Porous jump conditions are used to model a thin "membrane" that has known velocity (pressure-drop) characteristics. The governing equation is:

$$\Delta p = -\left(\frac{\mu}{\alpha} V + C_2 \frac{\rho V^2}{2} \right) \Delta m \tag{4-1}$$

where α is the permeability, V is the velocity normal to the porous face, C_2 is the pressure jump coefficient, and m is the thickness of the medium. The first term on the righthand side is a porous media inertial loss term, which is negligible in our simulations. The second term shows the skin friction pressure drop, which can be adjusted by calibrating the C_2 value based on the obtained pressure drop from the 1-D finite volume model.

The flow chart of the presented method is illustrated in Figure 4-3. In order to run the model, first, the whole flow field is solved by the CFD solver without applying any pressure drop in microchannel tubes, which gives the refrigerant mass flow rate and the pressure at the inlet of each microchannel tube. Then, the obtained pressure and mass flow rates are used as inputs for the 1-D finite-volume model, which gives the pressure drop and the heat transfer rate within microchannel tubes, as explained in the next section. The obtained pressure drop is utilized as an input to the CFD solution domain via the porous jump condition. The obtained heat transfer rate is also employed to find the microchannel tube outlet refrigerant temperature. The average values of the microchannel outlet temperatures in each header are then used to calculate the mean fluid properties, and the whole flow field is solved once again using CFD. This process is repeated until the mass flow rate residual in each microchannel tube is within the predefined value, which is chosen as the convergence criteria of the algorithm.

The MCHX headers are simulated with a commercial CFD code, ANSYS-Fluent. In Fluent, the governing conservation equations for the mass and momentum are solved using the finite volume method and non-staggered grid discretization. For simplicity, due to symmetry, only half of the domain is simulated. The coupled steady-state incompressible Navier-Stokes equations are solved using the SIMPLE scheme. The standard k-ε model is applied for the turbulence simulation, which uses two transport equations, one for the turbulent kinetic energy, K, and the other for the rate of dissipation of turbulent kinetic energy, ε, to model turbulence.

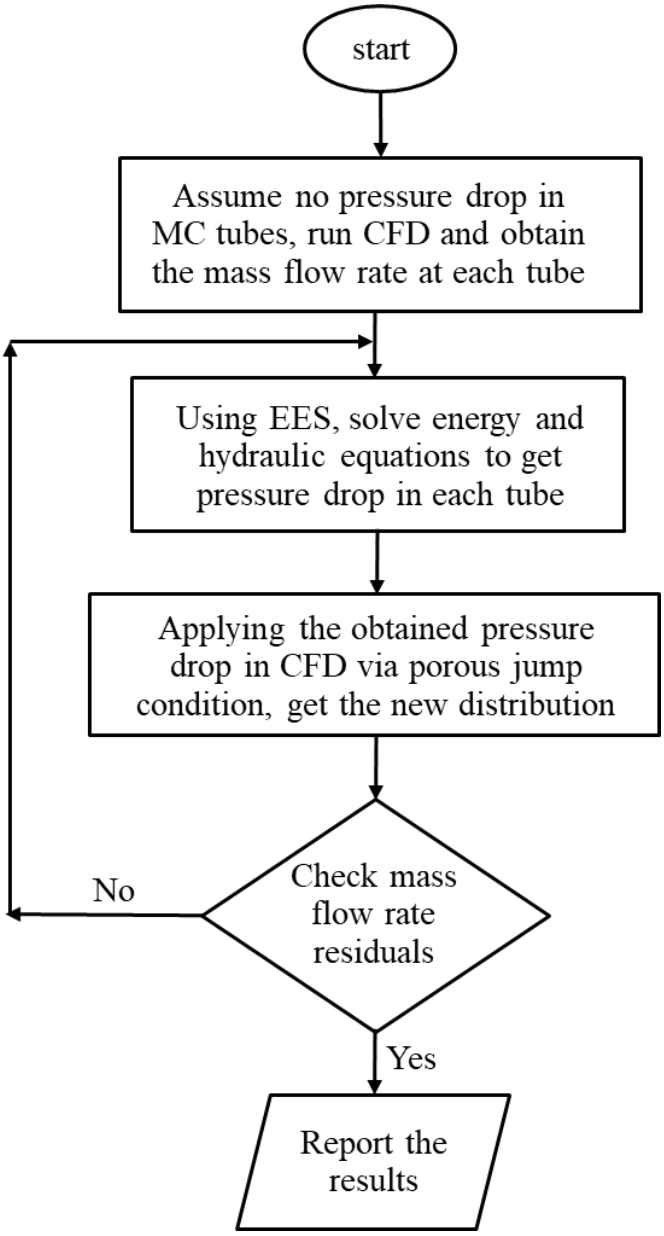

Figure 4-3: Hydraulic-CFD Linked model flowchart

Structured meshes, consisting of only hexahedral cells, are generated for computational zones using GAMBIT, as shown in Figure 4-4. Considerable care in the meshing of the MCHX model was required due to the large difference in the length scale of the geometries and to maintain mesh quality with minimal skewness. The grid independence study has been carried out, using three different meshes with around 580 thousand, 1.6 million, and 2.3 million cells for the headers. Using these three meshes, the simulations are conducted under the operating conditions in Table 4-2.

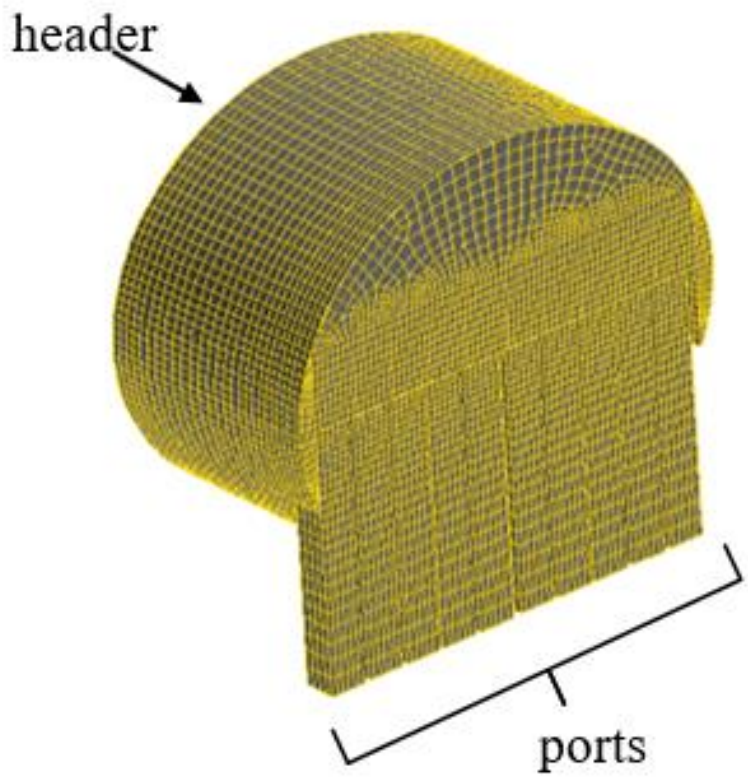

Figure 4-4: Generated mesh for one tube pitch

Table 4-2: Working conditions used as model inputs

Items	Unit	Value
Inlet mass flow rate	g/s	7.5
Inlet temperature	°C	80
Exit pressure	atm	1
Air inlet temperature	°C	25
Air face velocity	m/s	1

The pressure profile in the header is used as the criterion for grid independence study, as it is critical to the flow distribution. The results demonstrate that the calculated pressure profiles by the two largest meshes are almost the same, which indicates the mesh with 1.1 million computational zones is sufficiently fine for the tested case. However, to capture more flow details, the mesh with the largest number of nodes, 1.6 million, is selected. Then, this mesh is imported to ANSYS-Fluent for the flow simulation. The boundary conditions of velocity inlet and pressure outlet are used for the inlet and outlet of the microchannel heat exchanger, respectively.

4.3 HYDRAULIC 1-D MODEL

In order to predict refrigerant mass flow rate distribution among parallel microchannel tubes of a MCHX, a discretized finite volume 1-D model is developed. For simplicity, it can be assumed: 1) Heat conduction is negligible along the microchannel tubes and between those through fins; 2) Inlet and outlet headers are adiabatic; 3) Refrigerant is distributed equally among the ports of each microchannel tube; 4) Airside has uniform temperature and velocity. In this model, any single path through any microchannel tube connecting the heat exchanger inlet and the heat exchanger exit is considered as a unique flow path.

As shown in Figure 4-5, the overall pressure drop for each unique flow path can be expressed as:

$$\Delta p_i = \Delta p_{inlet\ header,i} + \Delta p_{cont,i} + \Delta p_{tube,i} + \Delta p_{\exp,i} + \Delta p_{outlet\ header,i} \quad (4\text{-}2)$$

Based on the principles of fluid mechanics, the overall pressure drop must be the same for all the flow paths. The mass flow rate at each location along the inlet and outlet headers is different due to refrigerant branching into and out of the microchannel tubes, respectively. These different mass flow rates give rise to different local minor pressure drops in the headers. Due to different minor pressure drops in the headers, the equality of overall pressure drop along all the flow paths is met by uneven mass flow rates among the microchannel tubes.

The pressure drop in a microchannel tube comprises frictional, momentum, and gravitational pressure drops. The frictional pressure drop in the microchannel tubes is calculated by the correlation developed by Churchill (1977). The pressure drop due to the contraction of the flow from the inlet header into the microchannel tube, and the expansion of the flow from the microchannel tube into the outlet header is calculated by the correlations in Idelchik hydraulic handbook (1994) (Section VII, Diagram 7-4; Section VII, Diagram 7-18).

To model the heat transfer between the air and the refrigerant, the *ε-NTU* method is used. As described in Incropera *et al*. (2007), the maximum possible heat transfer in one element is defined as:

$$Q_{\max} = C_a(T_{r,i} - T_{a,i}) \quad (4\text{-}3)$$

And the actual heat transfer rate in one element is given as:

$$Q_{actual} = \varepsilon Q_{\max} \quad (4\text{-}4)$$

Where ε is the effectiveness of the element. The effectiveness is a function of heat capacity ratio, C_r, and the Number of Transfer Unit *(NTU)*, as defined in Equation (4-5) and Equation (4-6), respectively. *NTU* is defined as the ratio of the overall heat transfer coefficient multiplied by the heat transfer area to the heat capacity rate.

$$C_r = \frac{\min(C_r, C_a)}{\max(C_r, C_a)} = \frac{C_{\min}}{C_{\max}} \tag{4-5}$$

$$NTU = \frac{UA}{C_{\min}} \tag{4-6}$$

Equation (4-7) is used for single-phase flow to correlate ε to *NTU* in cross-flow configuration.

$$\varepsilon = 1 - \exp\left[\frac{C_{\min}}{C_{\max}}.NTU^{0.22}.\left(\exp\left[-C_r.NTU^{0.78}\right]-1\right)\right] \tag{4-7}$$

The overall heat transfer coefficient, *U*, is defined in terms of the total thermal resistance to the heat transfer between the air and refrigerant:

$$\frac{1}{UA} = \frac{1}{\eta h_a A_a} + \frac{\delta_{wall}}{k_{wall} A_r} + \frac{1}{h_r A_r} \tag{4-8}$$

h_a is the air-side heat transfer coefficient and is determined by Chang and Wang (1997) correlation, where h_r is the refrigerant side heat transfer coefficient and is calculated by Gnielinski (1976) correlation. Moving downstream, h_{r} will change accordingly as refrigerant enthalpy decreases.

Pressure drop in each element of horizontal headers includes three components, frictional pressure drop $\Delta P_{f,i}$ acceleration pressure drop $\Delta P_{acc,i}$, and local loss $\Delta P_{\zeta,i}$, due to the halfway

protrusion of microchannel tubes into the header, as well as branching the refrigerant out of and into the inlet header and outlet header, respectively.

$$\Delta p_{header,i} = \Delta p_{f,i} + \Delta p_{acc,i} + \Delta p_{\zeta,i} \tag{4-9}$$

The frictional pressure drop in the headers is calculated by Equation (3-3), in which the friction factor is calculated by the correlation developed by Churchill (1977). Acceleration pressure drop is the change in dynamic pressure from upstream of the microchannel tube to downstream of that microchannel tube along the header, as expressed by Equation (3-2). To evaluate $\Delta P_{\zeta,i}$ in the 1-D finite volume model, the local pressure loss coefficients are calculated using three different methods, as follows:

1) Uniform pressure loss coefficients given by Yin *et al.* (2002)
2) Correlations generated by Ren *et al.* (2014)
3) Correlations for combining and dividing manifolds in Idelchik hydraulic handbook (1994) (Section VII, Diagram 7-4; Section VII, Diagram 7-20;). These correlations for converging and diverging cases are introduced by Zubov (1974) and Taliev (1952), respectively. The simplified version of these correlations for the MCHX geometry used in this study are:

$$\zeta_{conv} = 1.55\frac{Q_t}{Q_h} - \left(\frac{Q_t}{Q_h}\right)^2 \tag{4-10}$$

$$\zeta_{div} = 0.4\frac{Q_t}{Q_h} \tag{4-11}$$

Q_t and Q_h represent volume flow rate in the MC tube and the header, respectively.

The predictions for mass flow rate distribution in the hydraulic 1-D heat exchanger model, using the three above methods will be compared to the Hydraulic-CFD Linked model.

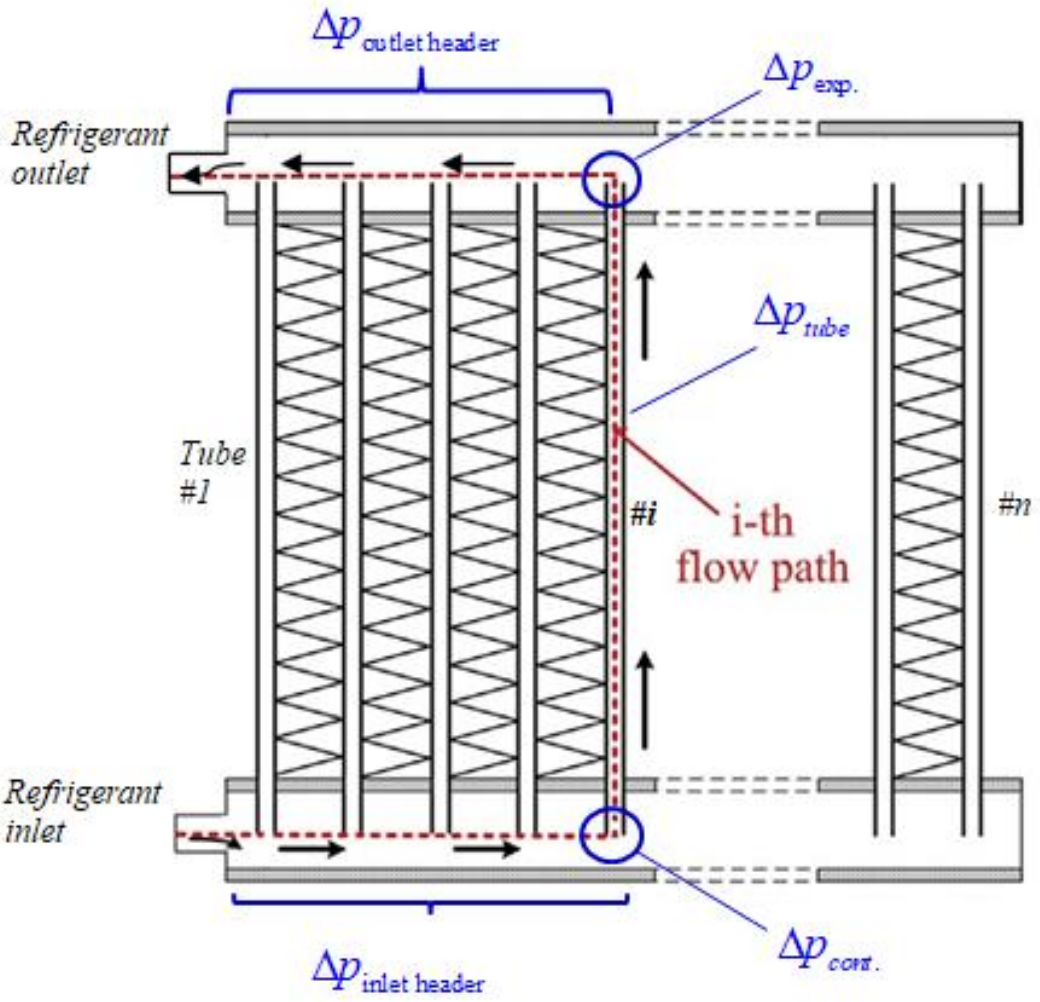

Figure 4-5: Pressure drop components in each flow path

4.4 RESULTS AND DISCUSSION

The above-proposed models were used to predict refrigerant distribution among parallel microchannel tubes of a single-pass MCHX to gain additional insight into how significant the values of local pressure loss coefficient in inlet and outlet headers are. The operating conditions used as inputs in the models are summarized in Table 4-2. The working fluid utilized in the models is nitrogen.

Figure 4-6 shows the comparison of mass flow rate distribution predicted by three different simulation approaches with Hydraulic-CFD Linked model for a single pass U-type MCHX. These models show a major difference between the predictions of the three 1-D finite volume approaches. However, according to the results, the mass flow rate distribution obtained by the correlations for dividing and combining manifolds in Idelchik hydraulic handbook (1994) matches the prediction by the Hydraulic-CFD Linked model much better.

Figure 4-7 shows the comparison of mass flow rate distribution predicted by three different simulation approaches with Hydraulic-CFD Linked model for a single pass Z-type MCHX. Similar to the U-type MCHX case, the 1-D models show different predictions of mass flow rate distribution, and the one achieved by the correlations for dividing and combining manifolds in Idelchik hydraulic handbook (1994) is very close to the prediction by the Hydraulic-CFD Linked model.

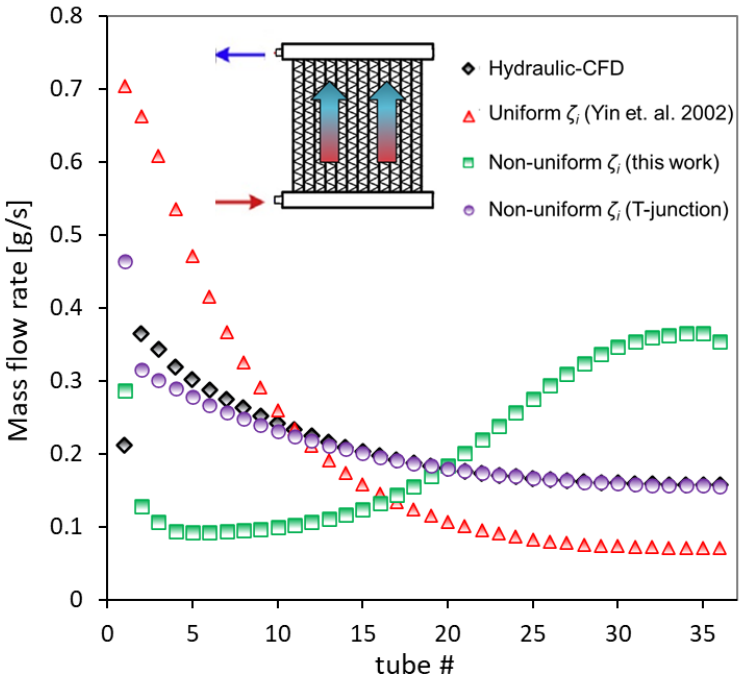

Figure 4-6: Comparison of flow distribution predictions of three 1-D models with Hydraulic-CFD Linked model for U-type MCHX

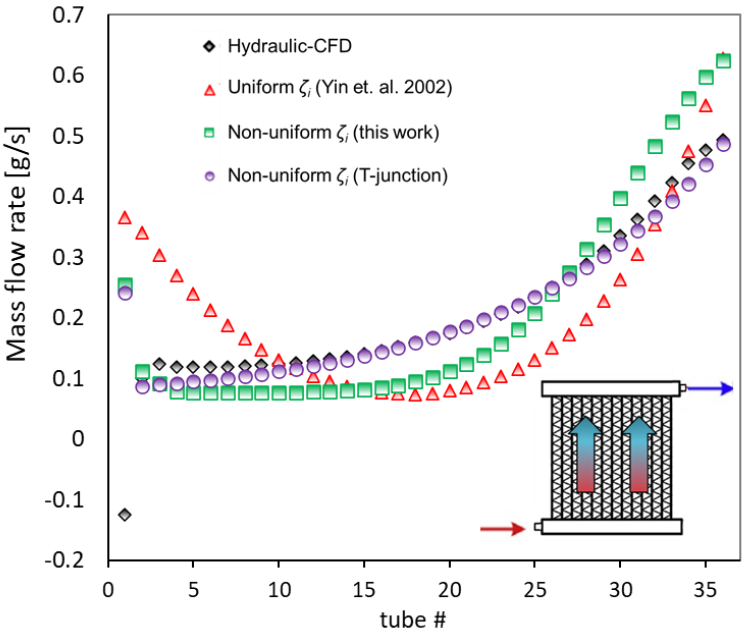

Figure 4-7: Comparison of flow distribution predictions of three 1-D models with Hydraulic-CFD Linked model for Z-type MCHX

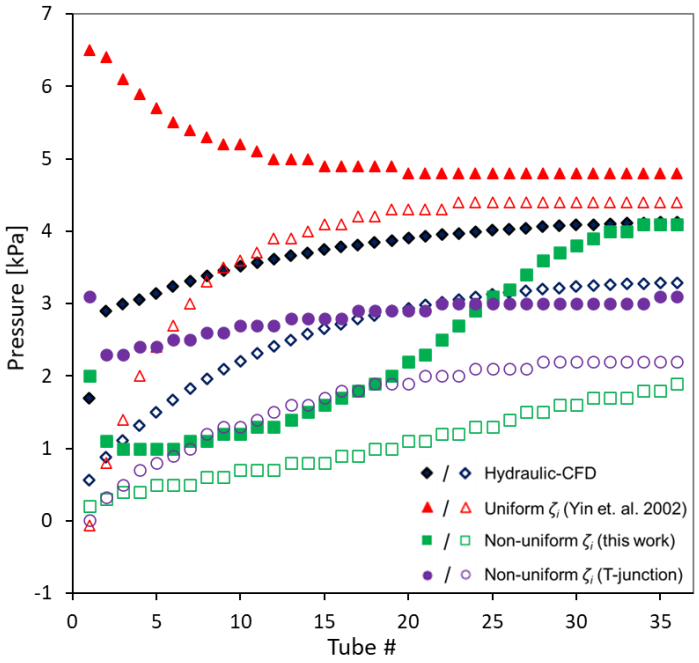

Figure 4-8: Predictions of pressure in inlet header and outlet header for three 1-D models and Hydraulic-CFD Linked model for U-type MCHX

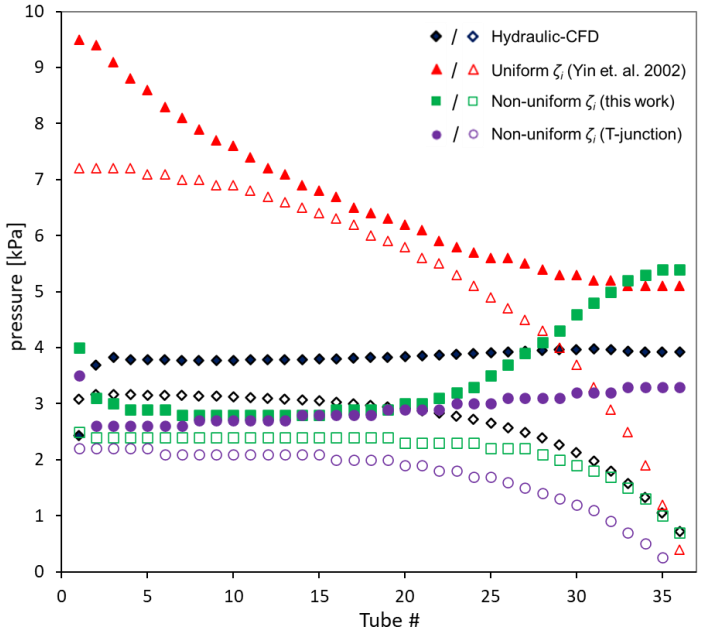

Figure 4-9: Predictions of pressure in inlet header and outlet header for three 1-D models and Hydraulic-CFD Linked model for Z-type MCHX

Pressure predictions by all four models along the inlet header and outlet header for U-type MCHX and Z-type MXHX are shown in Figure 4-8 and Figure 4-9, respectively. The discrepancy in pressure predictions between these models can be observed. However, it should be noted that the pressure difference on both sides of the microchannel tube dictates the mass flow rate in that tube. Despite the disagreement in pressure evaluation of the Hydraulic-CFD Linked model and the T-junction model, the difference between the pressure in the inlet and outlet header for any specific MC tube is very close to each other. Consequently, the mass flow rate distribution predictions are in good agreement. The discrepancy between the pressure values can be described as follows. First, the locations for which the pressures are provided in Figures 4-8 and 4-9 are not the same for the CFD model and other 1-D models. For the Hydraulic-CFD model, the pressures are for the mouth of the MC tubes, while for the other three 1-D finite volume models, the pressure values are for locations upstream and downstream of the MC tube along the inlet header and outlet headers, respectively. The other reason is the pressure distribution in the outlet header from the last MC tube to the exit. Dictating the ambient pressure at the exit of the MCHX in all the models defines the pressure variation in the heat exchanger. Within the CFD model, as shown in Figure 4-11, the pressure change near the exit due to the sudden expansion and contraction, as well as the sharp corner can be predicted more accurately. However, in the 1-D finite volume models, the effect of the aforementioned changes in the geometry is not captured.

As shown in Figure 4-10, in the third 1-D approach, it is assumed that the flow behavior over each microchannel tube mouth inside the header resembles a T-junction, with dividing flow and combining flow in the inlet header and outlet header case, respectively.

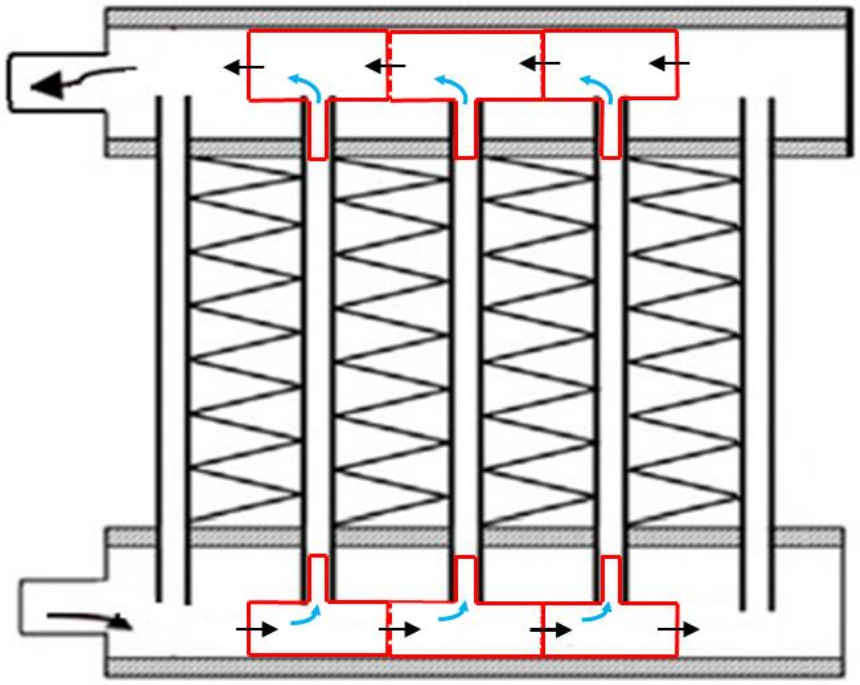

Figure 4-10: Schematic of the 1-D finite volume model with the assumption of T manifolds along the header, for U-type MCHX

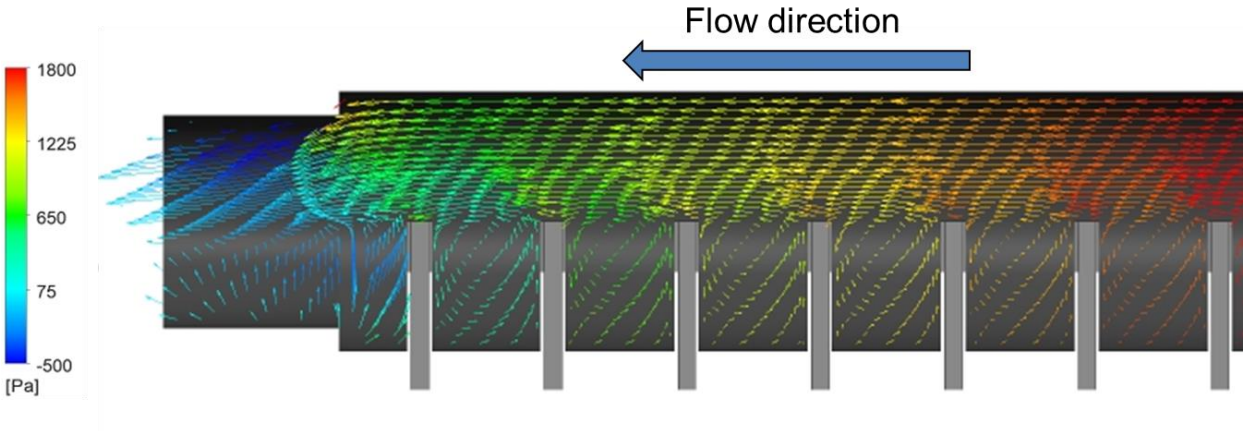

Figure 4-11: Velocity vectors, colored with pressure values near the exit of the outlet header, from the Hydraulic-CFD Linked model

Looking into the velocity vectors inside the headers from the Hydraulic-CFD Linked model, Figure 4-11 to Figure 4-13, illustrates that it is a reasonable assumption to simply consider T-junctions in place of the protruded regions in each segment of the headers.

The reason for this observation is that within the majority of the header, the flow rate in the microchannel tube is much smaller than that in the header. As a result, the streamlines in the header are not bent significantly, and pressure loss is mainly due to converging/diverging to/of the flow from the MC tube. In addition, thanks to the short distance between two adjacent microchannel tube, a secondary flow in the space between the protrusions are formed and the fluid in the header mostly flows on top of that recirculation zone. This also prevents any expansion and contraction from one microchannel tube mouth to the next one along the header.

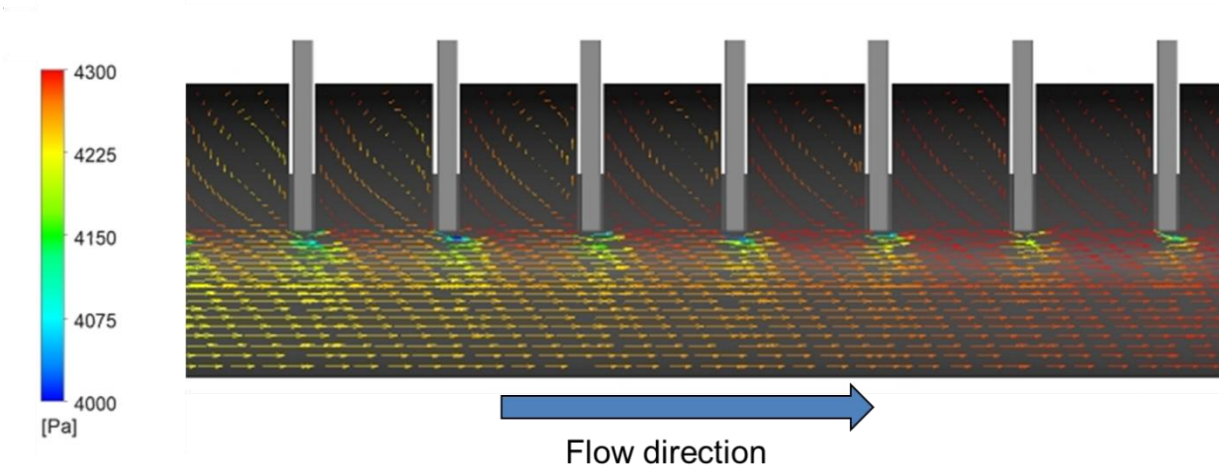

Figure 4-12: Velocity vectors, colored with pressure values in the middle part of the inlet header, from the Hydraulic-CFD Linked model

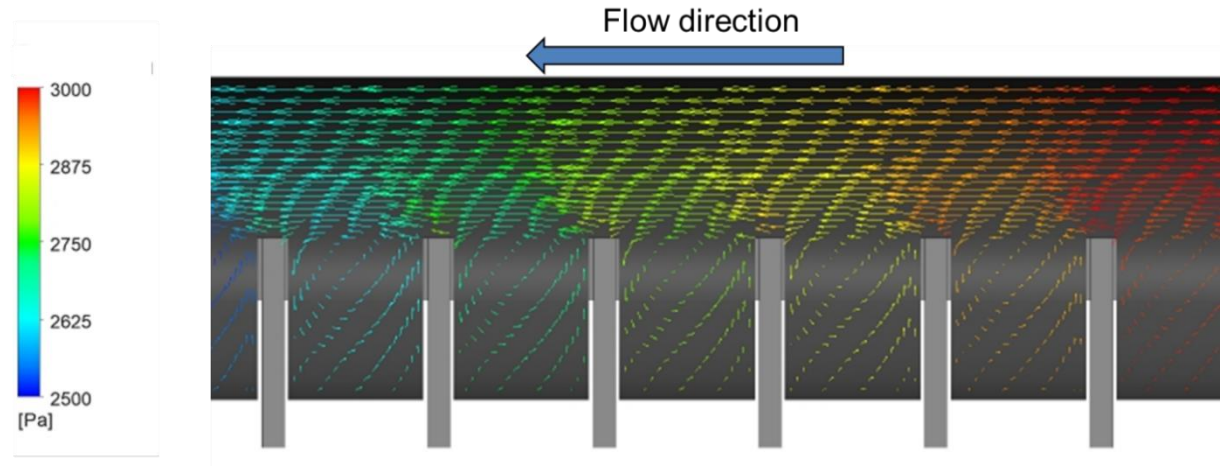

Figure 4-13: Velocity vectors, colored with pressure values, in the middle part of the outlet header, from the Hydraulic-CFD Linked model

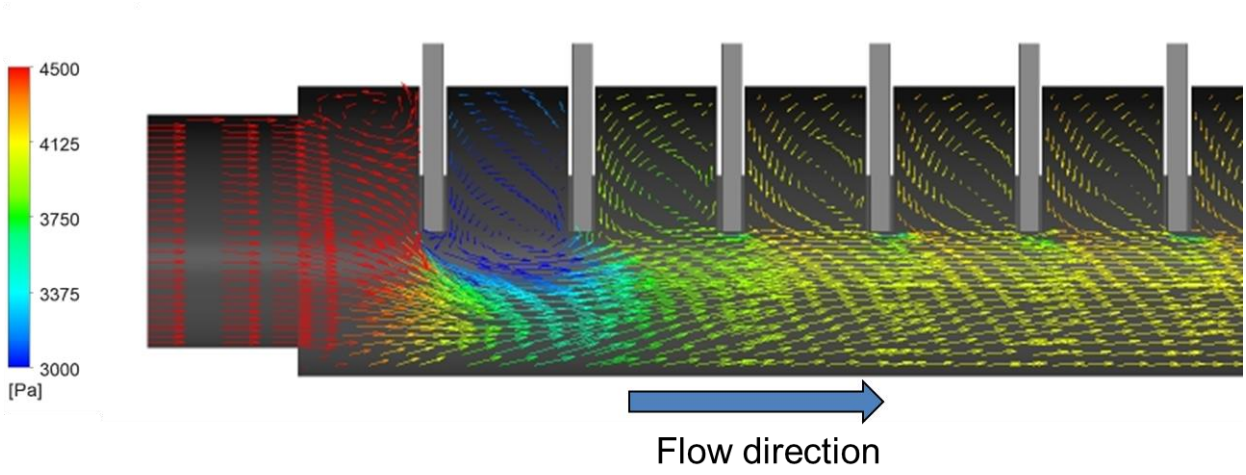

Figure 4-14: Velocity vectors, colored with pressure values, at the beginning of the inlet header, from the Hydraulic-CFD Linked model

The discrepancy between the mass flow rate distribution in the first several microchannel tubes (Figure 4-6 and Figure 5-7), predicted by the 1-D finite volume model with the assumption of T manifolds and Hydraulic-CFD Linked model, stems from the complex flow behavior in the initial part of the inlet header. The reason is that a big contraction and subsequent expansion only occurs when flow crosses over the protrusion of microchannel tube #1, as shown in Figure 4-14. In this region, the assumption of the flow behavior similar to T-junctions is not much reasonable. According to Figure 4-14, it takes some distance in the inlet header for the streamlines to become mostly parallel and uniform.

4.5 SUMMARY AND CONCLUSION

This chapter presents the numerical investigation of single-phase flow distribution in microchannel heat exchangers. Three different 1-D finite volume approaches to evaluate pressure drop in headers of MCHXs are proposed to predict mass flow rate distribution, and compared with a Hydraulic-CFD Linked model, in which the flow in headers is simulated by ANSYS Fluent. The 1-D finite volume models show a difference in the prediction of flow rate distribution. However, the model in which the flow passage in the header is assumed to be a series of dividing and combining T-manifolds shows a satisfactory agreement with the Hydraulic-CFD Linked model in the perspectives of mass flow rate distribution. The disagreement over the first multiple MC tubes is due to the complexity of the flow at the entrance to the inlet header, as well as the incapability of the 1-D model to capture the physics.

CHAPTER 5

TWO-PHASE FLOW PRESSURE DROP IN THE HEADER IN VERTICAL UPWARD FLOW

5.1 INTRODUCTION

Phase separation in the header is the main factor that causes refrigerant maldistribution in the two-phase flow and it is the most important in MCHX modeling. However, besides phase separation in the header, maldistribution in MCHX may also be caused by the pressure drop in the header in two-phase flow. As discussed in Section 4.3, the pressure drop in the header causes the pressure drop in the microchannel tube to be different between each tube, resulting in flow rate maldistribution. This chapter experimentally investigates the pressure drop in upward flow in a vertical header and explores the behavior of the pressure drop in the header for a range of inlet qualities and inlet mass flow rates based on experimental results. The pressure drop of two-phase R134a in the header was measured while the visualization of the two-phase flow in the header was recorded at the same time. Due to the complexity of two-phase flow in a real header, pressure drop is first analyzed in a header with no flow inside the microchannel tubes in Section 5.2, then the study goes further by adding flow into the tubes, investigating the inlet header in Section 5.3.

5.2 VERTICAL TUBE WITH HEADER-LIKE PROTRUSIONS

5.2.1 TEST FACILITY

The pressure drop measurement and flow regime visualization are obtained in the header shown in Figure 5-1.

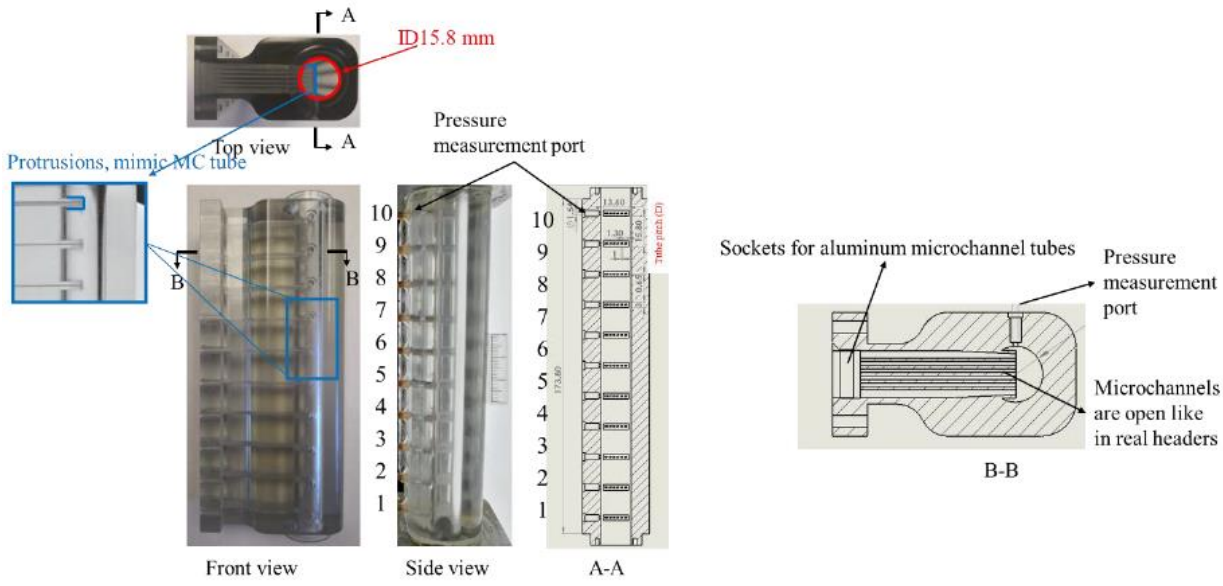

Figure 5-1: Test section for the two-phase upward flow in the vertical round tube with header-like protrusions

The test section is a fully transparent 3D printed part with an inner diameter of 15.8 mm, with the tube protrusion having a thickness of 3 mm and a width of 13.6 mm which has six microchannel ports. The microchannel tube protrudes halfway of the inner diameter of the round tube. At the other end of the microchannel tube, there is a socket for the aluminum, a microchannel tube connection, and a chamfer for the sealing with an O-ring. Two holes are made for the bolt and nut connection like a flange. The total length of this part is 173.8 mm. Aluminum microchannel

tubes are connected to the sockets with O-rings. The other end of the aluminum microchannel tubes is also blocked. The refrigerant flows in a tube with protrusions like in a real header. The seal will be removed when studying flow like in real MCHX (as presented in Section 5-3). There is a metal frame to support this section and connect to the facility. There is a port for the pressure measurement. The location of the pressure measurement port is at the inner wall of the transparent header. All ports are named 1 to 10 from the bottom to the top and connected to PFA tubes with a 1/8" OD. Upstream inlet geometry is a 500 mm PFA tube with a 3/8" OD.

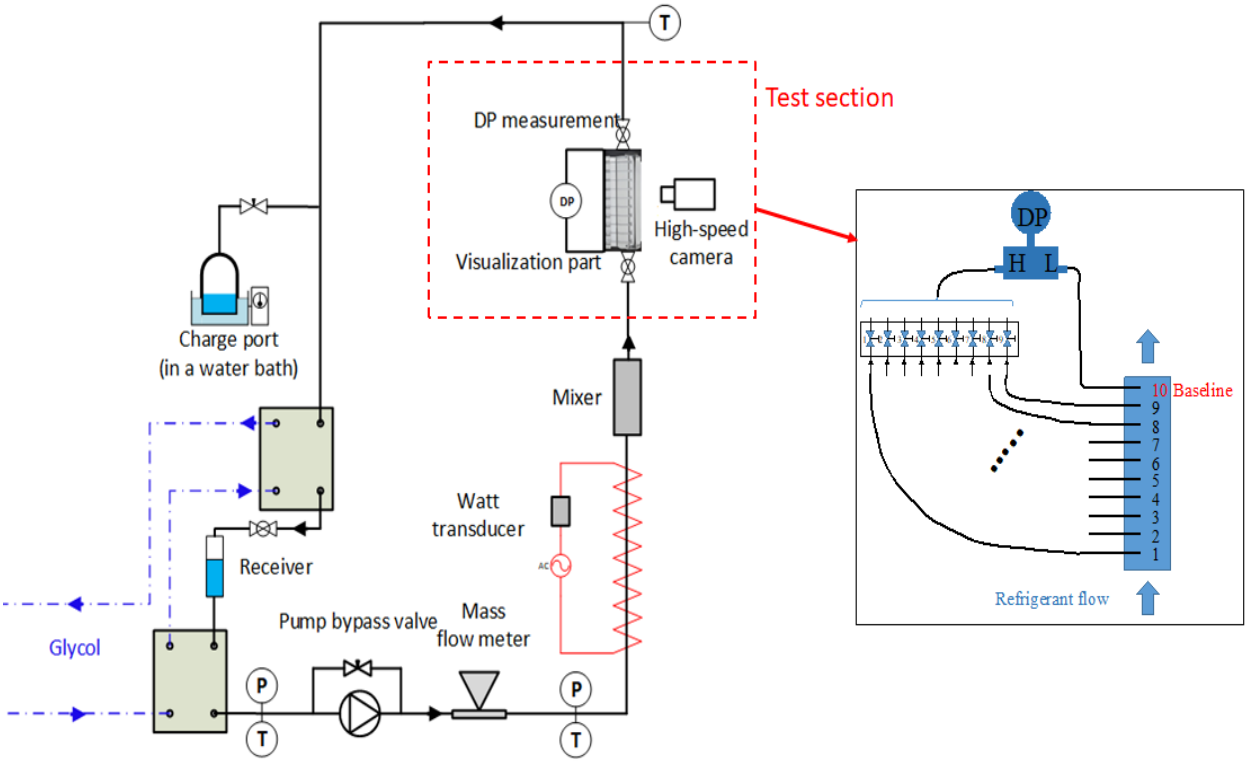

Figure 5-2: Facility for the two-phase upward flow in the vertical round tube with header-like protrusions

The schematic drawing of the facility is shown in Figure 5-2. Pure subcooled liquid refrigerant (R134a) is pumped through a mass flow meter with a gear pump (MICROPUMP GC M35). Local refrigerant enthalpy before the heater is obtained from the measured pressure (P) and temperature (T). The flow is then heated by an electric heater, and the power (Q) is measured by a watt transducer (Ohio Semitronics GW5-024CX5). Measured heater input power, mass flow rate, and inlet enthalpy determine refrigerant quality after the heater or at the inlet to the test section. After the refrigerant is mixed in the mixer to make the flow as homogeneous as possible, it continues into the test section. After the refrigerant passes the test section, it flows into two condensers with glycol as a secondary fluid. The subcooled liquid is then fed into the gear pump to complete the circuit. The saturation temperature in the test section is controlled by a refrigerant tank in a water bath.

After the system becomes stable (i.e., the temperature, pressure, and quality keep constant in the test section), a high-speed camera is used to capture flow regimes with a resolution of 512×512 and a speed of 2200 frames per second (fps). To measure the pressure difference, port number 10 is chosen to be the reference pressure and is connected to the lower pressure input of a DP sensor. All other nine ports are connected to nine small ball valves and then the higher-pressure input of the DP sensor (Figure 5-2). In such a way, the instrument errors from using multiple DP sensors are eliminated at the cost of additional time and work. All clear PFA tubes that connect the DP sensor and the pressure measurement ports are heated when liquid slugs appear inside. This is to make sure that the tubes to the DP sensor are all filled with vapor to avoid potential problems with gravity effects on DP due to liquid. Hence, the pressure drop along the header, and visualization results are obtained for each specific test condition.

Table 5-1: Working conditions for two-phase flow test for the round tube with header-like protrusions

Items	Unit	Value
Mass flow rate	g/s	3, 4.5, 6, 7.5
Mass flux	$kg/m^2 s$	28, 43, 58, 72
Saturation temperature	°C	14.5
Vapor quality	-	0.1 - 0.9
Working fluid	-	R134a

According to Bowers *et al*. (2006), when tube protrusions are present, it is more representative to define the mass flux by the smallest cross-sectional area. The mass flux calculation in this study is based on the minimum cross-sectional area of the header (104.03 mm^2). The test conditions are listed in Table 5-1.

Table 5-2: The uncertainty of the instruments in the round tube with header-like protrusions test

Instrument	**Measurement**	**Uncertainty**
Sensotec TJE	Pressure (*P*)	± 0.1% FS
T-type thermocouple	Temperature (*T*)	± 0.1 °C
Ohio Semitronics GW5-024CX5	Heater power (Q)	± 0.2% Reading/± 0.04% FS
Micromotion D40	Mass flow rate (m)	± 0.2% flow rate
Rosemount 1151	Pressure drop (DP)	±0.25% FS

5.2.2 DATA REDUCTION

The instrumental uncertainties of the devices used in this project are listed in Table 5-2. Error propagation rule is given in Equation (5-1). It estimates overall uncertainty based on measured values.

$$u_c = \sqrt{\sum_{i=1}^{N} \left(\frac{\partial y}{\partial x_i} \right)^2 u^2(x_i)} \tag{5-1}$$

where u_c is combined standard uncertainty, y is calculated values, x_i is measured values and $u(x_i)$ is the uncertainty of x_i. Equation (5-1) is built in the software Engineering Equation Solver (EES). The combined standard uncertainty can be obtained by following the procedure incorporated in EES.

5.2.3 RESULTS

In the control volume, the total pressure drop can be divided into four major contributions: hydrostatic ($\Delta P_{hydrostatic}$), frictional ($\Delta P_{frictional}$), local (ΔP_{local}, due to protrusions). Since all microchannels are closed, there is no acceleration pressure drop caused by mass addition or reduction in the test section. $\Delta P_{hydrostatic}$ is a function of two-phase density, ρ_{TP}:

$$\Delta p_{gra} = \rho_{TP} g l \tag{5-2}$$

$$\rho_{TP} = \rho_v \alpha + \rho_l (1 - \alpha) \tag{5-3}$$

where g is the acceleration of gravity and l is the length of the control volume. If the saturation temperature in the test section is set, $\Delta P_{hydrostatic}$ only depends on the local void fraction. When the inlet quality is lower, the local void fraction will also be smaller, and the hydrostatic pressure drop

is more significant. ΔP_{local} is caused by the presence of tube protrusions. Tuo and Hrnjak (2013) proposed:

$$\Delta p_{local} = k_{loss} \frac{G^2}{2\rho_{TP}} \tag{5-4}$$

where G is the mass flux and k_{loss} is the local loss coefficient which is determined by experiments. ΔP_{local} is again a function of local void fraction. $\Delta P_{frictional}$ is a function of many variables, including density, viscosity, and surface tension. In this study, it is calculated with the model from Friedel (1979). Due to the relatively low mass flux, $\Delta P_{frictional}$ only accounts for a small portion of the total pressure drop in most cases. Overall, the total pressure drop in the control volume is highly related to the gravitational pressure drop most of the time within the tested conditions.

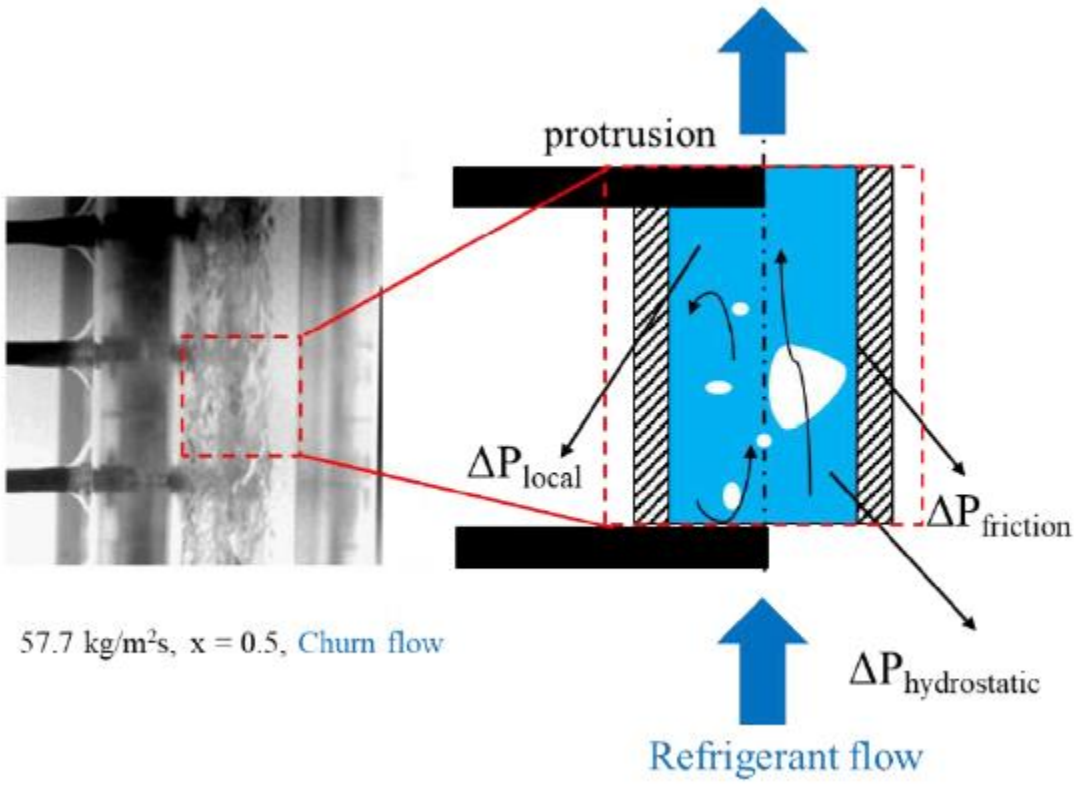

Figure 5-3: Schematic of the control volume of a measured pressure drop

Visualization results are studied to analyze flow regimes in the test section. In the explored mass flux range, three major flow patterns in the tube with header-like protrusions are observed: slug flow, churn flow, and semi-annular flow, as shown in Figure 5-4.

Slug flow: Vapor slugs appear periodically with the liquid bridges and small bubbles in the middle. The vapor slugs which are disturbed by protrusions are relatively smaller than those in the smooth vertical tubes.

Churn flow: The total effect of shear on the interface, pressure gradient, and gravity on a droplet is not constant upwards. Liquid droplets may oscillate in the section. Also, due to the disturbance of the tube protrusions, flow structures are very chaotic.

Semi-Annular flow: Liquid flows along the smooth portion of the tube wall, and vapor flows in the central core. Since some liquid is trapped between protrusions, it is called semi-annular flow. The interface between liquid and vapor core is wavy.

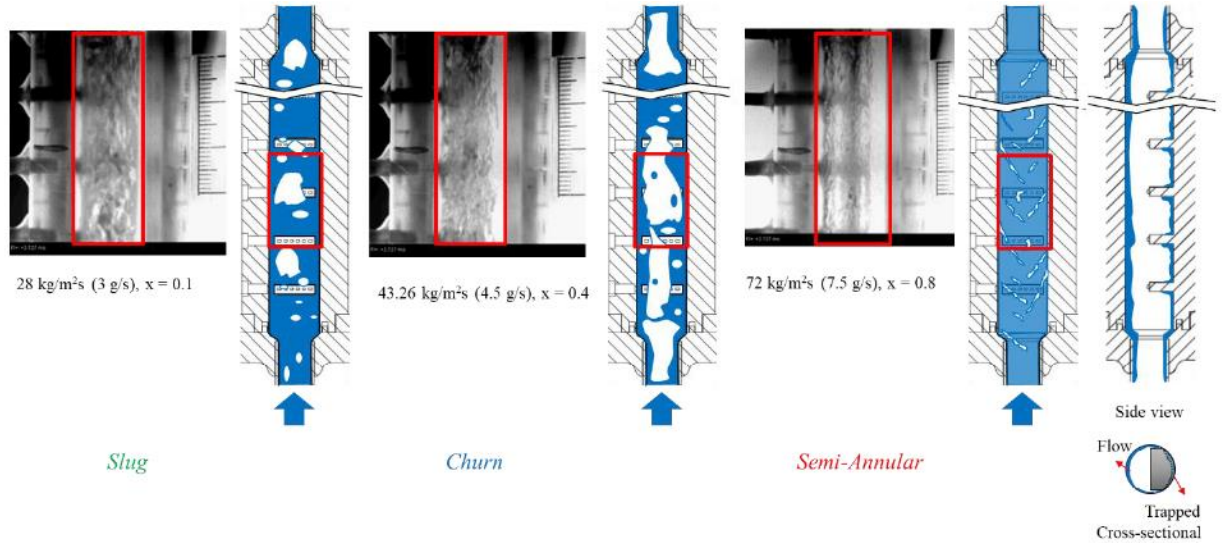

Figure 5-4: Flow patterns in the round tube with header-like protrusions

Figure 5-5 shows the pressure drop results for mass flow rates from 3 to 7.5 g s^{-1} (28-72 kg m^{-2} s^{-1}). Each line in the diagram depicts the results from a certain location. For example, line 1-2 represents the pressure drop between tubes 1 and 2 in Figure 5-2. When the inlet quality is 0 (fully liquid), the measured pressure drop in the control volume from all locations is close to the calculated hydrostatic pressure drop which is based on the geometry and thermal properties of R134a. In the lower mass flow rate and inlet quality region, in which the hydrostatic pressure drop is dominant, as the quality increases, the total pressure drop becomes smaller. However, in the higher mass flow rate and quality region, the total pressure drop is larger when the inlet quality is higher. In this region, the gravitational pressure drop is relatively small, but other contributions ($\Delta P_{frictional}$ and ΔP_{local}), especially ΔP_{local}, are more important. When the inlet quality equals 1 (fully vapor) at relatively higher mass flow rates, $\Delta P_{expansion}$ at the entrance of the section is more significant. It results in a very small or even negative pressure drop at the location of 1-2. Other than these conditions (full vapor at the location of 1-2), the pressure drop results for all locations of a specific test condition are very similar and agree well with the average value of that condition. The differences between 92% of all measured results and the average values are smaller than the measurement uncertainties.

Figure 5-6 shows the pressure drop components for mass flow rate 6 g s^{-1} at locations shown over the schematic. Pressure drop in the entire header (DP_{1-10}) shows clearly that frictional pressure drop is insignificant and hydrostatic pressure drop is the most important component in the majority of the vapor qualities. Local pressure drop plays an important role in higher qualities. This analysis for the pressure drop in the middle part of the header (DP_{6-7}) illustrates the same behavior as the entire header.

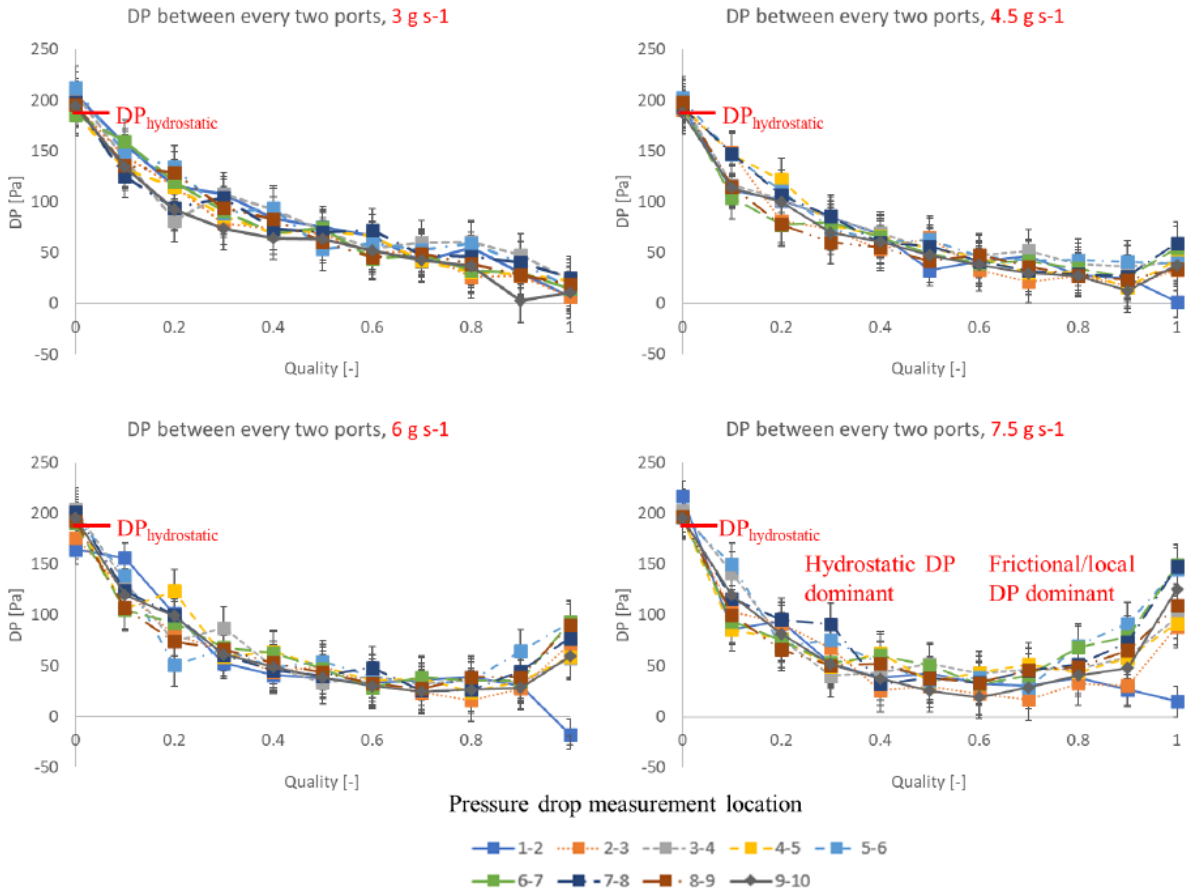

Figure 5-5: Pressure drop along the round tube with header-like protrusions

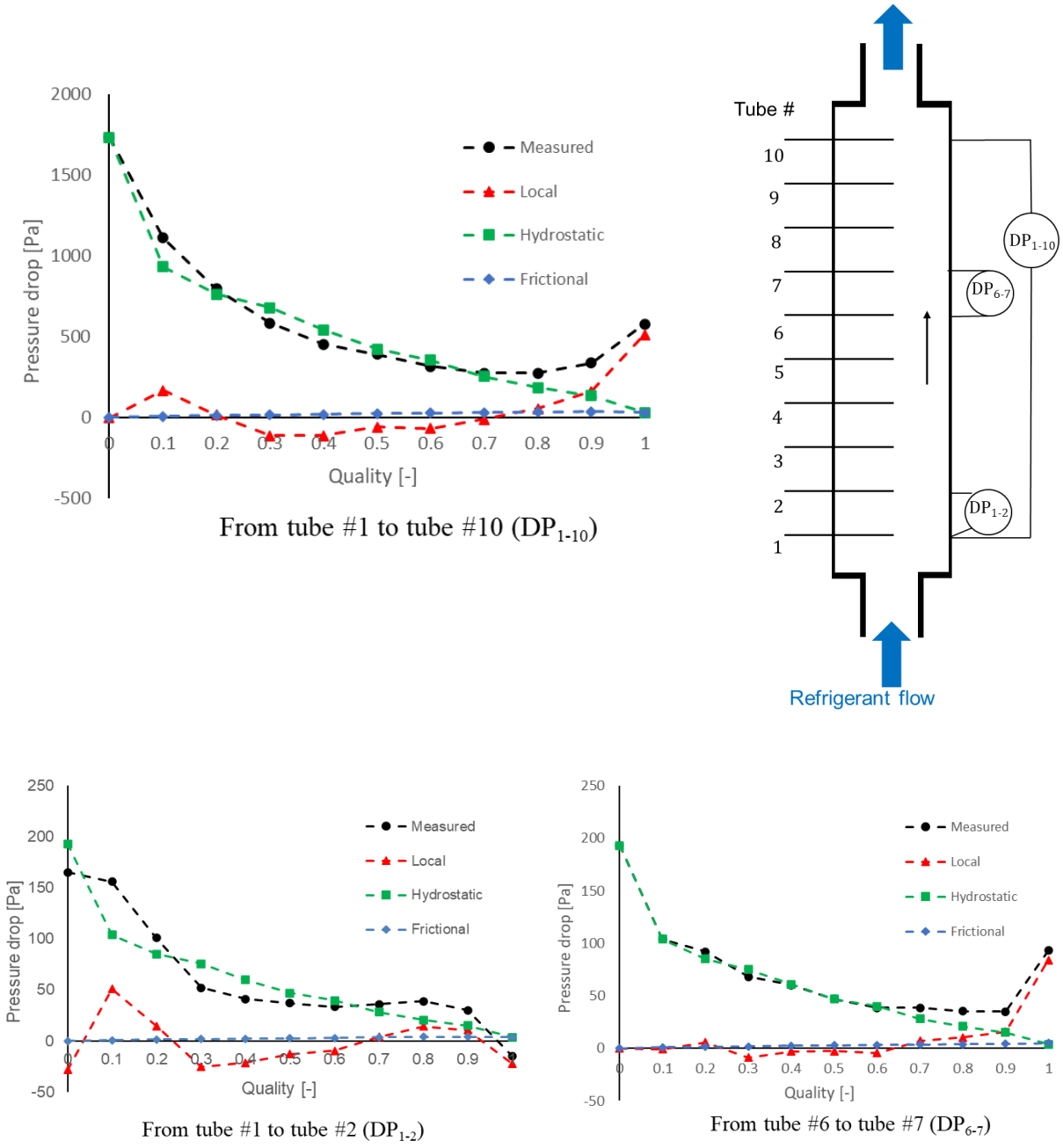

Figure 5-6: Comparison of pressure drop components along the round tube with header-like protrusions, $m = 6\ g\ s^{-1}$

5.3 VERTICAL INLET HEADER

5.3.1 TEST FACILITY

This section demonstrates the experimental measurement of pressure drop in upward flow in an inlet header with 10 microchannel tubes. Visualization results are also studied to analyze flow regimes in this configuration.

The test facility, Figure 5-7, was constructed to study R134a pressure drop in headers of MCHXs. To obtain the results of visualization, and pressure drop in the header for a certain test condition, a transparent header with pressure drop measurement ports is built. The header has the same inner diameter (15.8 mm) and tube pitch (15.8 mm) as the header in section 5.2. All the protrusions are ½ depth of the header's inner diameter, as widely used in the industry. Pure subcooled refrigerant is pumped through a mass flow meter (MicroMotion D40) with a gear pump (MICROPUMP GC M35). The mass flow rate (m_{in}) is controlled manually via a variable frequency drive (VFD) and a bypass valve. The refrigerant enters the inlet header from the bottom. A single electric heater is used to heat the refrigerant before the test section. The refrigerant enthalpy before the heater is obtained from the measured pressure (P_{sub}) and temperature (T_{sub}). Refrigerant is heated in the electric heater whose input power (Q_{in}) is measured by a Watt transducer (Ohio Semitronics GW5-024CX5). Before the test section, refrigerant quality (x_{in}) is determined by Q_{in}, $m_{in,}$ and the refrigerant enthalpy before the heater. The refrigerant flows into the test section after the mixer. The header has 10 microchannel outlets. For the header, two adjacent outlet tubes are combined into one with a Y-shape connection to maintain the same number of mass flow meters and heaters, as well as the control strategy. The refrigerant in the two combined outlet tubes is heated together, and the total mass flow rate is measured by a mass flow

meter. With the similar assumption made by Zou and Hrnjak (2013), this configuration should not affect the essence of the results. The two combined exits are assumed to have the same $x_{out,\,i}$ and $m_{out,\,i}$.

Table 5-3: Working conditions for two-phase test flow in the inlet header

Items	Unit	Value
Mass flow rate	g/s	3.2-5.3
Mass flux	Kg/m^2s	31-51.3
Saturation temperature	°C	14.5
Vapor quality	-	0.1 - 0.8
Working fluid	-	R134a

5.3.2 DATA REDUCTION

The instrument uncertainties of the devices used in this set of experiments are listed in Table 5-4. Error propagation rule is given in Equation (5-1). It estimates overall uncertainty based on measured values. The sum of the mass flow rate in all five outlet mass flow meters ($\sum_1^5 \dot{m}_{out,i}$) is not the same as the total inlet mass flow rate (m_{in}) due to the experimental uncertainties. The average and median deviations are 0.23% and 0.22%, respectively. Like the former study by Zou and Hrnjak (2013), the mass flow rate in each outlet tube is corrected.

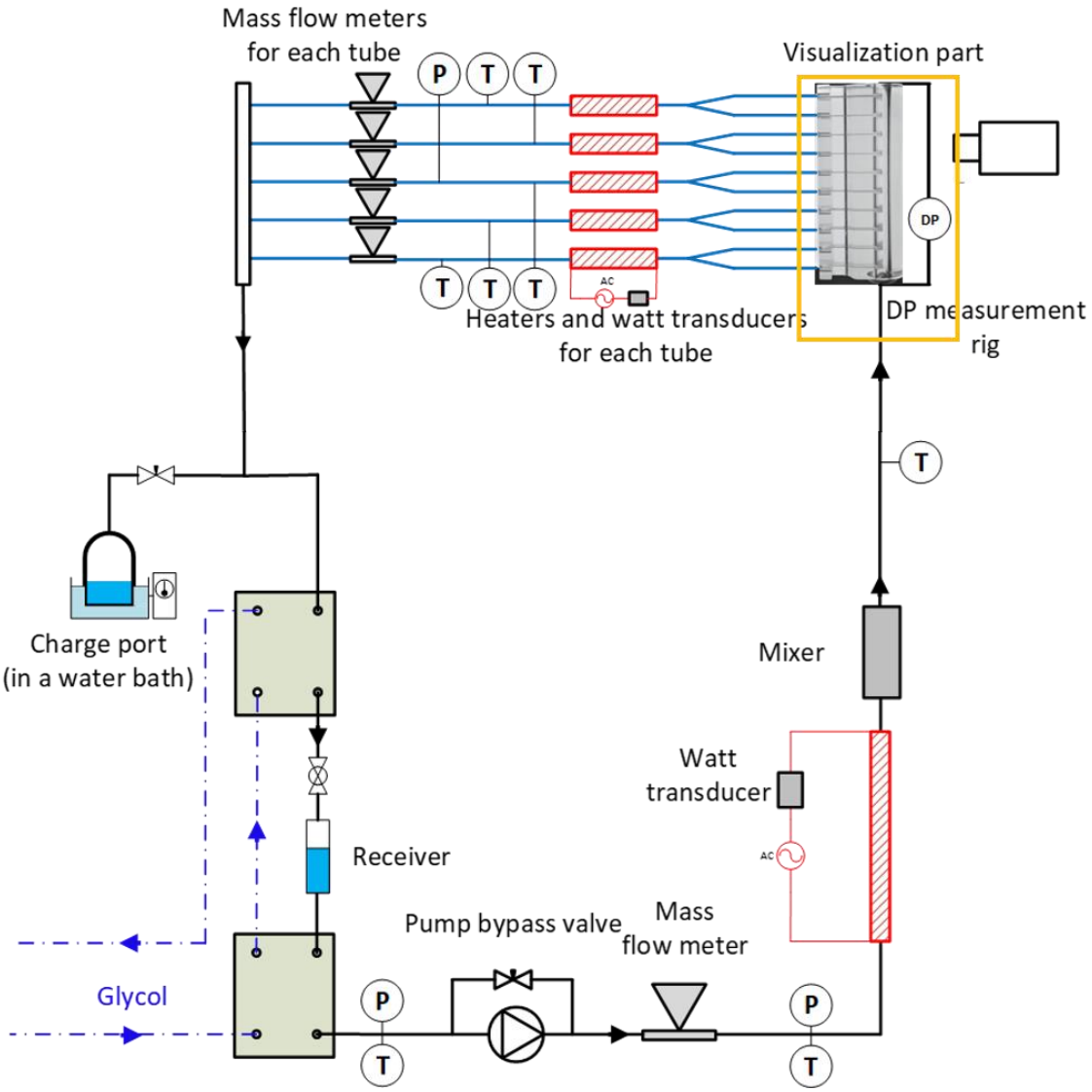

Figure 5-7: Test facility in the two-phase upward flow in vertical inlet header

$$m_{out,i}^{corrected} = m_{out,i}^{measured} . C_F \tag{5-5}$$

$$C_F = \frac{m_{in}^{measured}}{\sum_{i=1}^{n} m_{out,i}^{measured}} \tag{5-6}$$

The liquid mass flow rates in the five outlet tubes are also adjusted in such a way that the sum is equal to the total inlet liquid mass flow rate.

$$m_{L\ out,i}^{\ corrected} = m_{L\ out,i}^{\ measured} . C_{F_L} \tag{5-7}$$

$$C_{F_L} = \frac{m_{in}^{measured}(1 - x_{in}^{measured})}{\sum_{i=1}^{n} m_{L\ out,i}^{\ measured}} \tag{5-8}$$

The local variables in Figure 5-8 are calculated based on the mass balance, as shown in Equations (5-9) and (5-10). The mass flow rate at the top of the header, $\dot{m}_{11}$, is set to zero as the boundary condition since it is a stagnation point.

$$\dot{m}_{i+1} = \dot{m}_i - \dot{m}_{out,i} \tag{5-9}$$

$$\dot{m}_{i+1} x_{i+1} = \dot{m}_i x_i - \dot{m}_{out,i} x_{out,i} \tag{5-10}$$

Table 5-4: The uncertainty of the instruments in the vertical inlet header test

Instrument	**Measurement**	**Uncertainty**
Sensotec TJE	Pressure (*P*)	± 0.1% FS
T-type thermocouple	Temperature (*T*)	± 0.1 °C
Ohio Semitronics GW5-024CX5	Heater power (Q)	± 0.2% Reading/± 0.04% FS
Micromotion D40	Inlet mass flow rate (m)	± 0.2% flow rate
Micromotion D06	MC tube mass flow rates (m)	± 0.2% flow rate
Rosemount 1151	Pressure drop (DP)	±0.25% FS

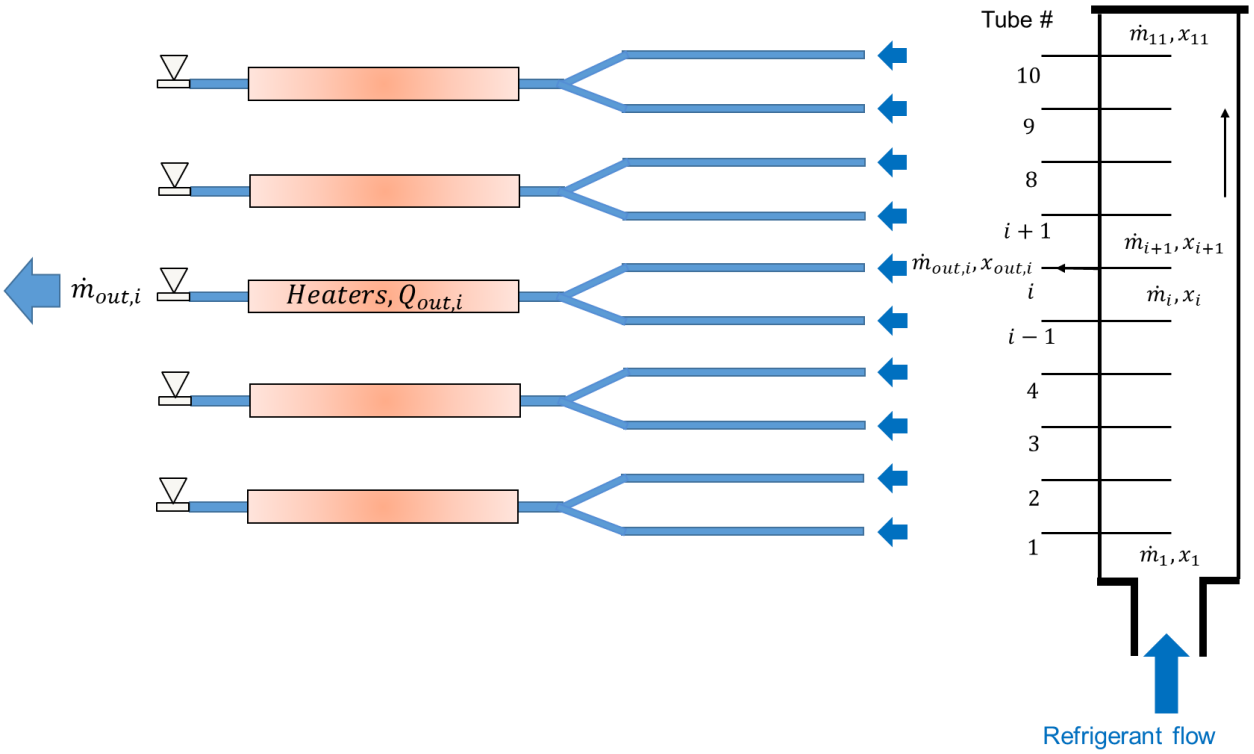

Figure 5-8: Measured and calculated variables in the inlet header

5.3.3 RESULTS

Figure 5-9 shows the flow regimes of upward flow in vertical inlet headers with m_{in}=5.3 g s^{-1}. Most of the liquid accumulates at the lower part of the header. The upper header is mainly occupied by the vapor phase. When the x_{in} is small, the flow regimes are very chaotic. The low-speed vapor goes upward with little entrainment. Liquid oscillates between protrusions. If x_{in} is relatively large, a thin liquid film is formed at the lower header. As x_{in} increases, less liquid enters the header, consequently, the highest positions that the liquid can reach become lower.

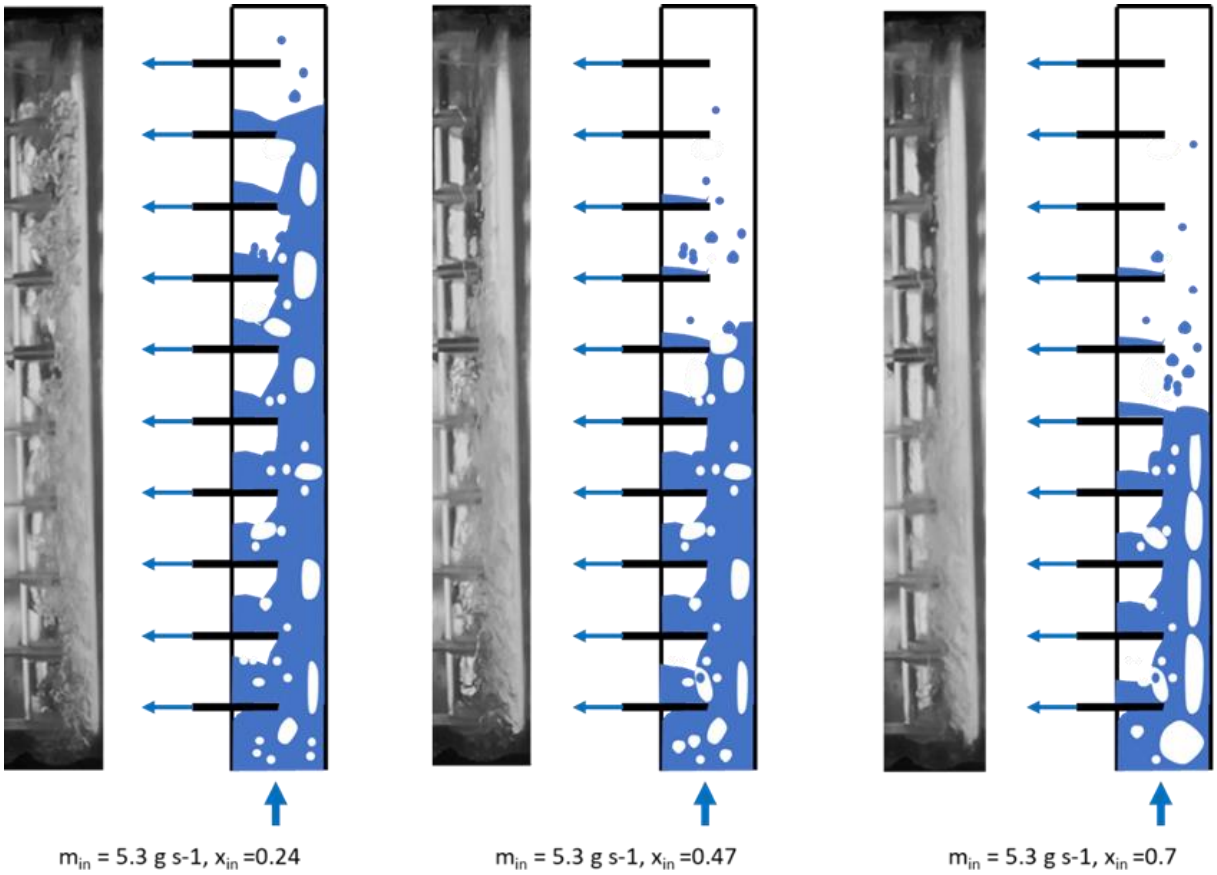

Figure 5-9: Flow regimes for vertical inlet header, m_{in}=5.3 g s^{-1}

The effect of inlet quality and inlet mass flow rate on pressure drop in the header is presented in Figure 5-10 and Figure 5-11. It can be seen that for all the cases the highest pressure drop happens over the first microchannel tube. This behavior can be expected due to the significant contraction from the entrance to the area above the first MC tube. Over the second microchannel tube due to the pressure recovery and expansion of the flow pressure drop decreases. Over tube #3, the flow starts to become more developed, and as the fluid goes further, the mass, especially of liquid, is removed from the main flow in the header. Therefore, as a general trend, the pressure drop gradually decreases as the flow goes further.

Due to the complexity of the pressure drop behavior in Figure 5-10 and Figure 5-11, the variation of the pressure along the header is evaluated, instead. However, for a fair assessment for all the inlet qualities and inlet mass flow rates, the pressure before the first microchannel tube (location 0 in figures 5-12 and 5-13) is set to zero, and pressure variation is plotted accordingly for all flow condition, as shown in figure 5-12 and 5-13.

Figure 5-12 shows the effect of inlet quality on pressure at different mass flow rates. It can be seen that pressure along the header decreases drastically over some number of first microchannels, with a linear trend. This region is dominated by liquids, resulting in higher gravitational pressure drop. Over the top vapor is dominated and pressure drop is much less. According to these plots, at a specific mass flow rate, for the lower inlet qualities, the liquid reaches higher microchannel tubes. As the inlet quality increases, less liquid will be present, and less hydraulic pressure drop exist, consequently.

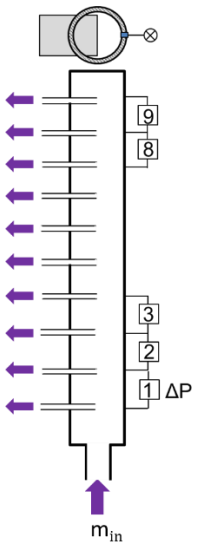

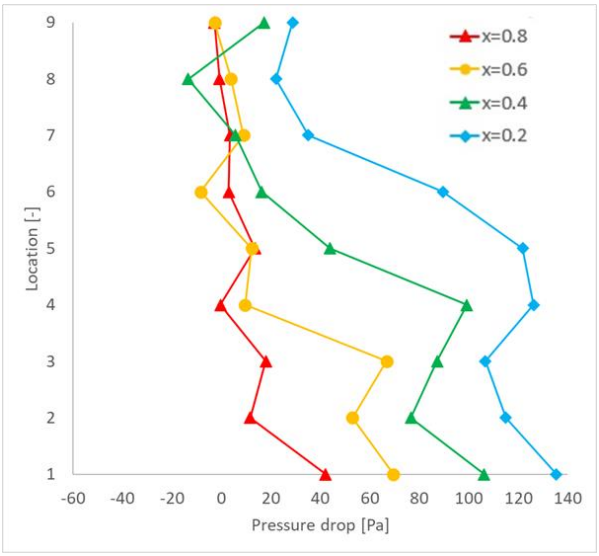

$\dot{m}_{in}$=3.2 g s^{-1}

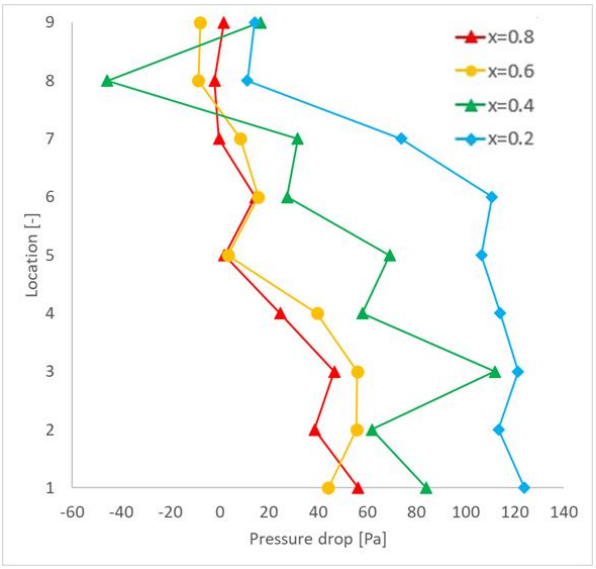

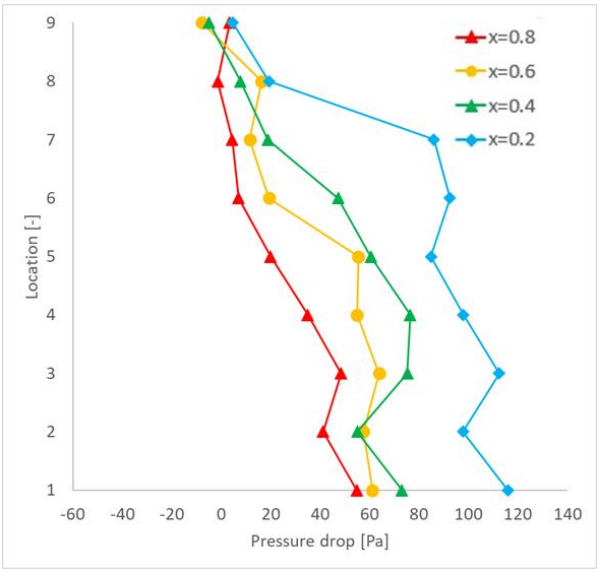

$\dot{m}_{in}$=4.3 g s^{-1}

$\dot{m}_{in}$=5.2 g s^{-1}

Figure 5-10: Effect of inlet quality on pressure drop at different mass flow rates

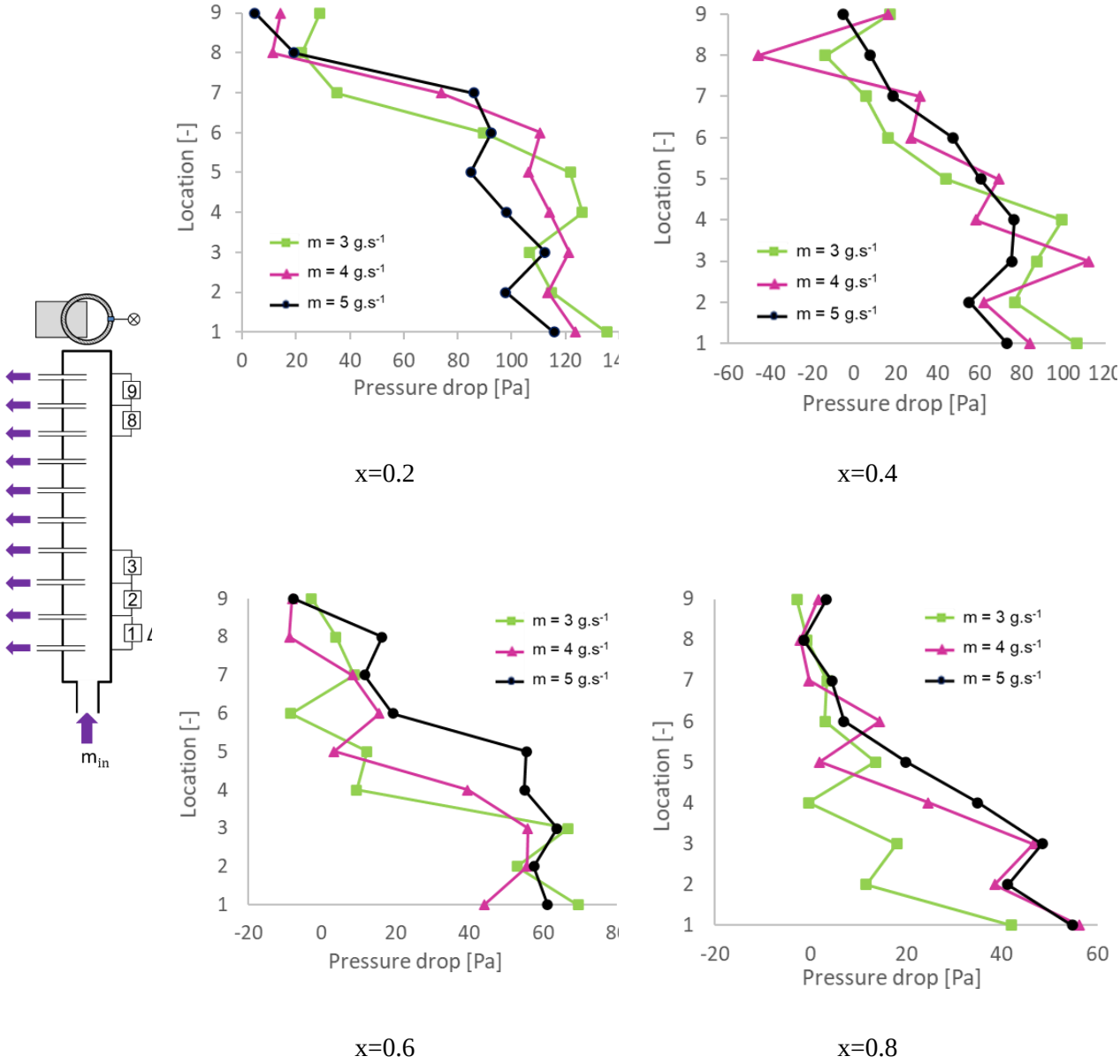

Figure 5-11: Effect of mass flow rate on pressure drop at different inlet qualities

.

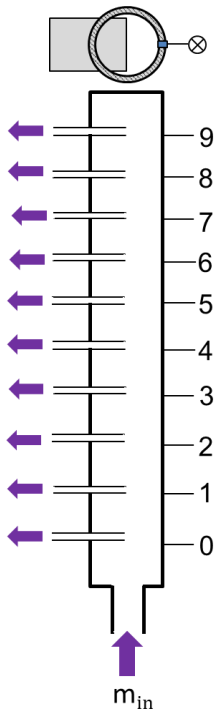

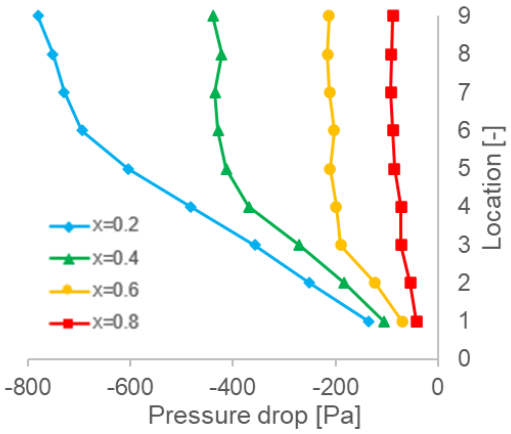

$\dot{m}_{in}$=3.2 g s^{-1}

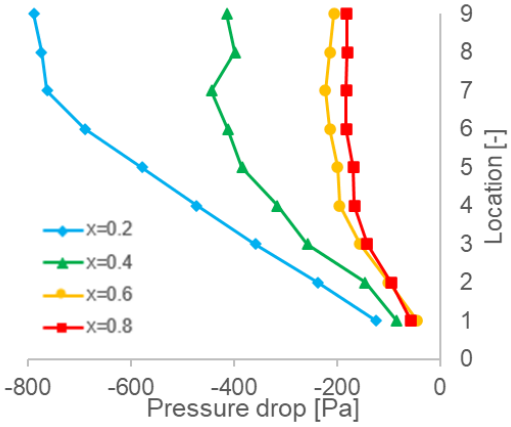

$\dot{m}_{in}$=4.3 g s^{-1}

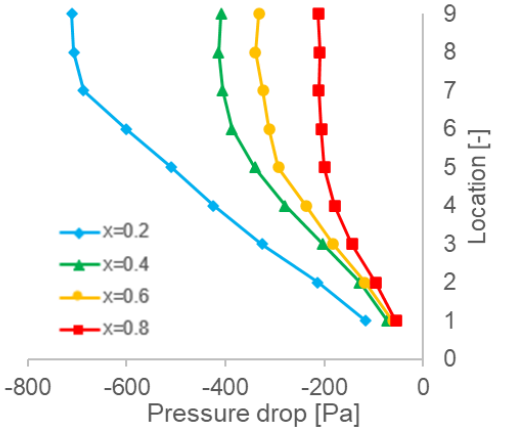

$\dot{m}_{in}$=5.2 g s^{-1}

Figure 5-12: Effect of inlet quality on pressure at different mass flow rates

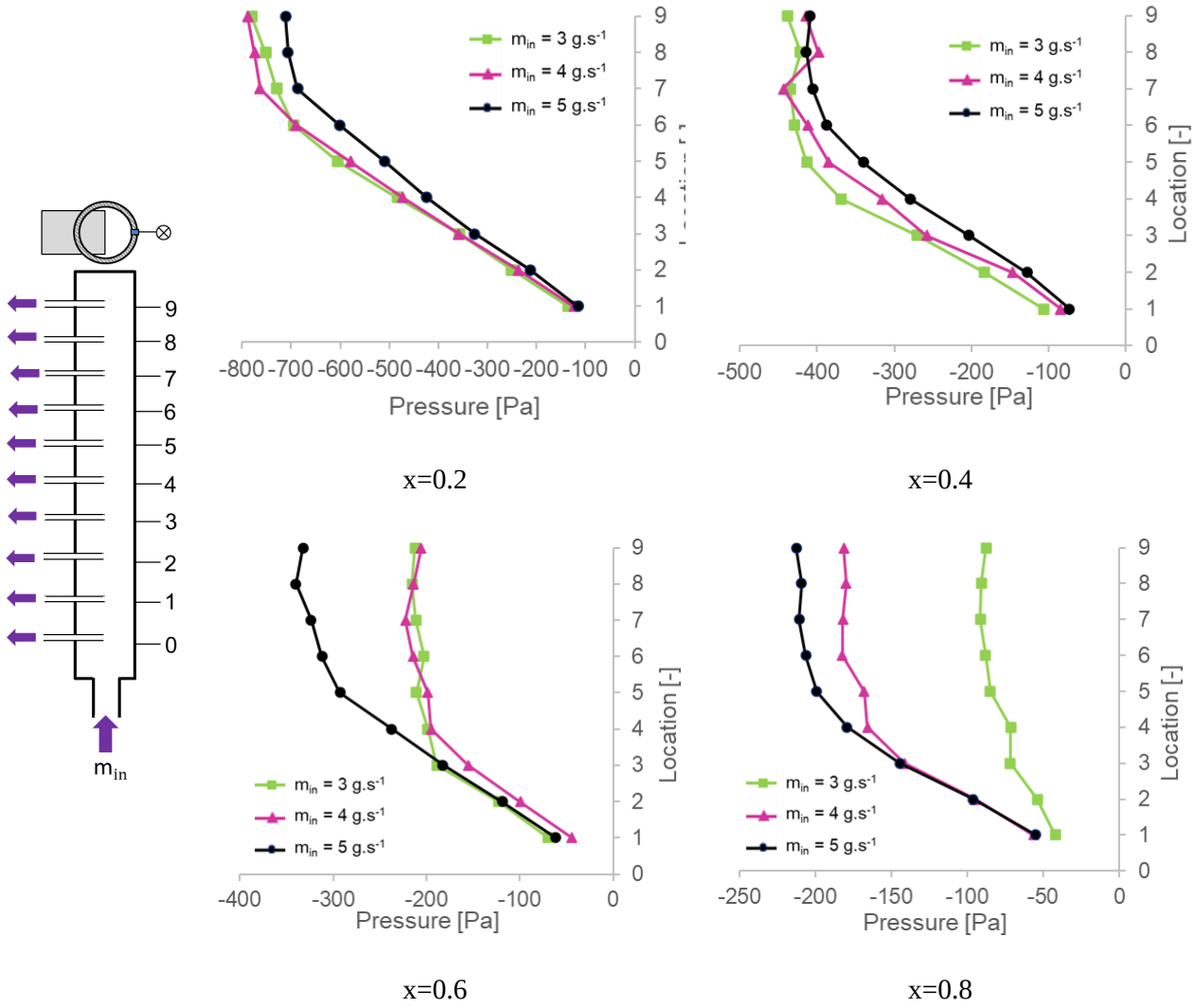

Figure 5-13: Effect of mass flow rate on pressure at different inlet qualities

Figure 5-13 shows the effect of inlet mass flow rate on pressure at different inlet qualities. The results show that at qualities of x=0.2 and x=0.4, increasing the mass flow rate decreases the pressure drop, while for the qualities of x=0.6 and x=0.8 the opposite behavior is observed. At the low qualities, because the hydrostatic pressure component is more dominant, increasing mass flow rate results in increasing void fraction, which results in smaller two-phase density and lower gravitational pressure drop. However, for higher qualities of x=0.6 and x=0.8, the higher the inlet mass flow rate, the more liquid is carried by the vapors toward the top. In addition, at higher qualities, as the vapor is more dominant, increasing the mass flow rate results in higher vapor velocity and higher local losses due to protrusions.

5.4 SUMMARY AND CONCLUSION

This chapter experimentally investigates two-phase R134a pressure drop in the vertical inlet header in upward flow and explores the behavior of the pressure drop in the header for a range of inlet qualities and inlet mass flow rates, while the visualization of two-phase flow in the header was recorded at the same time. According to the results, pressure drop is mainly affected by flow morphology in the header. For most of the inlet qualities and mass flow rates, gravitational pressure drop is very dominant and in the top region vapor is dominated and pressure drop is much less. In addition, the results demonstrate that at lower inlet qualities, as inlet mass flow rate increases pressure drop decreases, however, for higher qualities it shows the opposite behavior.

CHAPTER 6

SUMMARY AND FUTURE WORK

6.1 SUMMARY WITH CONTRIBUTIONS OF THIS RESEARCH

The major objectives of this study are to investigate pressure drop in headers of MCHEs. Both pressure drop for single-phase flow and two-phase flow in the headers of microchannel heat exchangers are studied and results are presented. A new set of correlations is generated to predict pressure loss coefficients, due to protrusions, in inlet and outlet headers. Then the generated correlation and two other methods are used in a 1-D finite volume approach to evaluate single-phase pressure drop in headers of MCHXs, to predict mass flow rate distribution in microchannel tubes, and the results are compared with a Hydraulic-CFD Linked model, in which the flow in headers are simulated by ANSYS Fluent. The 1-D finite volume models show a difference in the prediction of flow rate distribution. The model in which the flow passage in the header is assumed to be a series of dividing and combining T-manifolds shows a satisfactory agreement with the Hydraulic-CFD Linked model in the perspectives of mass flow rate distribution.

For two-phase flow analysis, flow visualization and pressure drop measurements are conducted in a vertical upward flow in a round inlet header. Flow regimes for a range of mass fluxes and vapor qualities are obtained and presented. The influence of mass flux and vapor quality on the pressure drop is also demonstrated.

6.2 RECOMMENDED FUTURE WORK

There are several opportunities for continued work in the area of two-phase flow distribution in heat exchangers. It is recommended that future work on this topic should be extended to horizontal headers and vertical headers of MCHXs with a downward flow. Studying pressure drop in headers with other widely used shapes (such as D-shape) can also be an interesting research direction. Also, in real-life HVAC&R systems, the working media are usually refrigerant and oil. It is very meaningful to extend this topic to real vapor-compression systems. Last but not least, the development of validated computational fluid dynamic (CFD) models in two-phase flow could provide local velocity and pressure information in the header and answer some of the outstanding questions in this field.

REFERENCES

Ablanque, N., Oliet, C., Rigola, J., Pérez-Segarra, C. D., & Oliva, A. (2010). Two-phase flow distribution in multiple parallel tubes. *International Journal of Thermal Sciences*, 49(6), 909–921. https://doi.org/10.1016/j.ijthermalsci.2009.11.005

Ahmad, M., Berthoud, G., & Mercier, P. (2009). General characteristics of two-phase flow distribution in a compact heat exchanger. *International Journal of Heat and Mass Transfer*, 52(1–2), 442–450. https://doi.org/10.1016/j.ijheatmasstransfer.2008.05.030

Anbumeenakshi, C., & Thansekhar, M. R. (2016). Experimental investigation of header shape and inlet configuration on flow maldistribution in microchannel. *Experimental Thermal and Fluid Science*, 75, 156–161. https://doi.org/10.1016/j.expthermflusci.2016.02.004

ANSYS-Fluent, (2018). ANSYS-Fluent Solver Theory Guide, ANSYS, Inc.

Aslam Bhutta, M. M., Hayat, N., Bashir, M. H., Khan, A. R., Ahmad, K. N., & Khan, S. (2012). CFD applications in various heat exchangers design: A review. *Applied Thermal Engineering*, 32(1), 1–12. https://doi.org/10.1016/j.applthermaleng.2011.09.001

Bajura, R. A. (1971). A model for flow distribution in manifolds. *Journal of Engineering Power*, 93(1), 7-12.

Bajura, R. A., & Jones, E. H. (1976). Flow distribution manifolds. *Journal of Fluids Engineering, Transactions of the ASME*, 98(4), 654–665. https://doi.org/10.1115/1.3448441

Bassiouny, M. K., & Martin, H. (1984). Flow distribution and pressure drop in plate heat exchangers U-type arrangement. *Chemical Engineering Science*, 39(4), 693–700. https://doi.org/10.1016/0009-2509(84)80176-1

Bowers, C.D., Newell, T.A., & Hrnjak, P. S., (2006). Experimental investigation of two-phase refrigerant distribution in a microchannel manifold, *ACRC Technical Report TR-245*, Univ. of Illinois, Urbana, USA.

Chang, Y.J., & Wang, C.C., (1997). A Generalized Heat Transfer Correlation for Louver Fin Geometry, *Int. J. Heat Mass Transfer*, 40(3), 533-544.

Chen, I.Y., Tseng C.-Y., & C. C. Wang (2012), Two-phase Flow Pressure Change across Sudden Contraction and Expansion in Small Channels. *Advances in Multiphase Flow and Heat Transfer*, 3, 55-83

Cho, H., K., & Kim, Y. S. (2003). *Mass Flowrate Distribution and Phase Separation of R-22 in Multi-Microchannel Tubes under Adiabatic Condition*. International Conference on Microchannels and Minichannels. Rochester, NY, The American Society of Mechanical Engineers, ICMM2003, 527-533.

Churchill, S. W. (1977a), Comprehensive Correlating Equations for Heat, Mass and Momentum Transfer in Fully Developed Flow in Smooth Tubes, *Industrial & Engineering Chemistry Fundamentals*, 16(1), 109-116

Churchill, S. W. (1977b), "Friction-Factor Equation Spans All Fluid-Flow Regimes," *Chemical Engineering*, 84(24), 91-92

Dario, E. R., Tadrist, L., Oliveira, J. L. G., & Passos, J. C. (2015), Measuring Maldistribution of Two-Phase Flows in Multi-Parallel Microchannels, *Applied Thermal Engineering*, 91, 924-937. https://doi.org/10.1016/j.applthermaleng.2015.08.103.

Datta, A. B., & Majumdar, A. K. (1980). Flow distribution in parallel and reverse flow manifolds. *International Journal of Heat and Fluid Flow*, 2(4), 253–262. https://doi.org/10.1016/0142-727X(80)90019-3

Datta, A. B., A.K. Majumdar (1983). A calculation procedure for two-phase flow distribution in manifolds with and without heat transfer. *Int. J. Heat Mass Transfer*, 26(9), 1321-1328.

Dharaiya, V. V., Radhakrishnan, A., & Kandlikar, S. G. (2009). Evaluation of a tapered header configuration to reduce flow maldistribution in minichannels and microchannels. *Proceedings of the 7th International Conference on Nanochannels, Microchannels, and Minichannels 2009*, ICNMM2009(B), 771–777. https://doi.org/10.1115/ICNMM2009-82288

EES, (2016). Engineering Equation Solver. Academic Professional Version 10.024-3D. F-Chart Software, Middleton, WI, USA.

Fei, P., & Hrnjak, P. S., (2004). Adiabatic developing two-phase refrigerant flow in manifolds of heat exchangers. *ACRC Technical Report TR-225*, Air Conditioning and Refrigeration Center, Univ. Illinois at Urbana-Champaign, Urbana, IL, USA.

Forinash, D. (2015). Novel Air-Coupled Heat Exchangers for Waste Heat-Driven Absorption Heat Pumps. *Mechanical Engineering, Georgia Institute of Technology*, Vol. Master of Science in Mechanical Engineering.

Friedel, L. (1979). Improved friction pressure drop correlations for horizontal and vertical two-phase pipe flow., *3R International*, 18(7), 485–491.

Garcia-Cascales, J.R., Vera-Garcia, F., Gonzalvez-Macia, J., (2010). Compact heat exchangers modeling, *Condensation. Int. J. Refrigeration*, 33, 135-137.

Garimella, S., Agarwal, A., & Killion, J. D. (2005). Condensation pressure drops in circular microchannels. *Proceedings of the Second International Conference on Microchannels and Minichannels (ICMM2004)*, 649–656. https://doi.org/10.1115/icmm2004-2393

Ghani, F., Duke, M., & Carson, J. K. (2012). Effect of flow distribution on the photovoltaic performance of a building integrated photovoltaic/thermal (BIPV/T) collector. *Solar Energy*, 86(5), 1518–1530. https://doi.org/10.1016/j.solener.2012.02.013

Gnielinski, V., (1976). New equation of heat and mass transfer in turbulent pipe and channel flow, *Int. Chem. Eng.*, 16(2), 359-368.

Graham, T.P., Dunn, W.E., (1995), Friction and Heat Transfer Characteristics for Single-Phase Flow in Microchannel Condenser Tubes. University of Illinois. ACRC *TR-78*. Air Conditioning and Refrigeration Center. University of Illinois at Urbana-Champaign.

Heun, M. K., & Dunn, W. E., (1995). Performance and optimization of microchannel condensers. *ACRC Technical Report TR 81*. Air Conditioning and Refrigeration Center. University of Illinois at Urbana-Champaign.

Hrnjak, P. S. (2004). Developing Adiabatic Two-Phase Flow in Headers—Distribution Issue in Parallel Flow Microchannel Heat Exchangers. In *Heat Transfer Engineering*, 25(3), 61–68. https://doi.org/10.1080/01457630490280128

Hrnjak, P., Tu, X., (2007). Single-phase pressure drop in microchannels. *Int. J. Heat. Fluid Flow*. 28, 14-20.

Huang, L., Lee, M. S., Saleh, K., Aute, V., & Radermacher, R. (2014). A computational fluid dynamics and effectiveness-NTU based co-simulation approach for flow mal-distribution analysis in microchannel heat exchanger headers. *Applied Thermal Engineering*, 65, 447–457. https://doi.org/10.1016/j.applthermaleng.2014.01.046

Hwang, S. T., Soliman, H. M., & Lahey, R. T. (1988). Phase separation in dividing two-phase flows. *American Institute of Chemical Engineers*, 14(4), 439–458. http://dx.doi.org/10.1016/0301-9322(88)90021-3

Hwang, Y., Jin, D. H., & Radermacher, R. (2007). Refrigerant distribution in minichannel evaporator manifolds. *HVAC and R Research*, 13(4), 543–555. https://doi.org/10.1080/10789669.2007.10390971

Idelchik, I. E. (1994). Handbook of Hydraulic Resistance, 2nd Edition. In *Begell House* (third edition, Issue 2). https://doi.org/10.1115/1.3264907

Kim, J.-S., Lee, K.-T., Kim, J.-H., Ha, S.-J., & Im, Y.-B. (2004). A relation between two-phase pressure drop and flow distribution in a compact heat exchanger header. *Proceedings of the 2nd International Conference on Microchannels and Minichannels*, (ICMM2004), 413–420.

Kim, N. H., Lee, E. J., & Byun, H. W. (2013). Improvement of two-phase refrigerant distribution in a parallel flow minichannel heat exchanger using insertion devices. *Applied Thermal Engineering*, 59(1–2), 116–130. https://doi.org/10.1016/j.applthermaleng.2013.05.026

Kim, N. H., & Sin, T. R. (2006), Two-Phase Flow Distribution of Air–Water Annular Flow in a Parallel Flow Heat Exchanger, *International Journal of Multiphase Flow*, 32(12), 1340-1353. https://doi.org/10.1016/j.ijmultiphaseflow.2006.07.005.

Kim, S., Choi, E., & Cho, Y. I. (1995). The effect of header shapes on the flow distribution in a manifold for electronic packaging applications. *International Communications in Heat and Mass Transfer*, 22(3), 329–341. https://doi.org/10.1016/0735-1933(95)00024-S

Kim, S. M., & Mudawar, I. (2012). Universal approach to predicting two-phase frictional pressure drop for adiabatic and condensing mini/micro-channel flows. *International Journal of Heat and Mass Transfer*, 55(11–12), 3246–3261. https://doi.org/10.1016/j.ijheatmasstransfer.2012.02.047

Kulkarni, T., Bullard, C. W., & Cho, K. (2004). Header design tradeoffs in microchannel evaporators. *Applied Thermal Engineering*, 24(5–6), 759–776. https://doi.org/10.1016/j.applthermaleng.2003.10.016

Lee, J. K. (2009). Branching of two-phase flow from a vertical header to horizontal parallel channels. *Journal of Mechanical Science and Technology*, 23(6), 1628–1636. https://doi.org/10.1007/s12206-009-0408-2

Lee, J. K., & Lee, S. Y. (2004), Distribution of Two-Phase Annular Flow at Header–Channel Junctions, *Experimental Thermal and Fluid Science*, 28(2), 217-222. https://doi.org/10.1016/S0894-1777(03)00042-6.

Luan, H. B., Kuang, J. P., Cao, Z., Wu, Z., Tao, W. Q., & Sundén, B. (2017). CFD analysis of two types of welded plate heat exchangers. *Numerical Heat Transfer; Part A: Applications*, 71(3), 250–269. https://doi.org/10.1080/10407782.2016.1264761

Mahvi, A. J., & Garimella, S. (2017), Visualization of Flow Distribution in Rectangular and Triangular Header Geometries, *International Journal of Refrigeration*, 76, 170-183. https://doi.org/10.1016/j.ijrefrig.2017.02.002.

Manikanda Kumaran, R., Kumaraguruparan, G., & Sornakumar, T. (2013). Experimental and numerical studies of header design and inlet/outlet configurations on flow mal-distribution in parallel microchannels. *Applied Thermal Engineering*, 58(1–2), 205–216. https://doi.org/10.1016/j.applthermaleng.2013.04.026

Marchitto, A., Fossa, M., & Guglielmini, G. (2012), The Effect of the Flow Direction inside the Header on Two-Phase Flow Distribution in Parallel Vertical Channels, *Applied Thermal Engineering*, 36, 245-251. https://doi.org/10.1016/j.applthermaleng.2011.10.008.

Moffat, R.J., (1988). Describing the uncertainties in experimental results. *Exp. Therm. Fluid Sci.*, 1(1), 3-17.

Muhana, A., & Novog, D. R., (2008). Validation of fluent for prediction of flow distribution and pressure gradients in a multi-branch header under low flow conditions. *16th International Conference on Nuclear Engineering*, ICONE16-48128, American Society of Mechanical Engineers.

Nielsen, K. K., Engelbrecht, K., Christensen, D. V., Jensen, J. B., Smith, A. & Bahl, C. R. H. (2012), Degradation of the Performance of Microchannel Heat Exchangers Due to Flow Maldistribution, *Applied Thermal Engineering*, 40, 236-247. https://doi.org/10.1016/j.applthermaleng.2012.02.019.

Panghat, K., & Mehendale, S. (2016). A Critical Assessment of Two-Phase Flow Distribution in Microchannel Heat Exchangers. *International Compressor Engineering, Refrigeration and Air Conditioning, and High-Performance Buildings Conferences*, 2089, 1–10.

Ren, T., Chavoshi, A., Ding, G., & Hrnjak, P. S. (2014). *Single Phase Pressure Drop in Round Cylindrical Headers of Parallel Flow MCHXs*. 15th International Refrigeration and Air Conditioning Conference, *1977*, 1–10.

Rong, X., Kawaji, M., & Burgers, J. G. (1995), Two-Phase Header Flow Distribution in a Stacked Plate Heat Exchanger, *Gas-Liquid Flows,* 225, 115-122

Said, S. A. M., Ben-Mansour, R., Habib, M. A., & Siddiqui, M. U. (2015). Reducing the flow mal-distribution in a heat exchanger. *Computers and Fluids*, 107, 1–10. https://doi.org/10.1016/j.compfluid.2014.09.012

Stevanovic, V. D., & Hrnjak, P. (2017). Numerical simulation of three-dimensional two-phase flow and prediction of oil retention in an evaporator of the automotive air conditioning system. *Applied Thermal Engineering*, *117*, 468–480. https://doi.org/10.1016/j.applthermaleng.2017.02.027

Tae, S. J., & Cho, K. (2006). Two-phase split of refrigerants at a T-junction. *International Journal of Refrigeration*, 29(7), 1128–1137. https://doi.org/10.1016/j.ijrefrig.2006.02.004

Taliv, V. N. (1952), Calculation of Local Resistances of Wyes, *Gosstroiizdat Press*, 35

Tompkins, D., Newell, T., & Hrnjak, P. (2002). Single Phase, Two-Phase Modeling; X-Ray Visualization for a Microchannel Manifold Distribution System. *Air Conditioning and Refrigeration Center,* University of Illinois at Urbana-Champaign, *TR-206*. http://www.ideals.illinois.edu/handle/2142/12125

Tong, J. C. K., Sparrow, E. M., & Abraham, J. P. (2009). Geometric strategies for attainment of identical outflows through all of the exit ports of a distribution manifold in a manifold system. *Applied Thermal Engineering*, 29(17–18), 3552–3560. https://doi.org/10.1016/j.applthermaleng.2009.06.010

Tuo, H., & Hrnjak, P. (2013). Effect of the header pressure drop induced flow maldistribution on the microchannel evaporator performance. *International Journal of Refrigeration*, 36(8), 2176–2186. https://doi.org/10.1016/j.ijrefrig.2013.06.002

Vist, S. (2004). *Two-Phase Flow Distribution in Heat Exchanger Manifolds*. Energy and Process Engineering, Norwegian University of Science and Technology, 306. http://ntnu.diva-portal.org/smash/get/diva2:123809/FULLTEXT01

Vist, S., & Pettersen, J. (2004). Two-phase flow distribution in compact heat exchanger manifolds. *Experimental Thermal and Fluid Science*, 28(2–3), 209–215. https://doi.org/10.1016/S0894-1777(03)00041-4

Wang, X. A., & Yu, P. (1989). Isothermal flow distribution in header systems. *International Journal of Solar Energy*, 7(3), 159–169. https://doi.org/10.1080/01425918908914252

Watanabe, M., Katsuta, M., & Nagata, K. (1995). General Characteristics of Two-Phase Flow Distribution in a Multipass Tube. *Heat Transfer – Japanese Research*, 24(1), 32–44.

Webb, R. L., & Chung, K. (2005). Two-Phase Flow Distribution to Tubes of Parallel Flow Air-Cooled Heat Exchangers. *Heat Transfer Engineering*, 26(4), 3–18. https://doi.org/10.1080/01457630590916239.

Wen, J., & Li, Y., (2004). Study of flow distribution and its improvement on the header of plate-fin heat exchanger. *Cryogenics*, *44*(11), 823-831.

Wijayanta, A. T., Miyazaki, T., & Koyama, S. (2017). Refrigerant distribution in horizontal headers with downward minichannel-branching conduits: Experiment, empirical correlation and two-phase flow pattern map. *Experimental Thermal and Fluid Science*, 81, 430–444. https://doi.org/10.1016/j.expthermflusci.2016.09.011

Yin, J.M., Bullard, C.W. & Hrnjak, P. S., (2001) R-744 gas cooler model development and validation. *Int. J. Refrig.*, 24(7), 692-701.

Yin, J. M., Bullard, C. W., & Hrnjak, P. S. (2002). Single-phase pressure drop measurements in a microchannel heat exchanger. *Heat Transfer Engineering*, 23(4), 3–12. https://doi.org/10.1080/01457630290090455

Zhang, Z., & Li, Y. Z. (2003). CFD simulation on inlet configuration of plate-fin heat exchangers. *Cryogenics*, *43*(12), 673–678. https://doi.org/10.1016/S0011-2275(03)00179-6

Zou, Y., & Hrnjak, P. S., (2010). Performance measurement and visualization of the refrigerant distribution in the vertical manifold of the microchannel tube heat exchanger. *ACRC Report CR-73* Univ. of Illinois, Urbana, USA.

Zou, Y., & Hrnjak, P. S. (2014). Single-phase and two-phase flow pressure drop in the vertical header of microchannel heat exchanger. *International Journal of Refrigeration*, 44, 12–22. https://doi.org/10.1016/j.ijrefrig.2014.05.007

Zou, Y. & Hrnjak, P. S. (2016). CFD Simulation of R134a and R410a Two-Phase Flow in the Vertical Header of Microchannel Heat Exchanger. *International Refrigeration and Air Conditioning Conference*. West Lafayette, USA, Purdue University Libraries, 2367, 1-10.

Zou, Y., Tuo, H., & Hrnjak, P. S. (2014). Modeling refrigerant maldistribution in microchannel heat exchangers with vertical headers based on experimentally developed distribution results. *Applied Thermal Engineering*, 64(1–2), 172–181. https://doi.org/10.1016/j.applthermaleng.2013.12.033

Zubov, V. P. (1974), Concerning the resistance of an ordinary Wye with converging flows, *The Problems of Hydraulics*, 124, 55-60.